Characterization of Nek9 as a transcriptional regulator of p53-mediated networks involved in cellular arrest and apoptosis

by

Leandro G. V. Crisostomo

A Thesis submitted to the Faculty of Graduate Studies of

The University of Manitoba

In partial fulfillment of the requirements of the degree of

Doctor of Philosophy

Department of Microbiology

University of Manitoba

Winnipeg, Manitoba, Canada

Abstract

Oncogenesis is the consequence of the transformation of normal cells into cancerous cells. Cellular kinases are vital enzymes that facilitate the transfer of phosphate groups between two molecules. The disruption of these messengers may lead to genomic instability, resulting in death, or oncogenesis. NEK9, a human kinase, is responsible for mitotic progression and spindle formation. This thesis describes how the dysregulation of NEK9 in human cells alters the expression of tumour-suppressing pathways, disrupting mitotic progression, leading to transformation, cell cycle arrest, and the induction of apoptosis. The overexpression of NEK9 in adenovirus-infected MEF cells was shown to enhance the transformative properties of the virus, suggesting it may possess oncogenic properties. NEK9 was shown to suppress p53 activity independent of adenovirus, suggesting an inherent ability to regulate p53-promoters. The depletion of NEK9 in p53-mutant cells led to the upregulation of tumour-suppressor genes such as *PIG3*, *PUMA*, and *GADD45α*. The expression of proapoptotic and antiapoptotic markers in NEK9-depleted cells were mainly cell-dependent, despite their p53 wild-type status. A kinase-inactive variant (D194N) and RCC1-deletion variant (ΔRCC1) of NEK9 were shown to cause a delay in the S-phase of cells. Cells with prolonged expression of these variants also exhibited signs of apoptosis. Altogether, these findings support the hypothesis that NEK9 acts as a transcriptional regulator to p53-regulated genes responsible for the induction of cell cycle arrest and apoptosis.

A high throughput *in vivo* screen was developed to identify NEK9 substrates. Co-localization between an mCherry-NEK9-LacI fusion protein with a GFP-tagged NEK6 consensus site indicated a positive interaction. However, co-localization was also detected between an mCherry-LacI fusion protein that lacked NEK9 and the GFP-tagged NEK6 consensus sequence,

suggesting further optimization of the assay is required. Establishment of NEK9's binding partners would aid in characterizing it's involvement in various cellular pathways.

Additionally, this thesis set out to map the temporal expression of adenoviral genes during infection of normal human cells. The boundaries of early, intermediate, and late viral gene activation were defined and discussed. Overall, these results detail the transcriptional cycle of adenovirus, by carefully examining the chronological events that occur during infection.

“Once you eliminate the impossible, whatever remains, no matter how improbable, must be the truth.”

- Sir Arthur Conan Doyle

Acknowledgements

I would like to acknowledge my supervisor, Dr. Peter Pelka. He provided invaluable feedback, teachings and philosophies which enabled my growth as a scientist and academic over the last couple of years. It was a pleasure to be introduced to Ace of Base, listen to the entirety of the Star Wars OST every Christmas and to watch Bladerunner 2049 at the theatres in the middle of the workday. These experiences have made my time at the lab enjoyable and I will always be grateful for the memories. I would also like to acknowledge my co-advisor; Dr. Deborah Court and the rest of my committee; Dr. Brian Mark and Dr. Spencer Gibson for their continued support and input over the years.

I want to thank the past and present members of the Pelka Lab. I was fortunate enough to experience different eras and iterations of the lab. I am deeply honoured to have spent these years with all of you and each one of the members of this lab has blessed me with memories I will forever cherish. Aside from teaching me the technical procEdUres, the past members (Jasmine, Ola, Alennie, Andrea, Megan) taught me how to dress better and take care of myself. As for the present members (Drayson, Nik, Scott), thank you for helping me grow as a mentor and teaching me to appreciate the little things in life. We shall sling spells again someday. I wish you all luck moving forward.

I would like to thank the Microbiology department and support staff. It is difficult to put into words the appreciation I have for all of you. You exemplify what it means to be a community. I can always count on someone to vent to when my cloning has failed for the n'th time. Keep caring for each other.

Finally, I would like to recognize that this research made possible by the financial assistance from the National Sciences and Engineering Research Council of Canada (NSERC), the Cancer Research Society and the University of Manitoba.

Dedication

This thesis is dedicated to my family and friends. To Maria and Gerardo Crisostomo, who chose to move to Canada and worked tirelessly, day and night, in hopes of providing a better life for their son. Thank you for your unconditional love and support. To my Lolo and Lola, my Tito's and Tita's, to my younger cousins; thank you for always checking up on me and making sure I am eating well. To my brother, Sam; I am grateful for your advice and kind words to lift me up when I am down.

Finally, to my partner, Theresa. Thank you for your unending patience and understanding. You have stuck with me even through all the times I was late for a date because I had to count plaques or infect cells. You made tea for me when I was working on my comprehensive exam, and you baked carrot cake for me while I wrote this thesis. Your love gave me strength to continue when I struggled through the hardest times. I am ready for the next chapter, and I am blessed to share this life with you and our lovely boyo, Apollo.

Table of Contents

List of Tables

List of Figures

List of Abbreviations

52K EP: 52K encapsidation protein
9S – 13S: 9S Svedberg unit
A549: Adenocarcinoma-549 cells
Act D: Actinomycin D
Ad-CMV: Adenovirus vector (does not express any protein of interest)
AdRC: Adenoviral replication center(s)
AdV pol: Adenovirus polymerase
AKT: Protein Kinase B/RAC-alpha serine/threonine-protein kinase
ANOVA: One-way analysis of variance
APAF-1: Apoptotic protease activating factor 1
APC/C: Anaphase-Promoting Complex/Cyclosome
ARDS: Acute respiratory syndrome
ATP: Adenosine triphosphate
AURK: Aurora kinase(s)
BAD: BCL-2 associated agonist of cell death
BAK: BCL-2 homologous antagonist killer
BAX: BCL-2 associated X
BCL-2: B-cell lymphoma 2
BCL-xL: B-cell lymphoma-extra large
BH3: BCL-2 homology 3 domain
BIM: BCL-2-like protein 11
Bim: Blocked in mitosis
BRCA1: Breast cancer type 1 susceptibility protein
BRCA2: Breast cancer type 2 susceptibility protein
BSA: Bovine serum albumin
C3G: Canadian Centre for Computational Genomics
CAR: Coxsackie and adenovirus receptor
CC: Coiled coil (domain)
CD46: Cluster of differentiation 46
CDC25C: Cell division cycle 25C
CDK: Cyclin dependent kinase(s)
CDK2: Cyclin dependent kinase 2
CDKN1A: Cyclin dependent kinase inhibitor 1A (p21)
cDNA: Complementary DNA
CHK1: Checkpoint kinase 1
CHO: Chinese hamster ovarian cells
CMV (Ad-CMV): Cytomegalovirus (Adenovirus vector)
CR3: Conserved region 3
D194N: Kinase-inactive variant of NEK9 (substitution of asparagine 194 with aspartic acid)
DBP: DNA binding protein
DCIS: Ductal carcinoma *in situ*
ddH_2O: Double distilled H_2O
ddPCR: Digital droplet polymerase chain reaction
DDR: DNA damage response

DEG: Differentially regulated gene(s)
DISC: Death inducing signaling complex
*dl*309: Human adenovirus serotype 5 with a deletion in the *E3* region (removal of the RID associated genes and 14.7K proteins[1])
DMEM: Dulbecco's modified eagle medium
DNA: Deoxyribonucleic acid
DBP: DNA-binding protein
DNA-PK: DNA-Protein Kinase
DREF: Zinc finger BED-type containing 1
DSB(s): Double-stranded breaks
dsRNA: Double-stranded RNA
DYNLL1: Dynein light chain LC8 type 1
E1A – E4ORF6/7: Early region 1A
E2F1: E2F Transcription Factor 1
(E3) RID complex: Receptor internalization and degradation complex
ECM: Extracellular matrix
EdU: 5-ethynyl-2'deoxyuridine (assay)
EG5: Kinesin family member 11
EGFR: Epithelial growth factor receptor
eIF-2a: Eukaryotic initiation factor 2a
EML4-ALK: Echinoderm microtubule associated protein-like 4 – anaplastic lymphoma kinase
FACT: SPT16 Homolog, Facilitates chromatin remodeling subunit
FAM: 6-carboxyfluorescein
FasR: Fas cell surface death receptor
FSCA: Forward scatter area plot
FSC: Forward scatter plot
FSCH: Forward scatter height plot
FUBP1: Far upstream element binding protein 1
G0: Gap 0 (phase)
G1: Gap 1 (phase)
G2: Gap 2 (phase)
GADD45α: Growth arrest and DNA damage inducible alpha
GAPDH: Glyceraldehyde-3-phophate dehydrogenase
GO: Gene ontology
HADV: Human adenovirus (serotype-2, 5, 7, 9)
HCMV: Human cytomegalovirus
HCT116: Human colorectal carcinoma tumour cell line
HEK293: Human embryonic kidney cell line
HeLa: Henrietta Lack cell line
HFF(s): Human foreskin fibroblasts
HGSOC: High grade serous ovarian cancer
HNCC: Head and neck squamous cell carcinoma
HPV: Human papilloma virus
HR: Homologous repair
HR: Hormone-receptor
HRP: Horseradish peroxidase

HT1080: Human fibrosarcoma cell line
IDC: Invasive ductal carcinoma
IF: Immunofluorescence
IMR90: Normal lung fibroblast cell line
JMY: Junction mediating and regulatory protein, p53 cofactor
kDa: Kilo Dalton(s)
L1 – L5: Late protein 1
M: Mitotic phase
MAP2K4: Mitogen activated protein kinase kinase 4
MCPs: Major capsid protein(s)
MDM2: Mouse double minute 2 homolog
MEF: Mouse embryonic fibroblast cell line
mg: Milligrams
mL: Milliliters
MLP: Major late promoter
MLTU: Major late transcription unit
MOI: Multiplicity of infection
mRNA: Messenger RNA
MTT: 3-(4,5-Dimethylthiazol-2-yl)-2,5-diphenyltetrazolium bromidefor (assay)
NEDD1: neural precursor cell expressed, developmentally down-regulated 1
NEK: (Never in mitosis gene-a) related-kinase
NEK9: (Never in mitosis gene-a) related-kinase 9
NFI: Nuclear factor I
NHEJ: Non-homologous end joining
NIM: Never in mitosis
NIMA: Never in mitosis gene-a
NLS: Nuclear localization signal
NOXA: Phorbol-12-myristate-13-acetate-induced protein/ Immediate-Early-Response Protein APR
OIS: Oncogene-induced senescence
ORF: Open reading frame(s)
P16 (CDKN2A): Cyclin-dependent kinase inhibitor 2A
P300: E1A-associated protein 300
PARP: Poly(ADP-ribose) polymerase 1
PB: Penton base
PBS: Phosphate-buffered saline
PCNA: Proliferating cell nuclear antigen
PCR: Polymerase chain reaction
PEI: Polyethylenimine
pH: Potential of hydrogen
PI3K: Phosphoinositide 3-kinase
PIG3: Tumour protein 53 inducible protein 3
PKR: Protein kinase RNA-activated
PLKs: Polo-like kinase(s)
PML: Promyelocytic leukaemia
PNK: Polynucleotide kinase

PODs: PML oncogenic domain(s)
PP2A: Protein phosphatase 2A
PPB: Pelka Plasmid bank
pRb: Retinoblastoma protein
PRD: Proline-rich domain
PTM: Post translational modification
pTP: Precursor terminal protein
PUMA: P53 upregulated modulator of apoptosis
PVDF: Polyvinylidene fluoride (membrane)
R497: Nek9 mutation
RAN-GTPase: Ras-related nuclear protein (guanosine triphosphate) phosphatase
Rb protein: Retinoblastoma protein
RCC1: Regulator of chromosome condensation 1
RNA: Ribonucleic acid
RNA Pol II: RNA polymerase II
RNA SEQ: RNA sequence (analysis)
ROS: Reactive oxygen species
RPM: Rotations per minute
RSV: Rous sarcoma virus
RT-qPCR: Real-time-quantitative polymerase chain reaction
RuvBL1: RuvB like AAA ATPase 1
S: Synthesis (phase)
SF: Serum-free
SiRNA: Small-interfering RNA
SK-OV-3: Ovarian serous cystadenocarcinoma cancer cell line
SSC: Side scatter plot
SV40: Simian-virus 40
SW-480: Colorectal adenocarcinoma cancer cell line
T47D: Ductal carcinoma cancer cell line
TAD1: tRNA-specific adenosine deaminase 1
TAD2: tRNA-specific adenosine deaminase subunit
TBS-T: Tris-buffered saline-tween 20
TET: Tetracycline
TNFR-1: Tumour necrosis factor 1
TP: Terminal protein
TP53/P53: Tumour protein 53
TRK: Tyrosine-receptor kinase
U/mL: Units per milliliter
U2OS: Human bone osteosarcoma epithelial cells
UV: Ultra-violet (radiation)
VAI: (Adenovirus) virus-associated RNA I
VAII: (Adenovirus) virus-associated RNA II
WB: Western blot
WI-38: Human lung fibroblasts
XRCC6/KU70: X-ray repair cross-complementing protein 6
β-gal: Beta-galactosidase (assay)

ΔRCC1: RCC1-deletion variant of NEK9
μg: Micrograms
μL: Microliters

Chapter 1: Literature Review

The literature review below will provide information regarding cancer, the factors involved in tumour development and cellular networks that are responsible for the elimination of aberrant and damaged cells. This will be followed by a brief overview on kinases, and the relationship between the kinase of interest, NEK9, with cancer and related processes. Lastly, an introduction on adenovirus and its interaction with NEK9 to subvert host-cell machinery will be detailed.

1.1. The cell cycle

Normal mammalian cells undergo the cell cycle to replicate and divide. The process is composed of four main phases: G1-phase (Gap 1), S-phase (Synthesis), G2-phase (Gap 2) and M-phase (Mitosis). The G1-phase is a growth period for the cell in preparation for DNA replication. This is followed by the S-phase wherein DNA is replicated through DNA synthesis. Another growth phase, or G2-phase, permits preparation for mitosis and the subsequent division of the mother cell into two daughter cells[2]. In some specific cell types and organisms, such as Xenopus eggs, the G1 and G2-phases are skipped entirely as the S- and M-phases alternate to rapidly produce daughter cells[3]. Chinese hamster lung cells have also been found to skip G1 and/or G2-phases entirely[4,5]. There is a fifth phase in the cell cycle known as G0 (Gap-0), wherein cells may exit the cell cycle and enter a resting state in response to negative stimuli, such as a nutrient-deprived environment. Cells in G0 may re-enter the cell cycle given appropriate stimuli, like the introduction of growth factors and nutrients, or remain in G0 indefinitely[3]. Once prepared to divide, they undergo the final phase, mitosis. Mitosis is divided into several sub-phases: the prophase, prometaphase, metaphase, anaphase, and telophase. During prophase, the cell prepares for division through condensation of the chromosomes and initiation of the formation of spindle poles[6]. In the prometaphase, the nuclear envelope is broken down into small vesicles, allowing the spindle poles to attach to the chromosomes[7]. This is followed by the metaphase, wherein the chromosomes align along the midbody of the cell. In anaphase, the sister chromatids separate as they move towards the spindle poles. Throughout telophase, the chromosomes arrive at the spindle poles, and decondense as the nuclear envelope is remade in each daughter cell. Finally, the two daughter cells separate during cytokinesis as the mother cell is divided in two[6,7]. This orchestra of growth, replication, and division is governed by families of regulatory proteins that maintain cellular proliferation and genomic integrity.

1.1.1. Kinases and regulation of the cell cycle

Cyclins along with their counterparts, cyclin-dependent kinases (CDKs), are regulatory elements that control the cell cycle. The levels of CDKs within a cell remain constant throughout the various phases[8]. CDKs must associate with a cyclin in order to form an active complex capable of modifying substrates via phosphorylation, which is a post-translational modification (PTM) of a protein via the transfer of a phosphate group from one molecule to another[9]. This is generally facilitated by kinases and will be discussed in later sections in more detail. CDK-cyclin associations include the CDK4 or CDK6 complex with cyclin D, which drives the progression from G1 to S-phase via phosphorylation of the retinoblastoma tumour-suppressor protein, (pRb) (shown in middle of Fig 1). This allows the E2F transcription factors to target DNA replication genes[9,10]. Another example of CDK-cyclin activity may be observed during the transition from G2 to M-phase[11]. CDK1 activity peaks during this transition, wherein CDK1 is activated by cyclin B to phosphorylate Eg5. Eg5 is a motor protein involved in the migration of centrosomes to promote the formation of mitotic spindles[12]. The CDK1-cyclin B complex also phosphorylates condensin, a protein involved in the condensation of chromosomes during mitosis[13]. The CDK1-cyclin B complex promotes the activation of the Anaphase-Promoting Complex/Cyclosome (APC/C), an E3 ubiquitin ligase that ubiquitylates cyclin B proteins, resulting in their degradation (shown in top-left of Fig 1). The precipitous drop in cyclin B activity results in CDK inactivation, marking the return of cells to G1-phase after mitosis[14,15]. Aurora kinases (AURK) participate in centrosome assembly and chromosome alignment, while Polo-like kinases (PLKs) recruit γ-tubulin during spindle formation and cooperate with CDKs to regulate the progression throughout mitosis (shown in left of Fig 1)[16,17]. The present study will focus on a member of the NIMA-related kinases (NEK), NEK9. Dysregulation of NEK9 may cause the transformation of infected cells, delay the cell cycle and in extreme cases, induce apoptosis. The disruption of the ebb and flow of this network, unless immediately addressed, may lead to aberrant cell growth and the development of cancer.

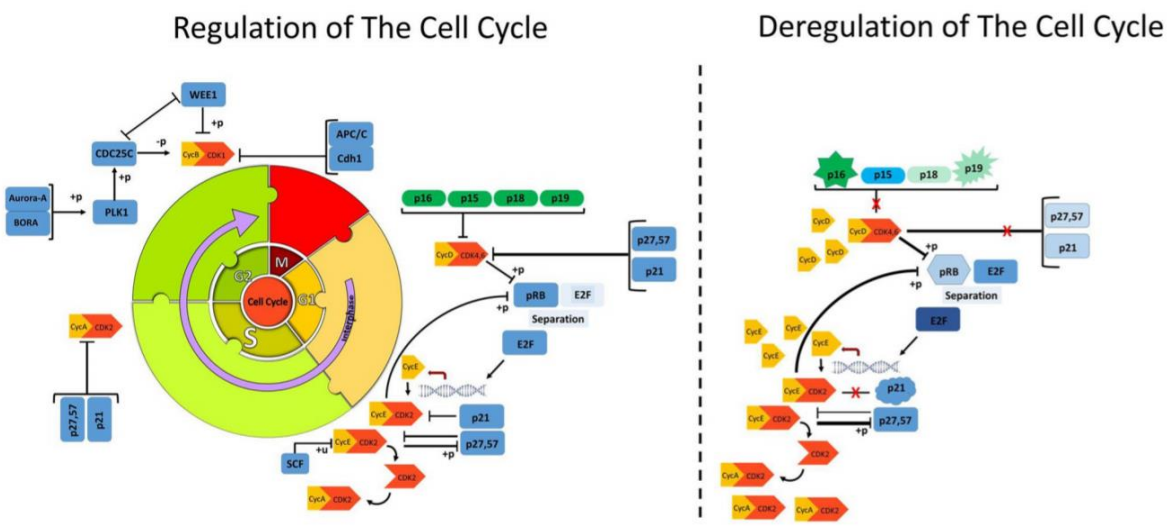

Fig 1. Regulation of the cell cycle

Overview of the various regulatory elements that govern the cell cycle. Obtained from Caglar and Avci, 2020[18].

1.2. Cancer

Cancer development is a consequence of dysregulating normal cellular processes. Normal cells that have undergone transformation may promote the formation of tumours, also known as tumourigensis. Communities of cancerous cells may metastasize into other locations inside the body. According to the landmark paper published by Douglas Hanahan and Robert Weinberg in 2002, there are six hallmarks that define and are shared by all types of cancers[19,20]. These include: uncontrolled cellular growth, evasion of growth suppressors, lack of proapoptotic signals, enhancement of growth signals, metastasis and angiogenesis[19]. Within the last decade, this framework has been expanded upon. These include new traits such as the evasion of immune destruction, tumour-promoting inflammation, promotion of genome instability and mutation and deregulation of cellular energetics[20]. These characteristics enable the proliferation and evasion of cancer cells, allowing the formation of tumours and eventual dissemination into the rest of the body, and are often preceded by the expression of oncogenes.

1.2.1. Oncogenes

Oncogenes are genes that promote oncogenesis, or the transformation of normal cells into cancerous cells. These are elements that are involved in driving cell growth, proliferation, and survival. They may be identified based on irregular expression patterns, or the presence of a gain/loss-of-function mutation which may lead to oncogenesis[21]. The first oncogene discovered was v-*src*, or Rous sarcoma virus (RSV) transforming gene in 1970[22,23]. Since then, several viral oncogenes have been examined, such as the large T antigen from the SV40 (simian vacuolating virus 40), the *E6* and *E7* from the human papillomavirus (HPV) and *E1A* from human adenovirus (HAdV)[24]. Oncogenes may also originate from within the cell, independent of pathogens.

A proto-oncogene is functionally normal under regular conditions but may be converted into an oncogene due to a mutagenic event[25,26]. This may occur through an internal spontaneous mutation that is undetected by "watchdog" systems within a cell's tumour suppressing pathway or by an external force, such as UV radiation, chemicals, or pathogenic agents[27–29]. The transformation of a proto-oncogene into an oncogene is marked with deregulated expression as mentioned above. If cells harbouring genetic mutations proceed unchecked towards mitosis and complete replication, the downstream effect may be the accumulation of abnormal cells and subsequent formation of tumours. Another avenue of transmission is brought about by genetic

inheritance from familial lineages[30]. The immune system is typically able to facilitate the removal of damaged cells[31]. However, in the case of congenital disorders stemming from inherited oncogenes, the immune system may be compromised and unable to remove aforementioned communities as depicted in Fig. 2.

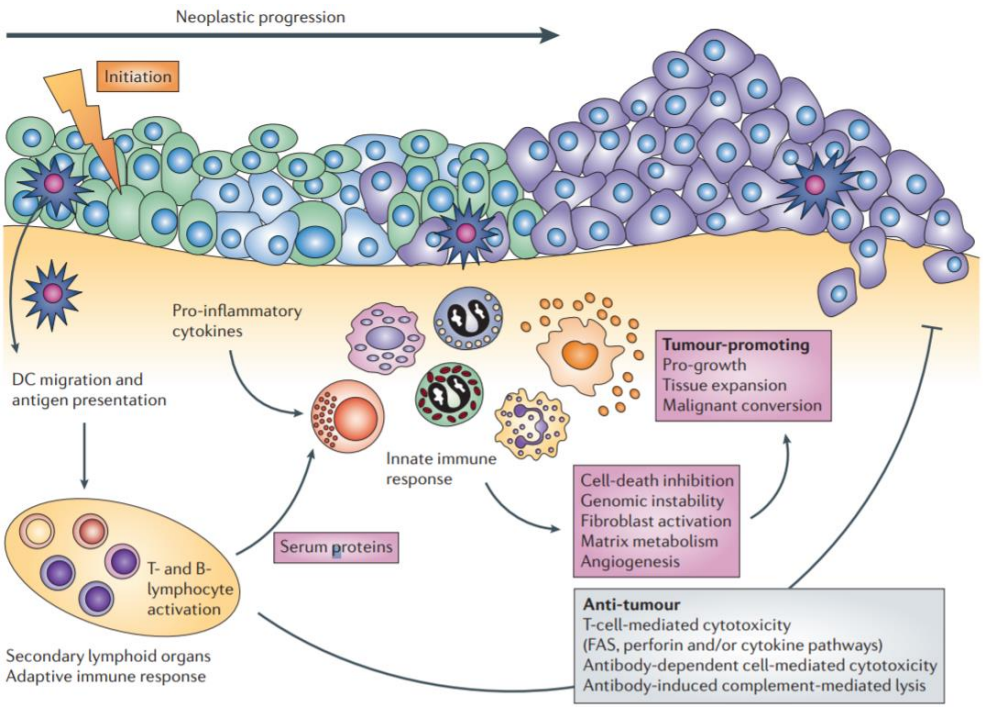

Fig. 2. Immune response to cancer cells

Overview of the immune response against development of cancer cells. Obtained from De Visser, Eichten, and Coussens, 2006[31].

1.2.2. Oncogenesis

A common misconception is that a single spontaneous occurrence and expression of an oncogene is enough to promote tumourigenesis. While an oncogene may initiate the domino effect that will eventually lead to unregulated neoplasticity, it is now understood that for efficient progression of tumourigenesis, several oncogenes must be activated[19,20]. The cascade, wherein expression of one oncogene may give rise to another oncogene to form tumours is best exemplified by the classic oncogene; breast cancer type 1 susceptibility protein (BRCA1)[32,33]. Dysregulation of this gene is strongly associated with high-risk patients for breast and ovarian cancers. Normally, BRCA1 acts as a tumour suppressor protein that participates in checkpoint activation and DNA repair by interacting with other DNA damage response (DDR) elements such as the breast cancer susceptibility protein 2 (BRCA2), or tumor protein p53 (p53)[34]. BRCA2 participates in the homologous repair (HR) of double-stranded breaks in DNA[35]. On the other hand, tumour-protein 53 (TP53, or p53) acts as a trans-activator of tumour suppressor genes[36]. In 50% of human cancers, p53 possesses mutations rendering it unable to inhibit the uncontrolled proliferation promoted by the listed oncogenes[33,37]. Oncogenic mutations may lead to the escape of a progenitor cell from the tumour-suppressing network, thus giving rise to a community of aberrant cells[27]. Common traits of neoplasms include an abnormal number of chromosomes (aneuploidy), irregular and/or amplified expression of specific oncogenes or the expression of mutant forms of tumour suppressor proteins that prevent induction of the DDR or cell cycle checkpoint pathways[19]. As a focal point in these roadblocks, p53 operates to prevent mutations that may lead to aberrant cell replication[38]. For example, it is highly expressed in spermatocytes (tetraploid cells) and initiates G1 arrest in cells experiencing cytokinesis failure, whereas those deficient for p53 proceed towards mitotic completion[39]. Past this point, the error-prone cell is examined by tumour-suppressor systems monitoring for replication stress, proapoptotic signals, pro-senescence signals and initiation of proper spindle formation. Abnormal expression of these signals may indicate the dysregulated expression of an oncogene[38–40].

1.2.3. Tumour suppressors

Tumour suppression pathways are responsible for maintaining the genomic integrity of the cell. Genes related to these networks participate in DNA repair, cell cycle arrest, induction of senescence or activation of programmed cell death[41]. Despite the harsh outcomes, the activation

of apoptotic or senescence programs is necessary to prevent the escape of cells harbouring mutations that may replicate and give rise to cancer communities[37]. For example, cells exposed to ionizing radiation may be subject to double stranded breaks (DSBs) in their DNA. In response, poly (ADP-ribose) polymerase (PARP) and DNA protein kinase (DNA-PK) are recruited to DSBs to prevent further damage[42]. PARP (PARP1 and PARP2) binds to DNA breaks whilst repair enzymes are recruited to the affected area[43]. DNA-PK is composed of three subunits: Ku70, Ku80 and DNA-PKcs. In the case of a DSB, a heterodimer consisting of Ku70 and Ku80 recruits the DNA-PK complex unto damaged DNA. DNA-PKcs promotes the formation of a DNA-repair complex involved in non-homologous end joining (NHEJ)[44]. p53 activation follows thereafter and induces the expression of downstream genes responsible for apoptosis in case the damage to DNA is irrepairable[42]. However, apoptosis is an energy-demanding process, and in nutrient-deprived environments, the cell may instead opt to undergo senescence. DNA repair enzymes such as ATM Kinase, Mre 11, Rad 50, and Nbs1 are recruited to sites of damage[45]. In this scenario, p53 levels are enhanced and activate CDKN1A (p21), which leads to cell cycle arrest. p21 inhibits DNA replication by binding to Proliferating Cell Nuclear Antigen (PCNA), a DNA replication factor, and preventing its interaction with DNA pol-δ[46]. Prolonged expression of p21 may lead to senescence[47]. Both of these responses highlight a critical component of the tumour suppression network, the p53 protein.

1.2.4. p53

p53 is a central figure in the cell's defence against uncontrolled neoplasticity and oncogenesis[37]. It was first discovered as a cellular protein that was capable of binding to the simian virus 40 large T antigen (SV40) in virus-mediated transformed cells[48]. p53 is 53 kDa and is composed of several domains including: two N-terminal transactivating domains (TAD1, TAD2), which regulate the expression of target genes, followed by a proline-rich domain (PRD), which acts as a protein-protein interaction domain. Next is the central core domain that acts as the DNA-binding site and the C-terminus, which includes the nuclear localization signal (NLS) and an oligomerization domain, responsible for protein-protein interactions[37,48].

1.2.5. p53 Function

The main function of p53 is to react to cellular stress, which may be induced through hypoxia, DNA damage, oncogene activation or nutrient deprivation[49]. Under regular conditions, p53 will prevent replication, and determine the appropriate action through cellular signaling regardless of the source of cellular stress directing the course of the cell's fate[36]. Activated p53 will form tetramers that bind to site-specific p53-target promoter of the genes. This stimulates the recruitment of transcription factors such as p300 and CBP (CREB-binding protein) which promote the expression of the target gene[36,37]. This dynamic nature is best described by Colleen A. Brady[37]: "The exact cell fate specified by p53 activation is dictated by cell type, environmental milieu and the nature of the stress". Cellular arrest may be induced by the expression p21, GADD45A, PCNA or 14-3-3sigma proteins[36]. GADD45A is responsible for arresting the cell cycle and promoting DNA damage repair[50]. 14-3-3σ acts to stabilize p53 expression and DNA interaction, and participates in growth arrest by inhibiting CDC25C activity[38]. Disruption of p53 function, through mutation, may result in deregulation of downstream activities.

1.2.6. p53 Disruption

The discovery of p53 as a central factor in tumour suppressor pathways has made it a prime target for oncogenic research. Due to the frequency of mutant p53 in human cancers, the consequence of these mutations on downstream processes is intensely studied. A method of studying p53 is to disrupt its function via knockdown (KD) or knockout (KO) through mutation or treatment with inhibitors[51]. Mice generated with p53 mutations ($p53^{-/-}$) developed tumours within the first 10 months as compared to a control litter ($p53^{+/+}$) which did not exhibit tumours 18 months into the study. Additionally, they found that animal cells exhibiting $p53^{-/-}$ mutations were less likely to undergo apoptosis in presence of DNA-damaging agents[52]. This was supported by another group that claimed thymocytes obtained from p53-knockout mice were resistant to γ-radiation[53]. These results reinforce the role of p53 in promoting apoptosis in presence of DNA damage, thereby preventing transformation. An independent study found that MEF (mouse embryonic fibroblast) cells infected with a retrovirus that expressed E1A and RAS proteins to promote transformation were less likely to form foci and instead, undergo senescence when p53 is present[54]. The efficacy of chemotherapeutic drugs also seems to vary based on the presence of wild type p53. Studies involving Adriamycin, a DNA-intercalating agent used for the treatment of cancer, has shown that

the depletion of p53 enhanced the sensitivity of transformed cells to the effects of the drug, as compared to cells with functional p53. On the other hand, the same cells lacking p53 were resistant to Fluorouracil, a drug that inhibits the synthesis of the pyrimidine thymidylate (dTMP), but not cells with p53[55]. Treatment of glioblastoma cells with SN-38, a DNA topoisomerase I inhibitor, also resulted differently based on presence of p53. Cells with p53 progressed towards senescence, whilst their counterparts were pushed towards apoptosis[56]. Each of these groups posited that the disruption of p53 resulted in the abnormal behavior of cells. The source of DNA-damage, the biology of the chosen cell or tissue and the type of p53 mutation are all important factors when considering the outcome of the cell following treatment.

1.3. Hypoxia

Hypoxia in the context of tumour microenvironments will be the focus of this section of the literature review. Hypoxia is used to describe the state of cells or tissues that are deficient for oxygen[57]. Extended periods of hypoxia may promote genomic instability in cells, resulting from DNA replication errors[57]. Under these conditions, Hypoxia Inducible Factor (HIF) genes are activated to prevent the MDM2-mediated ubiquitination of p53 amongst other functions[58]. Stabilization of p53 in the presence of DNA damage leads to cell cycle arrest, or apoptosis of cells experiencing hypoxia[59]. However, it is worth noting that HIF genes also promote the formation of new blood vessels. Also known as angiogenesis, this process is crucial to the rapid growth of a tumour, which often outpaces its supply of nutrients and oxygen[58]. Evidence has shown that cancer cells prefer to undergo aerobic glycolysis (this shift also known as the Warburg effect) to metabolize glucose, as opposed to oxidative phosphorylation even in the presence of oxygen[27]. Despite the inefficient conversion of ATP per molecule of glucose, it is proposed that aerobic glycolysis permits the proliferation of cancer cells in presence of suboptimal oxygen levels, allowing for continuous growth[60]. A switch to aerobic glycolysis is normally reserved to prevent the accumulation of ROS, and is induced by wild-type p53 through activation of antioxidant genes such as Sestrin 1, Sestrin 2 and TIGAR[37]. Ablation of p53 function through loss or mutation is associated with increased levels of ROS and DNA damage. In response, tumours have shown a capacity to induce DNA repair pathways to cope with high oxidative stress[27] while downregulating genes that govern cell death. In this manner, tumours can establish an environment to promote their growth, while simultaneously selecting against normal cells.

1.4. Apoptosis

Apoptosis, or programmed cell death, is one method initiated by damaged cells to maintain genetic integrity within a community. This response may be triggered by DNA damaging agents (e.g. UV, chemicals), reactive oxygen species (ROS) or lack of nutrients[40]. Exposure to these elements may result in the genetic destabilization through the development of mutations[40]. When cells sustain genomic damage, tumour suppression pathways are activated to induce cell cycle arrest. Once the damage is mitigated and repaired, the cell cycle is restarted, and mitosis progresses as normal. Otherwise, the cell undergoes permanent arrest or apoptosis[49,53]. Apoptosis is induced by p53 through two different means: The first method involves the activation of factors involved in stimulating *Fas*-related genes (FS-7-associated surface antigen) and death receptors found on the extracellular surface of the cell[61]. Upon binding of a Fas-ligand, the Fas Receptor (FasR) initiates the formation of the Death Inducing Signaling Complex (DISC) and the extrinsic apoptotic pathway[20]. The second method is through transactivation of proapoptotic factors from the BCL-2 family of proteins.

1.4.1. BCL-2 family

The BCL-2 family of proteins share BCL-2 (B-cell lymphoma 2) domains and consists of three types of members: proapoptotic, antiapoptotic and BCL-homology 3 (BH3)-only proteins. Proapoptotic members include BCL-2-like protein 4 (BAX) and BCL-2 homologous antagonist killer (BAK). Oligomerization of these two proteins leads to the formation of pores in the outer mitochondrial membrane[38,62]. This results in the release of cytochrome C into the cytoplasm and the induction of caspase-mediated apoptosis[62]. p53 can directly activate the proapoptotic protein, BAX, while suppressing the expression of the antiapoptotic BCL-2 protein[63,64]. The second group involves the antiapoptotic BCL-2, BCL-xL, MCL-1 and A1 proteins[65]. These members promote survival by binding BAX and BAK along the BH3 domain, thereby preventing the oligomerization of the proapoptotic enzymes[62]. The last group is reserved for proteins such as BCL-2-associated death promoter (BAD), p53 Upregulated Modulator of Apoptosis (*PUMA*) or Immediate-Early-Response Protein APR (*NOXA*)[66]. These effector proteins lack BH1 and BH2 domains, and only share the BH3 domain with other BCL-2 family members. BH3-only proteins bind to the BH1-BH2-BH3 groove of antiapoptotic members such as BCL-2 or BCL-xL, to prevent the their

interaction with proapoptotic counterparts[65]. BAX and BAK are then free to push the cell towards apoptosis[62,67]. Induction of this pore-forming event is achieved by recruiting transcriptional coactivators p300, in conjunction with JMY to enhance p53-mediated expression of proapoptotic factors such as BAX[36,68]. Another group involved in the apoptotic process are the members of the caspase family of proteins.

1.4.2. Caspases

Caspase-mediated apoptosis involves a group of proapoptotic proteins known as caspases. In all, there are 7 known members that include initiator caspases consisting of Caspase-2, Caspase-8, Caspase-9, and Caspase-10, as well as executioner or 'effector' caspases: Caspase-3, Caspase-6, and Caspase-7[39,40,62,69]. There are two distinct types of apoptosis that may be activated once initiator caspases are activated through dimerization: intrinsic or extrinsic (Fig. 3)[70]. Intrinsic apoptosis involves the formation of the apoptosome under cellular stress, wherein Caspase-9 is recruited by a APAF-1 and cytochrome C[40]. This leads to the subsequent activation of executioner caspases and the induction of apoptosis[70]. Extrinsic apoptosis involves the formation of the DISC following stimulation of the extracellular FasR. The DISC activates the initiator caspase-8 and resulting in the activation of executioner caspases[20]. In both cases, the activation of the executioner caspases is an irreversible event that eventually leads to cell death.

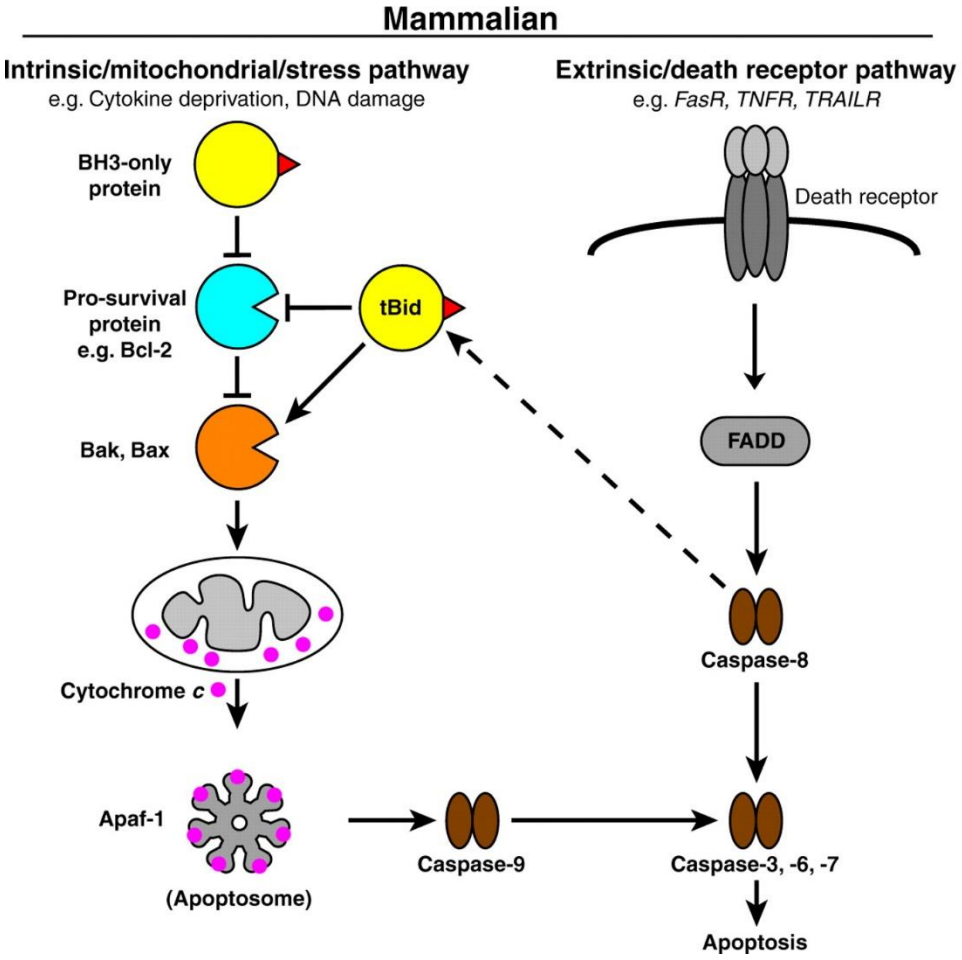

Fig. 3. Apoptotic induction in mammalian cells

Overview of intrinsic- and extrinsic-mediated death pathways in mammalian cells. Modified from Dewson and Kluck, 2009[71].

1.4.3. Secondary Necrosis

Programmed cell death is sequentially followed by one of two events: advanced apoptosis or secondary necrosis. Advanced apoptosis involves the presentation of molecules and receptors known as "consumption" signals to attract "scavengers" or phagocytic cells to remove cells undergoing apoptosis or dead cells[69]. Consumption signals are glycoproteins that are presented on the outer membrane to attract scavenger cells. These include macrophages, but eosinophils, neutrophils and dendritic cells may participate in situations wherein the apoptotic population (in case of mass necrosis or apoptosis on solid organs) exceed the macrophages' capacity, as in the case of hyper-inflammation[69,72,73]. Substitution may also take place if macrophages are unable to reach the location of apoptotic cells. Cellular elimination of these apoptotic and dying cells is an essential task for the maintenance of homeostasis and development of the host, otherwise the outcome of the cell may shift towards secondary necrosis.

Secondary necrosis occurs when advanced apoptosis is unable to proceed. One reason may be due to the lack of ATP available within the cell[69]. The physiological and biological shift during apoptosis (e.g. blebbing, formation of apoptotic bodies and microtubule spikes, cell shrinkage, etc) is an energy demanding process[40,69]. If a cell is not phagocytosed by a scavenger, it may undergo secondary necrosis[69]. DNA fragmentation and chromatin condensation are two features shared by apoptosis and secondary necrosis, but not with primary necrosis[40,69]. Cells undergoing secondary necrosis feature swollen cellular membranes, ultimately leading to disruption of the cell membrane. Another key difference between advanced apoptosis and secondary necrosis is the general lack of pro-inflammatory cytokines and molecules released during advanced apoptosis followed by phagocytosis. Primary and secondary necrosis lead to an inflammatory response, even when scavenger cells are present[69,72]. Studies of cell death conducted *in vitro* using cell culture must be thoroughly examined, as experiments using tissue culture may lack biological factors (e.g., scavenger cells) and as such, apoptosis is followed by secondary necrosis.

1.4.4. Senescence

Senescence is another outcome of the stress response, wherein cells undergo permanent arrest and exit the cell cycle[74]. It may be triggered by p53-mediated activation of p21 in presence of DNA damage. This is an irreversible process that includes the arrest of cells harbouring shortened telomeres or genetic mutations[49]. Nutrient deprivation or prolonged treatment with DNA

damaging agents (e.g. UV, DNA damaging chemicals, ROS) are factors that may initiate permanent arrest[75]. Common traits exhibited by cells experiencing senescence include enlargement, autophagy or the release of proinflammatory cytokines and insoluble extracellular matrix factors (ECM) that promote the arrest of surrounding communities[76,77]. Persistent stress and exposure to DNA damaging agents activate p53, which leads to expression of p21 and p16[38,78]. Studies have shown that senescence may be induced in transformed cells through overexpression of p21[38]. Enhanced levels of heterochromatin factors were found on E2F1 target genes in senescent cells, preventing the activation of DNA replication machinery[79]. The combination of these factors mediated by p53 prevent the propagation of mutated cells.

Senescence can be classified as replicative senescence or stress-mediated senescence[47]. Replicative senescence typically occurs in cultured cells following a high number of passages and is the consequence of the gradual deterioration of telomeres present along the ends of DNA[74,80]. Telomeres function to prevent damage during replication of DNA strands but degrade over time[38]. Prior to complete removal of telomeres, the DDR is triggered to initiate senescence and prevent the replication of damaged DNA[47]. Stress-mediated senescence may be triggered by various factors including heat, pH or pathogenic invaders such as Human Cytomegalovirus (HCMV) that promote the degradation of telomeres during viral replication[28,81,82]. This form of senescence is initiated by the DDR to suppress the propagation of cells harbouring mutant qualities that may promote oncogenesis[79]. The initial trigger for the two types of senescence may differ, but subsequent cascade of events remains similar. This results in the release of signaling molecules into the extracellular space which are detected by receptors of neighboring cells prompting the surrounding population to undergo permanent arrest[47]. Essential to the extrinsic and intrinsic signaling networks are a group of proteins known as kinases.

1.5. Kinases

The first kinase(s) was reported in 1954 by Burnett and Kennedy during their discovery of the phosphorylation of casein, a phosphoprotein isolated from milk. This process involved casein kinase-1 and/or casein kinase-2 in presence of Mg^{2+}, along with [γ-^{32}P]-ATP extracted from rat liver mitochondria[83,84]. As mentioned earlier, kinases are enzymes that catalyze the transfer of a phosphate group from adenosine-tri-phosphate (ATP) or a protein, to another molecule[85]. Vast networks depend on kinases to relay messages throughout the cell[86]. These cascades may be

initiated by an external stimulus, such as an extracellular ligand binding to a receptor on the cell membrane (e.g., tyrosine receptor kinase (TRK))[30]. TRKs subsequently transfer the terminal γ-phosphate group of an ATP to an acceptor molecule and passing the signal in a series of protein-protein interactions. This eventually travels into the nucleus wherein a gene will be activated in response to the primary stimulus[86]. Various types of kinases include: lipid, tyrosine and serine/threonine kinases. Lipid kinases, exemplified by the phosphatidylinositol-3 kinase (PI3K) family, play crucial roles in the signal transduction pathway involving the protein kinase B (AKT) pathway. PI3K activity, along with the AKT pathway, are frequent targets of mutation and are commonly dysregulated in tumours[87,88]. Tyrosine kinases phosphorylate the tyrosine residues on substrates, and while these events contribute less than 2% to the global protein phosphorylation events, they participate in vital cellular processes such as the epithelial growth factor receptor (EGFR) pathway[86]. Tyrosine kinases are may be found facilitating signal transduction across the cellular membrane or assisting in cell cycle regulation in the nucleus. Their counterparts, the serine/threonine kinases, phosphorylate acceptor molecules at serine and/or threonine residues and make up the majority of kinase activity within the cell[85,89]. Serine/threonine kinases have a host of functions involving signal transduction and gene regulation. For example, several prominent kinase families are involved in the cell cycle. Cyclin-dependent kinases (CDKs), Aurora kinases (AURK), Polo-like kinases (Plks) and NIMA-kinases (Nek) all play important roles in mitotic progression[90–92].

1.5.1. Kinases and Cancer

Communication throughout the cell is heavily dependent on the kinase networks, such that dysregulation of these pathways may lead to aberrant cell behavior. Kinases that are associated with cancer are often afflicted with mutations that impact expression, silencing, or gain/loss of function[93,94]. For example, elevated levels of Polo-like kinase 1 is a biomarker for breast cancer, ovarian carcinoma, colorectal carcinoma, uterine cancer and others[95]. The upregulation of cyclin D1 is a trait found in 50% of human breast cancers and has been identified in non-small-cell lung cancers, head and neck squamous cell carcinoma (HNCC), and other forms of tissue carcinomas[90]. Overexpression of Aurora Kinase A (AURK A) in patients suffering from HNCC has been found to correlate with poorer prognosis and general resistance to treatment[96]. NEK2 is elevated in several human cancers such as breast, cervical and prostate carcinomas but has not shown intrinsic

transformative properties *in vitro*[97]. The protein of interest discussed in this thesis, NEK9, belongs to the same family of kinases as NEK2.

1.5.2. Never-in-Mitosis-Gene-A

NEK9 is a serine/threonine kinase and a member of the Never-In-Mitosis-Gene-A (NIMA) family. The *NIMA* gene was the founding member of this group of kinases and was initially discovered by Ron Morris in the early 1980's during a screen of temperature sensitive mutants of *Aspergillus nidulans*. He discovered groups of mutants that were either blocked in mitosis (*bim*), or were never in mitosis (*nim*)[98]. The phosphorylation of NIMA is believed to be performed by p34 (Cdc2) and is essential for mitotic entry in *Aspergillus*[98,99]. NIMA is conserved across most eukaryotes, and orthologous proteins have been identified in *C. elegans, M. musculus* and most importantly in humans[100]. Since the initial discovery, the human NimA family has grown to 11 members. Despite differences in their length and protein domains, each member of the NimA family share a conserved sequence in their respective kinase domains[91].

1.5.3. NEK Family

The function and interaction between the members of the human NEK proteins have yet to be fully elucidated. Out of the 11 members (Fig. 4), NEK2 is the most studied and has been shown to participate in mitotic progression by assisting in microtubule organization[91,101]. NEK1 has been implicated in the DDR and apoptotic signaling[102]. NEK6 and NEK7, the two shortest members of the NEK family, are substrates of the principal subject of this thesis, NEK9. NEK6 activation leads to phosphorylation of the kinesin Eg5, which promotes mitotic spindle formation[103,104]. NEK7 phosphorylation is believed to play a role during cytokinesis and cilia development. Abrogation of NEK6 activation results in G2/M arrest, whilst expression of a kinase inactive NEK7 variant has led to arrest at the prometaphase and the induction of apoptosis[104,105]. Other members of the human NEK proteins are less understood, but have been associated in disease progression[106]. For example, NEK3 has been connected to tissue invasion and motility in a human ductal breast epithelial tumour cell line (T47D cells)[107]. NEK8 is dysregulated in primary breast tumours, and overexpression has shown to promote multi-nucleation in cells[108]. NEK8 has a RCC1 domain whose function is yet to be established[91]. Finally, NEK11 has been functionally identified to participate in the DDR through direct interaction with the dual specificity phosphatase, cell

division cycle 25A (CDC25A) leading to its degradation and the induction of mitotic arrest. A rare mutation in NEK11 that caused a loss-of-function has been identified in a family of five suffering from familial melanoma[109]. Based on these findings, there is a distinct connection between the dysregulation of these proteins and disease progression. The focus of this thesis, NEK9, does not fall far from the NEK family tree.

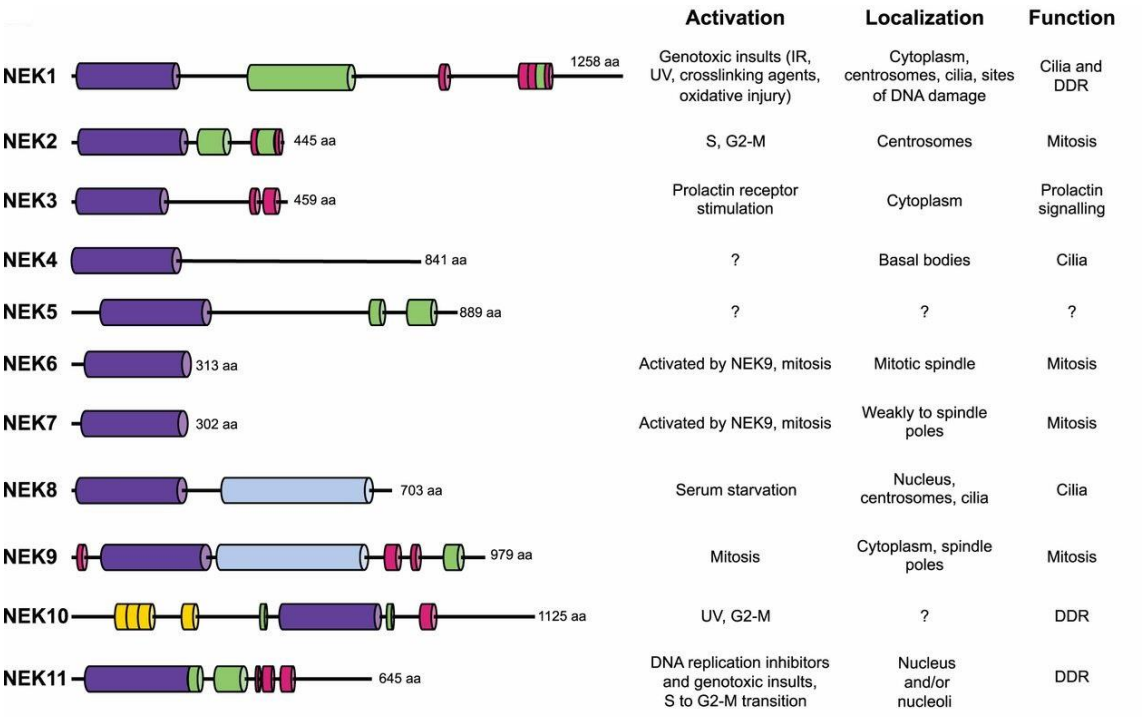

Fig. 4. Overview of NEK family members and protein domains

The human NEKs and their respective protein domains, activity, localization and know functions. Purple = conserved kinase domain, Green = coiled coil domain, Red = degradation motifs, Light blue = Regulator of Condensed Chromatin 1 (RCC1) domain, Yellow = armadillo repeats. Modified from Fry *et al*. 2012[110].

1.5.4. NEK9

NEK9 is a multifaceted protein kinase that participates in the regulation of mitotic spindle organization, chromosome condensation and alignment, as well as cytokinesis[111–113]. Sites of protein and substrate interaction have been identified across the length of NEK9 (Fig. 4). While levels of NEK9 remain constant throughout the cell cycle, its phosphorylation and activity are enhanced during mitosis[91]. The first step in NEK9 activation during prophase is carried out by an upstream kinase, CDK1 that phosphorylates Ser-869 during prophase[101]. This is followed by the phosphorylation of NEK9 at Thr-210 in its activation loop by Polo-like kinase 1 (Plk1)[101]. NEK9 is also capable of autophosphorylation[114]. The interaction between NEK9 and its substrates, NEK6 or NEK7, occur upon the onset of mitosis in a signaling cascade[115]. The conformational change in NEK7 when associated with NEK9 binding causes the release from an autoinhibitory state. The result of this signaling cascade is the phosphorylation of Histone H3[116]. Additionally, activation of NEK6 and NEK7 leads to Eg5-mediated centrosome separation during the prophase[117]. In accordance with its function in centrosome and mitotic spindle formation, NEK9 can be immunoprecipitated with γ-tubulin, along with other members of the γ-tubulin ring complex[118]. NEK9 also phosphorylates Dynein Light Chain 1 (DYNLL1), which is responsible for maintaining cytoskeletal distribution. Phosphorylation of DYNLL1 enhances its autoactivation, while reducing interaction and inhibition by NEK6[119,120]. NEK9 also promotes centrosome assembly through phosphorylation of a γ-tubulin recruiting protein, neural precursor cell expressed, developmentally down-regulated 1 (NEDD1)[121]. During the later stages of mitosis, NEK9 is re-localized towards the mid body and participates in the alignment of chromosomes[118,114]. A recent publication has shed light on NEK9 as a transcriptional repressor of p53-regulated genes during an infection with adenovirus[50]. The role of NEK9 in disease progression will be detailed below.

1.5.5. NEK9 Protein domains

Though originally identified through a screening experiment for kinases induced by IL-1, NEK9 is not activated by IL-1[101]. Never-in-mitosis A related-kinase 9, or NEK9, is amongst the largest members of the NEK family, at 979 amino acids in length[91]. It is composed of several domains as seen in Fig. 4. The N-terminus is followed by the conserved kinase domain (residues 52-308), which contains the catalytic loop responsible for NEK9's kinase activity. Next is the nuclear localization signal (NLS) which is essential for nuclear import. On the C-terminal side of

the NLS are six consecutive RCC1 (Regulator of Chromosome Condensation) repeats (residues 347-726), which are predicted to fold into a structure that resembles a seven-bladed propeller[122]. The RCC1 domain of NEK9 shares similarities with the RCC1 region found on NEK8[101]. The RCC1 is believed to act as a DNA-interacting domain, and an autoinhibitory domain for NEK9[91,123]. Mutants lacking this region show enhanced kinase activity, reinforcing of the role of RCC1 domain as a negatively regulator of kinase activity[124]. The RCC1 region of NEK9 has 27% identity and 43% similarity to another protein known as RCC1, which functions as a guanine exchange factor for Ran GTPase[125]. *In vitro* studies of the RCC1 domain of NEK9 report an interaction with Ran GTPase, mirroring the function of the RCC1 protein[124]. Downstream of the RCC1 region are nine consecutive glycine residues (residues 352-760), followed by a coiled coil domain (residues 891-940) and the C-terminus. The coiled coil domain is crucial to substrate and protein interactions and acts as a site for homodimerization during autophosphorylation. NEK9 variants with mutations in the coiled coil region exhibit reduced kinase activity[126].

1.5.6. NEK9 in disease progression

Recently there has been light cast unto NEK9 and its role in disease progression. A recessive mutation of NEK9 (R497) has been reported to cause skeletal dysplasia. Patients homozygous for the R497 mutation have reduced proliferation of their fibroblasts, attributed to loss of full length NEK9. Further to this, the R497 mutation resulted in reduced numbers of cilia found in patient fibroblasts, implicating NEK9 in fibroblast cilia maturation, thereby contributing to the development of skeletal dysplasia[100]. Mouse models that are knocked out for *Nek9* are embryonic lethal[127,128]. NEK9 was identified alongside MAP2K4 during a kinase outlier analysis in buparlisib-sensitive tumours. Buparlisib is an oral inhibitor of pan class 1 PI3K family of lipid kinases and is used in the treatment of breast cancer. Triple-negative-breast cancer tumour samples that were most resistant to buparlisib treatment had elevated levels of NEK9 and MAP2K4. Depletion of NEK9 or MAP2K4 resulted in a decreased rate of proliferation in the resistant tumour samples. This was corroborated with the reduction in levels of survivin, a central marker for many tumour networks[129]. In another study, NEK9 was upregulated in EML4-ALK positive lung cancer patients[123]. Low levels of NEK9 have also been associated with high grade invasive ductal carcinomas (IDCs) and overall larger tumour sizes[130]. NEK9 has garnered the attention of researchers as a potential target in certain cancers. Inhibition of NEK9 and CDK16 using

dabrafenib, an ATP-competitive inhibitor of the MAPK family, caused a reduction in the proliferation of *BRAF*- and *Ras*-mutant cancers *in vitro*[131]. Dabrafenib-mediated inhibition of NEK9 in *Ras*-mutant cells led to a reduction of phosphorylated CHK1, an important regulator of the DDR and cell cycle checkpoint response, and an increase in expression of p21, which is a p53-regulated gene responsible for promoting cellular arrest[132]. The same study also found the inhibition of NEK9, following treatment with dabrafenib, severely hampered the growth of p53 mutant HCT116 cells compared to p53 wild-type HCT116 cells, implicating enhanced drug sensitivity in cells lacking functional p53. In addition, the Kurioka lab published findings involving NEK9 as an essential component in the proliferation of p53-deficient transformed cells. Their study also looked into a delivery system to deplete NEK9 in tumours transplanted unto the back of female nude mice[78]. Tumours derived from p53-mutant cancer cells were noticeably smaller as compared to tumours taken from p53-wildtype cancer cells following treatment with NEK9 siRNA, suggesting NEK9 participates in the proliferation of cancer cells lacking functional p53[78].

NEK9 protein is commonly expressed in several types of lung cancer specimens, but was hardly detected in non-cancerous lung epithelial cells[123,133]. In addition to oncogenesis, the Pelka lab identified NEK9 as a prominent target of adenovirus to enable the effective growth of the virus[50]. During infection of adenovirus, NEK9 is re-localized from the cytoplasm into the nucleus, where it is recruited by a viral protein, E1A, to form a NEK9-E1A complex[134,135]. The first viral protein expressed by adenovirus during infection, Early Region 1A (E1A) is responsible for the transactivation of early viral genes as well as the transformation of the cellular environment to suit viral replication by inducing S-phase and partly suppressing the p53-tumour suppressor network[136]. E1A does not inherently possess DNA binding properties and must rely on host proteins to recruit it to p53-regulated promoters to exert transcriptional control. Previous reports have found the presence of NEK9 and E1A on the p53-regulated promoter of *GADD45α*, which participates in the prevention of abnormal DNA replication by arresting the cell cycle or pushing the cell into apoptosis[29,134]. Targets such as *GADD45α* are suppressed by adenovirus, because p53-regulated genes stand as obstacles to viral DNA replication. Inhibiting the interaction between NEK9 bindings sites on the N-terminus of E1A revealed diminished activation of p53-regulated genes, establishing the importance of NEK9 in efficient growth of adenovirus during infection by suppression of the tumour-suppressor pathways.

1.6. Adenovirus

Adenovirus is a non-enveloped, linear, double-stranded DNA virus belonging to the *Adenoviridae* family[136]. Adenoviruses have a wide range of hosts including canines, rodents, and humans amongst other species. There are 57 known serotypes that are capable of infecting humans[137]. Infection may cause mild conjunctivitis or pneumonia-like symptoms that are generally treatable, but severe respiratory failure or induction of acute respiratory distress syndrome (ARDS) may afflict young or immunocompromised individuals[138,139]. Deadlier strains in immunocompromised individuals may lead to complications and death as in the case of the 2018 outbreak of human adenovirus 7 (HAdV7) in a Detroit children's hospital[140]. Adenovirus is another model DNA-tumour virus. The E1A protein of adenovirus shares sequence homology with the HPV E7 protein[141]. The HPV E7 protein is also capable of transactivating the E2 promoter of adenovirus *in vitro*, which has led to the development of a replication-defective adenovirus. The replication of this replication-defective virus is limited to HPV-infected cells, resulting in their selective elimination[142]. Since its discovery in 1953, research on adenovirus has contributed to various aspects of molecular biology. Early mechanisms of transformation, including transcription factors and tumour suppressor components have been identified through this early work[143].

Adenovirus generally infects terminally differentiated epithelial cells, first binding to the Coxsackie/Adenovirus receptor (CAR) or CD46 and is subsequently taken up into the cell via integrin-mediated endocytosis[138]. Once inside the cell, the virus disrupts and dissolves the endosomal membrane, leading to the uncoating of the capsid and eventual release of the viral genome into the nucleus[136]. The viral genome is transported into the nucleus where RNA polymerase II (RNA pol II) initiates the transcription of viral genes[144]. This leads to the expression of the first viral protein, E1A, which activates downstream viral genes while simultaneously suppressing the host's tumour suppressing pathways[145]. The transcription of viral genes is divided based on expression before DNA replication (early) or after (late) as shown in Fig. 5[146]. Expression of early and late viral genes will be described in subsequent sections. The final phase of the infection wherein fully assembled viral particles accumulate within the host involves the lysing of the cellular membrane, then releasing and completing the generation of viral progeny[147].

1.6.1. Viral gene transcripts (Early)

Adenovirus was used as a model to study RNA splicing in the early 70s. RNA splicing is the process where sections of RNA are removed (introns) from the initial transcript in order to generate a mature transcript[148]. The regions that remain after are known as exons, and comprise the mature mRNA[149–151]. Mapping RNA transcripts of adenovirus type 2 eventually led to the discovery of the oncogenic E1A protein[145,152]. The precursor mRNA of E1A may be processed into five mature mRNA transcripts: 9S, 10S, 11S, 12S, and 13S. These are translated into their respective proteins: 55R, 171R, 217R, 243R, and 289R[153,154]. Each isoform dominates certain periods of the viral life cycle, as the expression of the 243R and 289R isoforms peak during the early stages of infection, whilst 10S slowly accumulates later in infection and the 55R isoform is generally the most abundant throughout infection[155,156].

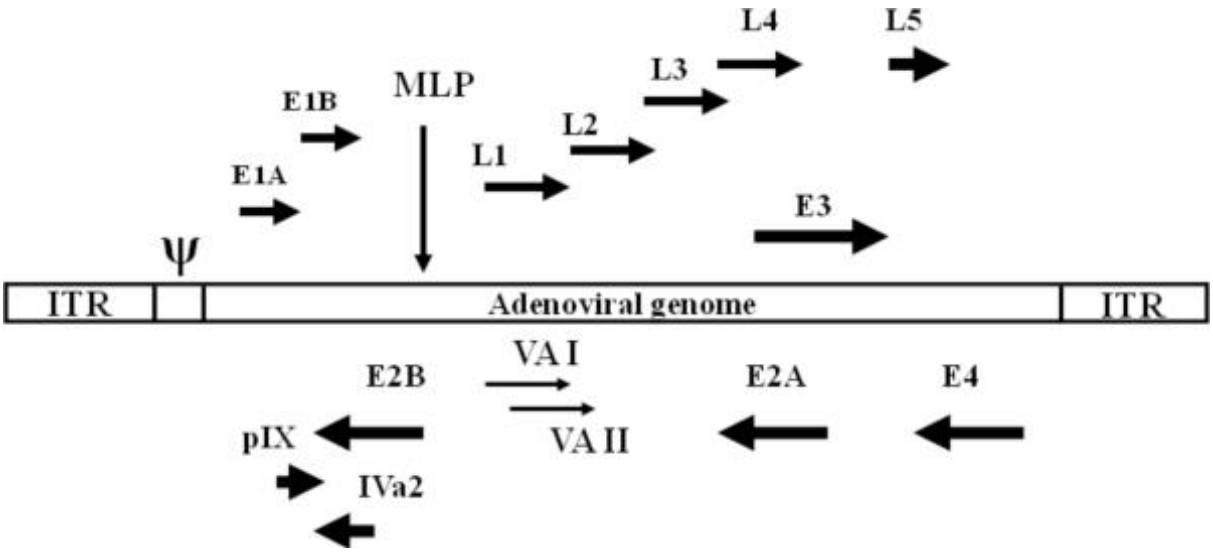

Fig. 5. Overview of human adenovirus serotype 5 transcript map

A map of the various early transcripts: E1A, E1B, E2A (DBP), E2B (pTP, DNA Pol), E3, E4 and VA I, VA II. Intermediate-early transcripts: pIX, IVa2. The Major Late Promoter (MLP) is also indicated, as with the Late transcripts: L1, L2, L3, L4, L5. Inverted terminal repeats present on either end of the genome along with the packaging (ψ) signal. Modified from Vetrini *et. al* 2010[157] and used under the Creative Commons Attributions License.

Adenovirus inhibits host defences against viral replication by preventing tumour-suppressor gene activation and induction of apoptosis. Some of these processes are mediated by the *E1B* gene. The *E1B* gene produces two different proteins: E1B-19K and E1B-55K. E1B-19K acts as a BCL-2 homologue which is able to bind and inhibit BAX, preventing BAX-mediated apoptosis[158]. E1B-55K on the other hand, directly binds and antagonizes p53, suppressing p53-dependent transcription[159]. Additionally, E1B-55K associates with another viral protein, E4-Orf6 to form an E3 ubiquitin ligase to target and degrade several cellular proteins such as p53, Bloom helicase, integrin α3, and Mre11 to promote viral replication[160–162].

Viral genome replication is facilitated by the E2 proteins. The *E2* gene encodes for three transcripts: precursor terminal protein (pTP), adenovirus DNA polymerase (AdV pol) and the DNA-binding protein (DBP). These viral proteins act in a concerted effort to initiate and facilitate DNA replication. pTP forms a heterodimer with AdV pol to form a complex that targets the origin of replication and initiates genome replication[163–165]. On the other hand, DBP stabilizes the pre-initiation complex on the origin of replication by enhancing the interaction between pTP, AdV Pol and a transcription factor, NFI (nuclear factor I)[163,166,167]. Moreover, DBP lowers the K_m for the linking of pTP to dCTP and unwinds DNA during replication in an ATP-independent manner through the formation of multimers[168].

Adenovirus employs immunomodulatory proteins in response to the host's adaptive immune response. The *E3* region is responsible for inhibiting the immune response, as well as mediating viral lysis[169]. The E3-gp-19K protein suppresses class 1 MHC antigen presentation in infected cells to prevent CTL-mediated killing of infected cells. The E3-6.7K protein is believed to associate with the E3 RID complex (receptor internalization and degradation complex) to degrade cell surface receptors such as FasR and TNFR-1 (tumour necrosis factor 1), preventing the premature lysis of infected cells[170,171].

The *E4* region of adenovirus consists of seven open reading frames (ORFs)[172,173]. The proteins that are generated in this region are responsible for the recruitment of transcription factors, regulation of protein phosphorylation, DNA replication and RNA splicing[174]. The first of these products, E4-Orf1, is believed to activate the PI3K pathway to promote cell growth and survival[175,176]. According to independent studies involving human adenovirus 9 (HAdV9), E4-Orf2 participates in oncogenesis, similar to E4-Orf1[177]. On the other hand, E4-Orf3 is responsible for the rearrangement of subnuclear structures known as PML (promyelocytic leukaemia)

oncogenic domains (PODs) in infected cells[174]. These PODs are linked to various types of proteins that include transcriptional regulators, DNA repair proteins or factors involved in cellular defence. During infection, PODs have been associated with viral replication, transformation and suppression of apoptosis and antiviral responses[178–180]. The E4-Orf4 protein binds to protein phosphatase 2A (PP2A) to downregulate viral and cellular transcription. It has also been observed to induce p53-independent apoptosis[181,182]. As previously described, E4-Orf6 associates with the viral protein E1B-55K, to form an E4 ubiquitin ligase that promotes the degradation of p53[160,161,174]. The interaction between E1A and Rb allow E4-Orf6/7 to form a complex with free E2F/DP transcription factors which leads to the induction and transcription of the *E2* promoter to promote the expression of early viral genes[183–186].

To evade detection by anti-viral processes within the host, adenovirus utilizes the virus-associated RNA I (*VAI*) and virus-associated RNA II (*VAII*) to suppress the activation of the protein kinase R (PKR)-response. Upon detection of double-stranded RNA (dsRNA), PKR is activated and phosphorylates the eukaryotic initiation factor 2 (eIF-2a) to inhibit the formation of the eIF2-GTP-Met-tRNA complex that is responsible for the initiation of protein synthesis[187]. During infection, accumulated *VAI* RNA bind and sequester PKR, preventing the phosphorylation of eIF-2a, permitting viral protein production[188,189]. Depletion of *VAI* significantly hampers viral growth, as *VAI*-mutant viruses saw a 20-fold decrease compared to wild-type[190,191]. Conversely, less is known about *VAII*. It is believed to participate in nonessential tasks during infection and may compensate for *VAI* in mutant viruses[192,193]. Despite the gap in current knowledge, *VAII* is highly conserved, and depletion of both *VAI* and *VAII* has led to a 60-fold decrease in yield as compared to wild-type[191].

1.6.2. Viral gene transcripts (Late)

Included in the late transcriptional program are the *L1 – L5* (Late) structural viral genes of adenovirus as indicated in Fig. 5. The expression of these structural genes stem from the alternative splicing of a single precursor RNA product known as the Major Late Transcription Unit (MLTU) produced from the Major Late Promoter (MLP)[194]. Early research conducted to characterize the MLTU provided insight into the temporal regulation and splicing events that produce mature mRNA transcripts of late viral genes. The *L1* gene is transcribed early during infection and produces two proteins: 52K and 55K[155]. The 52K and 55K proteins are important during packaging

of the viral genomes and capsid assembly[195]. Intermediate viral genes such as *IVa2* and *pIX* are transcribed after the activation of early genes, and before the majority of the late genes[196,197]. IVa2 is responsible for genome packing and assembly, whilst pIX functions as a cement protein to stabilize the viral capsid[197,198]. During viral genome replication, IVa2 alongside E1A and E4 Orf3, promote the expression of *L4* through an internal promoter found on the open reading frame of *L4-100K*[199,200]. This leads to the production of L4 proteins: 22K and 33K, which mediate the transition from early to late gene transcription. Once the Major Late Promoter (MLP) is activated, the transcription of the late genes commences. Compared to the L4 22K and 33K proteins, the L4 100K protein does not inherently affect the upregulation of the MLTU but instead has been shown to play a pivotal role in hexon trimer assembly[194].

Late into the infection, the major capsid proteins (MCPs) of adenovirus begin to assemble. This includes: hexon, followed by penton base (PB), and finally the fiber protein[201]. In addition to the MCPs, several cement proteins IIIa, VI, VIII, and IX, are incorporated into the viral capsid to stabilize the entire structure by adjoining the other capsid proteins to one another[202]. Inside the capsid, the viral core is composed of the viral genome, V protein, VII protein, μ protein, terminal protein (TP), and the viral protease[195]. The V and VII proteins participate in the transport of the viral core to the nucleus, while the μ protein has a role in viral chromosome condensation[203,204]. TP is the mature product of the pTP after it has been processed by the viral protease. TP is believed to act as the primer for the first round of viral replication, whilst pTP is utilized for subsequent rounds of replication, as the viral protease is not produced until late into infection[205,206]. The viral protease also plays a role during the entry of the viral genome into the nucleus. It is believed to degrade protein VI, releasing the viral DNA from its anchor during transport of the virus in the endosome. This enables the viral genome to exit the capsid once inside the nucleus[207]. All in all, the temporal expression of late viral genes from the MLTU provides an exciting avenue of research into the tight regulation exerted by adenovirus to ensure viral assembly advances smoothly. The MLTU showcases the efficient nature of adenovirus, utilizing alternative splicing once more to generate a handful of late structural transcripts from a single precursor.

1.7. Thesis goals and objectives

The primary goal of this thesis is to further our understanding of NEK9's role within the cell cycle. Previous work had characterized NEK9's function as a regulator of spindle dynamics during mitosis, but recent studies have identified NEK9 upregulated in tumour samples[118,121,208]. Furthermore, this research may contribute to future studies aiming to inhibit NEK9 to treat specific cancers. Our hypothesis was that NEK9 participates as a negative regulator to p53-target genes relating to cell cycle and apoptotic induction in transformed cells.

The first goal of this thesis was to investigate NEK9's role in cellular transformation in conjunction with the adenoviral protein, E1A. The current study is a continuation of an earlier publication from our lab that described the recruitment of NEK9 during adenovirus infection by E1A to suppress p53-regulated promoters[134]. This was the first time NEK9 had been implicated as a transcriptional regulator of p53-promoters and served as the basis of the second objective. The focus of this second objective was to characterize the interaction between NEK9, p53 and p53-regulated genes. We hypothesize that NEK9 downregulates the expression of p53-related genes through suppression of p53 promoters. Our approach aimed to answer two primary questions. First, to determine whether the suppression of p53-regulated genes by NEK9 was a by-product of adenovirus infection or an intrinsic ability to regulate tumour suppressing pathways. Second, to examine the protein domains responsible for the regulatory activity of NEK9. This would permit us to explore whether the regulatory mechanisms of NEK9 is reliant on its ability phosphorylate substrates or is due to the association with other protein domains, similar to the interaction between the RCC1 domain with RAN-GTPase[126].

Unexpectedly, utilization of these variants led to the discovery that NEK9 may participate in the induction of cell cycle arrest or apoptosis. This property is common amongst the NEK family of proteins, as other members have demonstrated participation in similar events[91,133]. The focus of the third goal of the thesis was to investigate the consequences of NEK9 dysregulation through knockdown of NEK9, or the expression of NEK9 variants. Our hypothesis is that the disruption of regular NEK9 function through depletion, or overexpression of wild-type or variants induces cell cycle arrest or apoptosis. Understanding the consequences of deregulating NEK9 in transformed cells through expression of these variants may provide insight into NEK9 as a novel target for cancer research.

As a fourth goal, a high throughput *in vivo* substrate screen was developed as a method to identify NEK9 binding partners. We hypothesized that the consensus site of known Nek9 substrates will bind to full-length wild-type Nek9, but not to kinase-inactive mutants. Optimization of this assay may yield important information regarding the proteins and pathways that are regulated by NEK9.

The final goal explored in this thesis was the chronological expression of adenoviral genes during infection. Earlier studies have explored this subject and provided critical insight into the dynamics of viral gene expression during infection[155,209]. The intention of this research was to apply digital droplet PCR technology to detect the initial activation of viral genes and quantify their relative expression throughout infection. Our working hypothesis was that the activation of early and late viral genes would be delayed in arrested IMR-90 cells infected with HAdV5, as compared to the early models using HeLa cells and HAdV2. However, we expected that the order in which the viral genes would be expressed will remain similar. This work means to supplement previous findings by probing normal human cells and provide insight using a new platform in which to investigate rare or miniscule quantities of gene copies in environmental or patient samples.

Chapter 2: Characterization of NEK9 as a transcriptional regulator of p53-mediated networks responsible for cellular arrest and induction of apoptosis in human cells

2.1. Introduction

This chapter will focus on the human cellular kinase, NEK9 and its relation to p53-regulated tumour-suppressing pathways. The expression of NEK9 seems to vary between different types of cancers. Elevated levels have been associated with lower rates of survival in patients with triple negative breast cancer, or certain melanomas[129,131]. Interestingly, enhanced expression has also been linked with low-grade breast cancers as compared to aggressive counterparts, leading to a better prognosis[130]. There does not seem to be a correlation between survivability and the expression of NEK9 in cancer patients. NEK9 is also a target of adenovirus during infection, as it is co-opted to suppress p53 activity, thereby facilitating the transformation of the cellular environment to suit viral replication[50,78,135]. Our investigation into the consequences of disrupting NEK9 in transformed cells will be detailed in the following sections.

2.2. Materials and methods

2.2.1. Antibodies

Primary and secondary antibodies used in western blot assays were diluted in Tris-Buffered Saline-Tween 20 (TBS-T) containing 5% milk (powder). Primary and secondary antibodies used in immunofluorescence assays were diluted in blocking (1% goat serum, 1% bovine serum albumin (BSA), 0.2% Tween 20 in phosphate-buffered saline (PBS) or 5% BSA, 0.2% Tween 20 in PBS).

Table 1. NEK9 Antibodies

Antibodies	Details	Use	Dilution Factor	Source	Catalogue Number
NEK9 (Commercial)	Rabbit	Primary	1:1000 (WB) 1:600 (IF)	Abcam	Ab138488
PARP	Mouse	Primary	1:1000	Millipore	AB3565
Actin	Mouse	Primary	1:1000	Abcam	Ab3280
Myc (9E10)	Mouse	Primary	1:200	In house	N/A

Alexa Fluor 594 Anti-Rabbit	Goat	Secondary	1:600	Jackson Immunoresearch	AB_2632469

2.2.2. Cell lines

HT1080 human fibrosarcoma cells, A549 human lung adenocarcinoma cells, SK-OV-3 human ovarian cancer cells, T47D triple-negative breast cancer cells, SW-480 human colon cancer cells, 293 Human embryonic kidney cells, MEF cells, IMR-90 and WI-38 human lung fibroblast cells were grown on Dulbecco's modified Eagle's medium (DMEM) (Hyclone) supplemented with either 10% or 5% fetal bovine serum and 1% streptomycin/penicillin (100 µg/mL streptomycin, 100 U/mL penicillin) (Hyclone). CHO Chinese hamster ovarian cells were grown on Ham's F-12 nutrient mixture media supplemented with 10% fetal bovine serum and 1% streptomycin/penicillin (100 µg/mL streptomycin, 100 U/mL penicillin) (Hyclone). Cell culture kept in T175 flasks (SARSTEDT) at stable temperature of 37°C at 5% CO_2.

Table 2. Cell lines

Cell line	Origin/Tissue	Status	ATCC Catalogue Number
IMR-90	Human/lung	P53+	CCL-186
WI-38	Human/lung	P53+	CCL-75
HT1080	Human/connective tissue	P53+	CCL-121
A549	Human/lung	P53+	CCL-185
SW-480	Human/colon	P53-	CCL-228
SK-OV-3	Human/Ovary: ascites	P53-	HTB-77
T47D	Human/Mammary gland; derived from metastatic site: pleural effusion	P53-	HTB-133
MEF*	Mouse/embryo	P53+	N/A

CHO**	Chinese hamster/ovary	P53+	N/A

*NEK9-TET$^{(-)}$-inducible MEF cells generously provided by Dr. Peter Pelka and gifted by Dr. Peter Whyte.

**CHO-LacO cells generously provided by Dr. AJ Berk as referenced in Hsu *et al*. 2018[210].

2.2.3. Infection

Cells were grown to 90% confluency. Cells were washed with serum-free (SF) media and the infection mixture virus volume dependent on experiment, topped to 500 µL of SF-media. Cells were rocked gently every 15 minutes for 1 h at 37°C. Subsequently, complete media (DMEM supplemented with 5% or 10% fetal bovine serum, 1% streptomycin/penicillin (100 µg/mL streptomycin, 100 U/mL penicillin) (HYCLONE (GE Life Sciences), Chicago, Illinois, United States)) was added to top up each well. Infection was carried for time points indicated per experiment and samples were harvest for processing or kept in -80°C freezer for storage.

Table 3. NEK9 Viruses

Virus	Feature
Ad-CMV	Viral expression vector with CMV promoter
Wild-type-NEK9	Viral expression vector with CMV promoter to express Myc-tagged NEK9
D194N	Viral expression vector with CMV promoter to express Myc-tagged D194N
ΔRCC1	Viral expression vector with CMV promoter to express Myc-tagged ΔRCC1

NEK9 viruses generously provided by Dr. Peter Pelka. NEK9 mutants generated as described in Pelka *et al*. 2007b[211] and inserted into adenoviral expression vectors as described in Hardy *et al*. 1997[212].

2.2.4. Titration Assay

HT1080 cells were counted using a hemocytometer and plated at 250,000 cells per well in 6-well plates (SARSTEDT). Cells were infected with 100 µL, 300 µL and 600 µL of NEK9,

D194N and ΔRCC1-expressing viruses for 24 h. Cells were harvested, lysed and processed for western blot assay (Fig. 22). Protein concentrations were normalized to 125 µg/µL and 25 µg of protein was loaded per well. Myc-tagged-NEK9, myc-tagged-D194N and myc-tagged ΔRCC1 were detected with myc (9E10) primary antibody at a dilution of 1:200 (in-house).

2.2.5. Transfection

HT1080 cells were counted using a hemocytometer and plated at 250,000 cells per well in 6-well plates (SARSTEDT). Cells were transfected by adding a master mix (2 µg of p53-reporter plasmid DNA, 2 µg of protein expressing plasmid DNA, 20 µL polyethylenimine (PEI) (1 mg/mL)[213]. Cells were treated for 24 h to allow uptake and expression of proteins. Samples were harvested at 24 h and kept in -80°C freezer.

Table 4. NEK9 Plasmids

PPB	Name	Features
1	pCAN-Myc	Mammalian expression vector with an N-terminal myc tag and Neomycin resistance marker[a]
46	pCDNA3-E1A 13S	Mammalian expression vector for 13S isoform of wild-type-E1A
207	pCAN-Myc-NEK9	Mammalian expression vector with an N-terminal myc-tagged NEK9 and Neomycin resistance marker [b]
417	pTRE-ΔRCC1	Expression vector of myc-tagged ΔRCC1 mutant and ampicillin resistance marker [c]
470	pG13-luc wt p53 binding sites	Luciferase reporter with p53-binding sites (http://www.addgene.org/16442/)
471	pcDNA3 p53 wt	p53 expressing plasmid (http://www.addgene.org/69003/)

[a]Generously provided by Dr. Peter Pelka, generated in Dr. Peter Whyte's lab[214].

[b]Generously provided by Dr. Peter Pelka, generated in Dr. Peter Whyte's lab[215].

[c]Generously provided by Dr. Peter Pelka.

2.2.6. Induction of NEK9 in MEF-NEK9-inducible cells

MEF cells inducible for NEK9 expression were grown to 90% confluency in Tet+ (DMEM supplanted with 5% fetal bovine serum, 10 µL Doxycycline (100 mg/mL) (Sigma-Aldrich, St. Louis, Missouri, United States), 100 µg/mL streptomycin/penicillin. To induce NEK9 expression, MEF cells were washed 3 times in serum-free media (SF-media) and incubated in SF-media for 3 h. Cells then were infected with *dl*309 and subsequently grown in Tet$^-$ media (DMEM supplanted with 5% anti-biotic special fetal bovine serum). MEF cells generously provided by Dr. Peter Pelka, and generated as described previously[215].

2.2.7. Knockdown of NEK9

Cells were depleted for NEK9 by directly adding a knockdown master mix (500 uL serum-free DMEM media, 5 µL siLentFect Lipid Reagent for RNAi (1 mg/mL) (BioRad), 0.6 µL *Nek9* siRNA (50 µM) (Thermofisher) or 0.6 µL Control Negative siRNA (50 µM) (Thermofisher). Cells were treated with siRNA for 24 h or 72 h for NEK9 knockdown. Samples were harvested at 24 or 72 h and kept in 15-mL conical tubes (SARSTEDT) and kept in -80°C freezer.

2.2.8. EdU Incorporation Assay

2.2.8.1 Serum induction

IMR-90 cells were grown until 100% confluent on Lab Tek II 4- Chamber Slides (Thermo-Fisher). NEK9 knockdown and control knockdown were carried out by adding *Nek9* siRNA (50 µM) or Control Negative siRNA (50 µM) directly to cells (both at 5 µg/mL) and topped with conditioned media (media harvested from cultured cells) for 72 h to allow for cellular arrest. Following treatment and arrest, cells were pulsed with EdU in the Chamber Slides for 1 h as per manufacturer's specifications using the Click-It EdU labeling kit for microscopy (Life Technologies). After labeling with EdU, cells were fixed in 3.7% formaldehyde, stained for EdU using the Click-It kit with Alexa Fluor 488, and labelled for NEK9 using NEK9 commercial antibody (dilution 1:600) (ab138488) (Abcam) and AlexaFluor-594 conjugated secondary antibody (dilution 1:600) (AB_2632469) (Jackson Immunoresearch, West Grove, Pennsylvania,

United States). Cells were visualized using ImageXpress Micro 4 live cell imager (Molecular Devices) and analyzed using MetaXpress software package version 7 (Molecular Devices).

2.2.8.2 NEK9 Overexpression

HT1080 cells were grown until 90% confluent on Lab Tek II 4- Chamber Slides (Thermo-Fisher). Knockdown of NEK9 and a control knockdown were carried out by adding *Nek9* siRNA (50 µM) or Control Negative siRNA (50 µM) directly to cells (both at 5 µg/mL) for 24 h. Infections were carried out by adding Ad-CMV, NEK9, D194N and ΔRCC1 viruses directly onto cells at a MOI of 10 for 24 h. Following knockdown and infection, cells were pulsed with EdU in the Chamber Slides for 1 h as per manufacturer's specifications using the Click-It EdU labeling kit for microscopy (Life Technologies). After labeling with EdU, cells were fixed in 3.7% formaldehyde, stained for EdU using the Click-It kit with Alexa Fluor 488, and labelled for NEK9 using Myc monoclonal antibody. Cells were visualized using ImageXpress Micro 4 live cell imager (Molecular Devices) and analyzed using MetaXpress software package (Molecular Devices).

2.2.9. Promoter Luciferase Assays

HT1080 cells were plated onto 6-well plates and grown to 90% confluency. Cells were then transfected by directly adding 2 µg of p53-reporter plasmid (PPB 471) and 2 µg of the p53 (PPB 472), NEK9 (PPB 207), 13S E1A (PPB 46) or ΔRCC1 (PPB 417) expressing plasmid alongside 20 µL polyethylenimine (PEI) (1 mg/mL) to the cells (Table 4). Cells were harvested 24 h post transfection and 300 µL 5x Cell Culture Lysis Buffer (Promega E397A) was used to lyse samples in microfuge tubes. Samples were centrifuged for 10 minutes at 13,000 rpm (ThermoScientific, Waltham, Massachusetts, United States) (Sorvall Lynx 4000 Centrifuge). 50 µL of lysate was pipetted into white opaque bottom detection plates (ThermoScientific). Plates were placed immediately in the SpectraMax ID3 (Molecular Devices) and 50 µL of Luciferase Substrate (Promega E151A) was injected into each well prior to the detection of signal. Fluorescence emission was measured using the SoftMax Pro 7 software package and promoter activity was based on the fold change difference between mock cells (no reporter) against cells transfected with the p53-reporter plasmid.

2.2.10. Real-time gene expression analysis

A549, HT1080, SK-OV-3 and SW-480 cells were counted using a hemocytometer and plated in 6-well plates (250,000 cells per well). Knockdown of NEK9 and control knockdown were carried out when cells reached 90% confluency by adding *Nek9* siRNA (50 µM) or Control Negative siRNA (50 µM) directly to cells (both at 5 µg/mL) for 24 h. After knockdown, cells lysed and total RNA was extracted using the TRIzol Reagent (Sigma) or NucleoZOL (Machery Nagel, Düren, Germany). Cells were placed into microfuge tubes and 500 µL of NucleoZOL was added per sample. Subsequently, 100 µL of NucleoZOL of RNA-free water was added to the sample, shook vigorously for 15 seconds and incubated for 15 minutes at room temperature. Samples were centrifuged at 12,000 x g for 15 minutes at 4°C. The supernatant (500-600 µL) was transferred into a fresh tube and kept on ice. The RNA was precipitated by adding 250 µL isopropanol per 500 µL of supernatant, invert and incubate for 10 minutes on ice. The samples were centrifuged at 4°C for 10 minutes. The supernatant was aspirated, leaving a small white pellet of RNA. The pellet was washed with 500 µL of ethanol by inversion at room temperature. The samples were spun at 12,000 x g for 5 minutes to settle pellet. The ethanol was aspirated, leaving the RNA pellet. The samples were placed in the biosafety cabinet for 2-5 minutes to allow the ethanol to evaporate. Once the pellet became clear, 50 µL of double-distilled syringe-filtered (0.22 µm filter) H_2O (ddH_2O) was added per sample. The RNA pellet was allowed to dissolve into ddH_2O on ice for 30 minutes. Once dissolved, 6.6 uL of DNAse I master mix (1 µL DNAse 1 (2,000 units/mL) per 5.6 µL DNAse 1 Buffer (10X reaction buffer)) (New England Biolabs, Ipswich, Massachusetts, United States) was pipetted per sample, vortexed vigorously and centrifuged briefly to spin down sample. The samples were placed in a 37 C water bath for 30 minutes. Afterwards, 0.7 µL of EDTA (Stock 0.5 M EDTA, pH 8) was added to each sample, vortexed and spun down. The samples were placed into a 75°C heat block for 10 minutes, and subsequently placed on ice. Complementary DNA (cDNA) was generated by adding total RNA (up to 2.5 µg) with 2 µL of SuperScript VILO Reverse Transcriptase Master Mix (Thermofisher) for a total volume of 10 µL. The samples were vortex, spun down and incubated at 42 C for 1 h. The samples were diluted by adding 90 µL of ddH_2O per tube and kept on ice. Real-time expression analysis was conducted using the BioRad CFX96 real-time thermocycler alongside the SYBR Select Master Mix (Applied Biosystems, Foster city, California, United States) (Reaction steps detailed below). Gene expression was normalized

relative to the percentage of GAPDH (glyceraldehyde 3-phosphate dehydrogenase) mRNA. Data was analyzed using the CFX Maestro version 1.1 (BioRad) software package.

Table 5. Reaction steps for PCR (CFX96 – SYBR Select Master Mix)

Steps	Temperature	Duration	Cycles
Uracil-N-Glycosylase	50°C	2 minutes	Hold
SYBER Select Master Mix activation	95°C	2 minutes	Hold
Denature	95°C	15 seconds	40x
Anneal/Extend	60°C	1 minute	40x
End	4°C	-	Hold

Reaction steps as described from SYBR Select Master Mix manual[216].

Table 6. Nek9 Primers

Gene	**Forward (5'-3')**	**Reverse (3'-5')**
Human GAPDH	GAGTCAACGGATTTGGTCGT	TTGATTTTGGAGGGATCTCG
mGADD45A	GCTCAACGTAGACCCCGATA	GTTCGTCACCAGCACACAGT
PIG3	GCTTCAAATGGCAGAAAAGC	AACCCATCGACCATCAAGAG
PUMA	AGCAGGGCAGGAAGTAACAA	GCTGCTGCTCCTCTTGTCTC
P21	GGAAGACCATGTGGACCTGT	AAGATGTAGAGCGGGCCTTT
P38a	TGACTCAGATGCCGAAGATG	ATCATAAGGATCGGCCACTG
MDM2	GGTGGGAGTGATCAAAAGGA	GTGGCGTTTTCTTTGTCGTT
BCL-2	ACAGGGTACGATAACCGGGA	CATCCCAGCCTCCGTTATCC
BCL-xL	TCCCCATGGCAGCAGTAAAG	GGGCTGCATGTAGTGGTTCT
BAX	CATGAAGACAGGGGCCCTTT	GTCTTGGATCCAGCCCAACA
BAD	AGACTCCAGCTCTGCAGAGA	CCAAAGGAGACAGCACGGAT

2.2.11. Western blot

SK-OV-3 cells were grown to 90% confluency and infected at 24, 48 and 72 h with Ad-CMV, wild-type-NEK9, D194N and ΔRCC1 expressing viruses a MOI of 10. Samples were scraped into Eppendorf tubes and lysed using NP-40 lysis buffer (150 mM NaCl, 1% NP-40, 50

mM Tris-Cl at 8 pH)[217]. Samples were centrifuged at 13,000 RPM (Sorvall Lynx 4000 centrifuge) for 10 minutes at 4°C. A Bradford assay was conducted to determine and normalize protein concentrations. Supernatant was transferred into a separate microfuge tube and 2X Sample Buffer (2 mL Tris (1M, pH 6.8), 4.6 mL glycerol (50% w/v), 1.6 mL SDS (10% w/v), 0.4 mL bromphenol blue (0.5% w/v), 0.4 mL β -mercaptoethanol) was added[218]. Samples were boiled for 10 minutes at 100°C. Samples were placed in an ice bucket to cool and was subsequently ran on SDS-PAGE Gel. Once separated, the proteins were transferred unto PDVF membrane. The PVDF membrane was placed into a container with Blocking Buffer (5% skim milk powder dissolved in TBS-T solution) and gently rocked for 1 h. Actin (dilution 1:1000), Myc (9E10) (dilution 1:200), NEK9 (commercial) (dilution 1:1000) or PARP (dilution 1:1000) primary antibody was applied (Primary antibody diluted in 3% BSA solution, or Blocking Buffer (5% skim milk diluted in TBS solution)) overnight, rocking at 4 C. The primary antibody was removed, and the membrane was washed using ~30 mL of TBS-T solution (100 mL TBS solution, 900 mL of ddH_2O, 1 mL Tween 20) and rocked at room temperature for 10 minutes. This wash step was repeated three times. After the third wash, a secondary antibody is applied to the membrane for 30 minutes, gently rocking at room temperature. Subsequently, the membrane is washed several times with TBS-T. Immobilon Forte Western HRP Substrate (Horseradish peroxidase) (Millipore, Burlington, Massachusetts, United States) is applied to the membrane for 5 minutes and film is used to detect protein bands.

2.2.12. Flow cytometry

SW-480 cells were grown to 90% confluency in 10-cm plates (SARSTEDT). Infection was carried out by directly adding Ad-CMV (150 µL), NEK9 (300 µL), D194N (300µL) and ΔRCC1 (150 µL) to the cells for 24, 48, and 72 h (infection volumes based on a titration assay). Cells were washed with PBS and harvested into 50-mL conical tube (SARSTEDT). Cells were spun down at 3,000 RPM (Sorvall Lynx 4000 centrifuge) and washed with PBS. Cells were spun down again and cold ethanol (70% (v/v) solution) was administered to fix cells for 30 minutes. Cells were washed twice with PBS and spun down prior to addition of propidium iodide (1 mg/mL (Thermo Fisher)). Cells were kept at 4°C overnight or kept on ice for transport.

Stained cells were placed in Beckman Coulter CytoFlex LX Digital Flow Cytometry Analyzer 4 Laser System (Laser: 488 nm, Mirror/Filter: 610/20 BP). Initial gating method was based on forward (FSC) vs. side (SSC) plot to exclude cell debris or aggregated cells. Second

gating was based on forward scatter height (FSCH) vs. forward scatter area (FSCA) to exclude doublet cells. Final population of cells was analyzed for cell cycle distribution based on size, granularity and DNA content using the cell-cycle analysis software package FlowJo version 10.7.1 (BD Biosciences, San Jose, California, United States). Ancestry (gated populations) of cell cycle analysis may be found in *5.3. Supplementary Data*.

2.2.13. Scratch Assay

HT1080 cells, SK-OV-3 cells, A549 cells and T47D cells were counted using a hemocytometer, plated at 250,000 cells and grown to 90% confluency in 6-well plates (SARSTEDT). Cells were depleted for NEK9 by directly adding *Nek9* siRNA (50 µM) or Negative Control siRNA (50 µM) for 24 h. Cells were infected with Ad-CMV, NEK9, D194N or ΔRCC1 at a MOI of 20 for 24 h. After infection, a pipette tip was used to administer a horizontal and vertical scratch across the monolayer of cells. A breathable film (Breathe-Easy sealing membrane) (Sigma-Aldrich, St. Louis, Missouri, United States) was fixed upon the plate and subsequently placed into the live-cell imager (ImageXpress Micro 4) (Molecular Devices) set to 37°C and pumped with air (78.09% Nitrogen, 20.95% Oxygen, 0.93% Argon, 0.04% Carbon Dioxide). The scratches were monitored for 24, 48 and 72 h and time lapse videos were taken. Images and videos were analyzed using the MetaXpress version 6.6 software package (Molecular Devices).

2.2.14. Propidium Iodide Staining

HT1080 cells, SK-OV-3 cells, A549 cells, T47D cells and SW-480 cells were grown to 90% confluency in 6-well and 96-well plates. Cells were depleted for NEK9 by adding *Nek9* siRNA (50 µM) or Negative Control siRNA (50 µM) directly to cells for 24, or 72 h. Cells were infected with Ad-CMV, NEK9, D194N or ΔRCC1 at a MOI of 20 for 24 h. Cells were stained by adding 20 µL of propidium iodide (1 mg/mL) (Thermo Fisher) to each well post-infection, including a mock-infected propidium iodide only well. Cells were monitored under the live-cell imager (ImageXpress Micro 4) (Molecular Devices) set at 37°C and supplied with modified air (78.09% Nitrogen, 20.95% Oxygen, 0.93% Argon, 5% Carbon Dioxide) for 24, 48 and 72 h post-infection.

2.2.15. MTT assay

HT1080 and SW-480 cells were counted using a hemocytometer and plated at 12,000 cells per well in a 96-well plate (Eppendorf, Hamburg, Germany). Cells were depleted for Nek9 by adding *Nek9* siRNA (50 µM) or Negative Control siRNA (50 µM) directly to cells for 24, 48, and 72 h. The cells were treated with *Nek9* siRNA (50 µM) or Negative Control siRNA (50 µM) to deplete NEK9. The cells were infected by directly adding Ad-CMV (5 µL), NEK9 (25 µL), D194N (25 µL) or ΔRCC1 (75 µL) (infection volume based on titration assay (Fig. 22)) for 24, 48, and 72 h. 24 h prior to MTT kit application, cells were plated at 2,000, 4,000, 8,000, 16,000 and 32,000 cells per well to generate a standard curve. After each 24, 48 and 72 h time points, the MTT assay kit (Abcam, Cambridge, United Kingdom) was applied to each well. The media was aspirated from the cells and the MTT Reagent mixture (50 µL MTT Reagent, 50 µL SF media) was added per well and cells were incubated at 37 C for 3 h. The control well consisted of the MTT Reagent mixture without any cells. Subsequently, 150 µL MTT soluble solution was added to each well and the plate was covered in foil and was gently rocked for 15 minutes at room temperature. The plate without the lid was placed into the plate reader (SpectraMax iD3) (Molecular Devices) and the colorimetric shift of MTT to formazan was measured at 590 nm. The data was analyzed using SoftMax Pro version 7 software package (Molecular Devices).

IMR-90 and WI-38 cells used in MTT experiments were subjected to arrest by incubating the cells in conditioned media for 3 days. The cells were treated with *Nek9* siRNA (50 µM) or Negative Control siRNA (50 µM) to deplete NEK9. The cells were infected by directly adding Ad-CMV (5 µL), NEK9 (50 µL), D194N (50 µL) or ΔRCC1 (75 µL) (infection volumes based on titration assay (Fig. 22)). The standard curve for IMR-90 and WI-38 cells were not arrested but plated at the same quantity as previous experiment. Cells were subjected to MTT assay at the same timepoints as indicated above.

2.2.16. Transformation Assay

MEF cells inducible for NEK9 expression were counted using a hemocytometer and plated at 500,000 cells per 6-cm plate (SARSTEDT). Cells were induced to express NEK9 and subsequently infected with a wild-type adenovirus 5 strain, *dl*309, at a MOI of 30. Cells were maintained to grow in Tet- media to constitutively express NEK9. Uninduced and induced mock cells, along with infected cells had media replaced every 3 days and monitored for 30 days post

infection and induction. After 30 days, cells were washed using PBS. Crystal violet was applied to the wells and stained the foci. Foci were enumerated after staining.

2.2.17. β-galactosidase Senescence Assay

WI-38 cells were counted using a hemocytometer and plated at 250,000 cells per well in a 6-well plate (SARSTEDT). Cells were infected with Ad-CMV, NEK9, D194N and ΔRCC1 expressing viruses at a MOI of 20 by directly adding the infection mixture (virus volume, topped to 500 µL SF-media) onto the cells. After 24 h of infection, the media was removed, and the cells were washed with twice with PBS. The cells were fixed with 4% formaldehyde for 3 minutes at room temperature. The cells were washed twice with PBS. The cells were stained with β-gal senescence stain (1 mL per well) and incubated overnight at room temperature. Plates were stored at 4°C for future observation.

2.2.18. Statistics

Data was analyzed using one-way analysis of variance (ANOVA) followed by a post hoc comparison of Tukey's test or Student's T-test (two-tailed) comparing Ad-CMV samples to NEK9 virus-infected samples. Statistical analysis was conducted using Graphpad Software package. Flow cytometry data analyzed using FlowJo v10.7.1 software package. Data significant to p-value <0.05, or otherwise indicated.

2.3. Results

2.3.1. Differential expression of Nek9 mRNA in different cell lines

Based on reports that detailed the upregulation in certain breast cancer tissues and the impact on the proliferation of p53-mutant transformed cell lines, it was necessary to first establish the basal expression of *Nek9* across our available pool[78,219]. The level of *Nek9* mRNA was measured across ten different cell lines as indicated in Fig. 6. The assay included primary cells such as IMR-90 (lung fibroblasts), WI-38 (lung fibroblasts) and transformed cells such as HT1080 (fibrosarcoma cells), HEK293 (kidney epithelial cells), HEK293T (kidney epithelial cells expressing SV40 Large T antigen), U2OS (human bone osteosarcoma epithelial cells), A549 (lung adenocarcinoma cells), SK-OV-3 (ovarian cancer cells), T47D (triple negative breast cancer cells) and HeLa (cervical cancer cells). Transcripts were measured using complementary DNA (cDNA) generated from RNA that was extracted from each cell line and the expression of *Nek9* was displayed according to the relative expression compared to the housekeeper gene, glyceraldehyde 3-phosphate dehydrogenase (*GAPDH*). This experiment allowed us to narrow our focus to the cell lines that had relatively high expression.

Expression of *Nek9* between IMR-90 cells and WI-38 cells was less than 2% relative to *GAPDH*. Comparatively, HT1080, 293, 293T, U2OS, A549 and HeLa cells also expressed *Nek9* at approximately 2% relative to *GAPDH*. The presence of Large SV40 T-Antigen had little effect on *Nek9* production as 293 and 293 T cells had similar levels. T47D (ductal carcinoma) and SK-OV-3 (ovarian) cell lines were observed to express significantly higher levels of *Nek9* as compared to the other lines tested. T47D cells expressed three times the amount of *Nek9* as compared to HT1080 or HEK293 cells, whereas SK-OV-3 cells expressed six times that amount (Fig. 6).

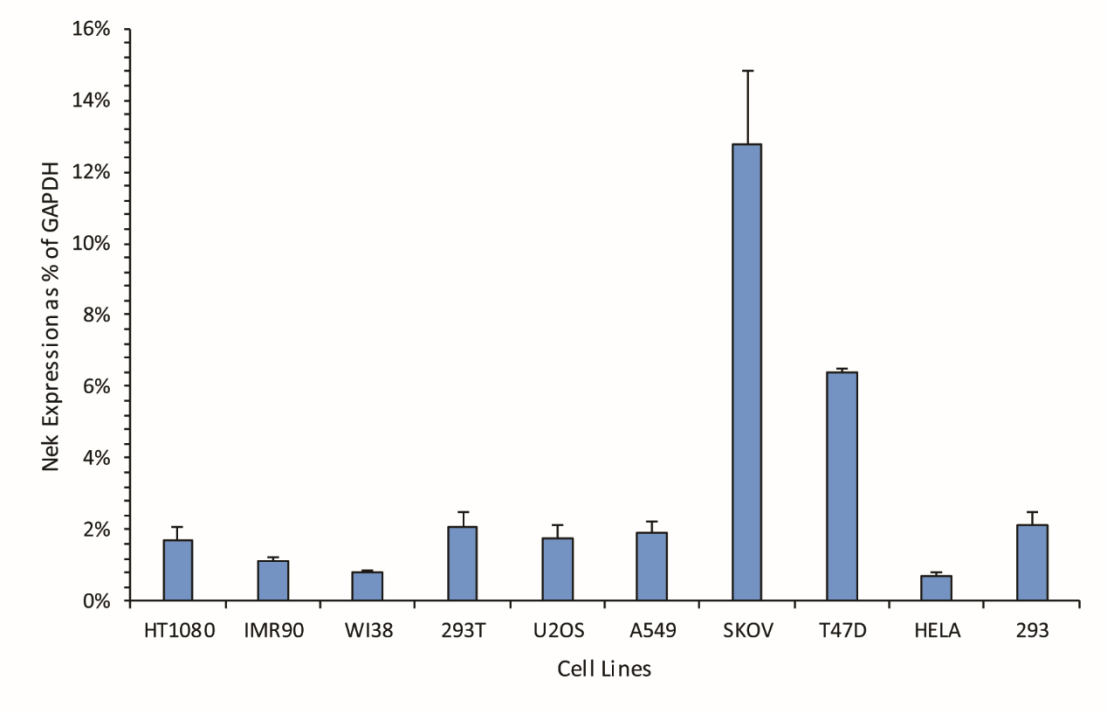

Fig. 6. Expression of Nek9 mRNA as percentage of GAPDH across various cell lines.

The indicated primary and transformed cells were grown and lysed and RNA was extracted as described in Chapter 2 (2.2.10. Real-time gene expression analysis). The purified RNA used as template for RT-qPCR to measure relative levels of *Nek9* and *GAPDH* transcripts. The signal produced using Nek9 primers is given as percentage of that using GAPDH primers. n = 3, error bars represent SD.

2.3.2. NEK9 overexpression enhances transformation of adenovirus infected MEF cells

Given our observations of the differential expression of *Nek9* transcripts in various tumour cell lines and the recent publication of adenovirus-mediated recruitment of NEK9 to suppress the p53-network, we was opted to determine the role of NEK9 in the transformation of rodent cells[50,220]. The transformative properties of NEK9 were examined by conducting a foci-forming assay using MEF cells inducible for NEK9 overexpression, along with infection of our wild-type-adenovirus strain (*dl*309) as shown in *Fig. 7*. Mock (uninfected) and uninduced (-NEK9) MEF cells displayed few formations of transformed cells (foci) as indicated by the lack of aggregated cells visible after crystal violet staining. This was mirrored by mock MEF cells that were induced for NEK9 expression (+NEK9) (*Fig. 7*A). In contrast, MEF cells infected with *dl*309 and induced (+NEK9) had a high quantity of foci forming. This was unlike infected, uninduced (-NEK9) MEF cells, which had few foci present. The foci of a second experiment were counted and between two replicates, MEF cells infected with *dl*309 and induced (+NEK9) had twice the amount of foci present compared to uninfected MEF cells that were not induced for NEK9 expression. These results suggest that increased expression of NEK9 in MEF cells could enhance the transformative properties of adenovirus in MEF cells.

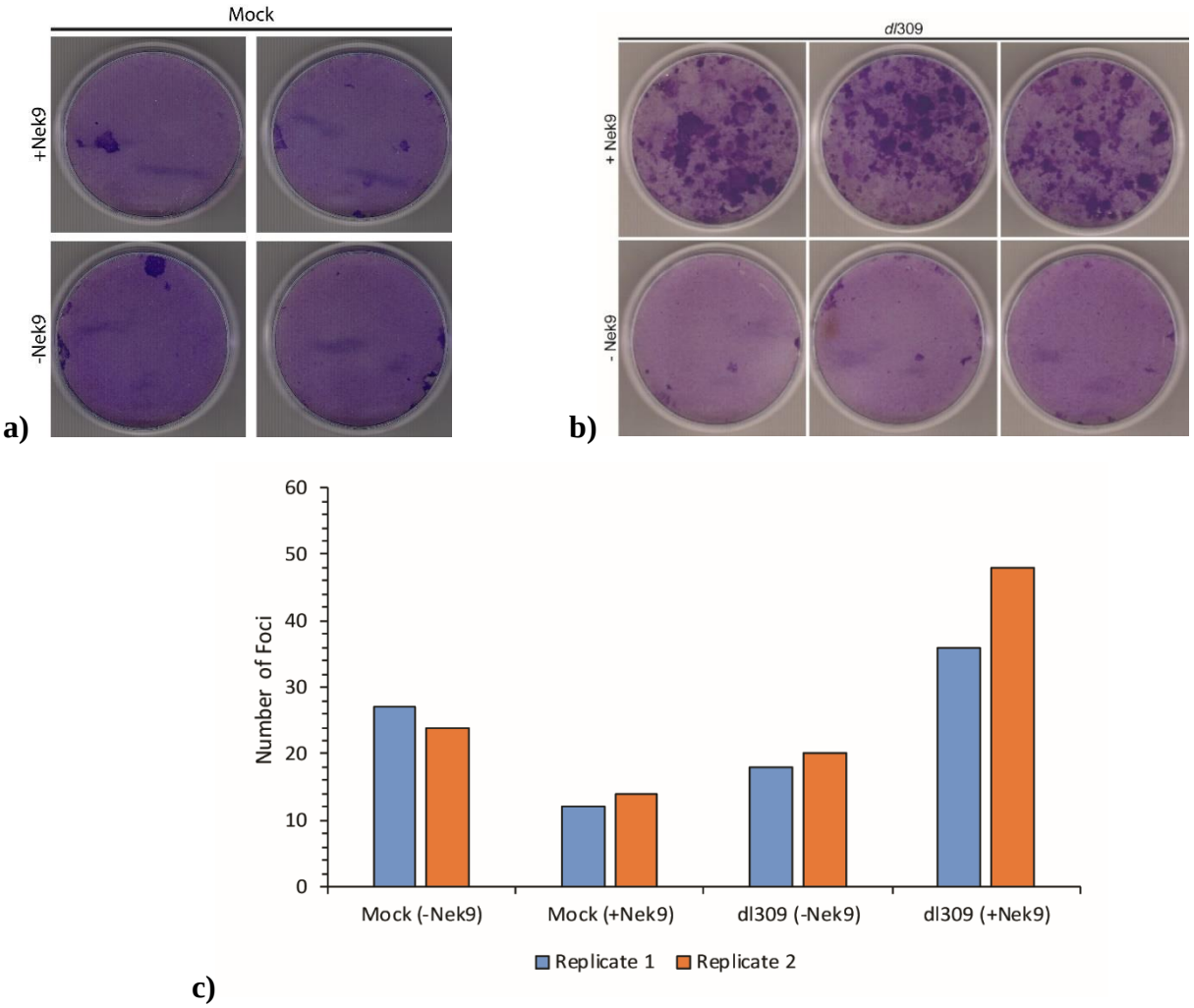

Fig. 7. Foci forming (transformation) assay

NEK9-inducible MEF cells were induced to overexpress NEK9, followed by mock-treatment or infection with wild-type adenovirus (*dl*309) at an MOI of 30 for 24 h. Induced cells were grown on *tet*$^{-}$ and uninduced cells were grown on *tet*$^{+}$media. A) Mock-infected cells displaying little foci in uninduced and induced cells. B) *dl309*-infected cells induced to express NEK9 show enhanced transformation as compared to uninduced infected cells. Cells were grown and monitored for 30 days prior to being treated with crystal violet to stain foci. C) Foci from replicate 1 and replicate 2 were enumerated and graphed, n = 2.

2.3.3. NEK9 suppresses p53-mediated activation

It had been previously observed that the recruitment of NEK9 by the adenoviral protein E1A leads to formation of a complex (NEK9-E1A) to suppress p53-regulated activation[50]. E1A enhanced the recruitment of NEK9 onto the promoter of *GADD45α*, resulting in its suppression. It was of interest to determine whether NEK9 possessed an innate property to exert transcriptional control over p53-regulated genes in absence of E1A. A luciferase reporter assay was used to measure the activity of p53 on a p53-regulated promoter in the presence of NEK9 (Fig. 8). HT1080 cells that were only transfected with the reporter plasmid was used to measure background p53 activity. Based on two trials, cells transfected with a p53-expressing plasmid acted as positive controls and saw the highest activity amongst the tested conditions. Between the replicate samples, cells that were transfected with a NEK9 expression plasmid saw little change when compared to reporter-only cells. Most importantly, the cells transfected with both the p53 and NEK9 expressing plasmids did not achieve the same level of activity as the cells transfected for only the p53 expressing plasmid and reporter.

A second experiment included the expression of the 289R isoform of E1A or the ΔRCC1 variant (deleted for the RCC1 domain) of NEK9 alongside the reporter plasmid (Fig. 9). The primary motivation of this experiment was to investigate whether the largest isoform of E1A, 289R, would enhance the previously observed NEK9-mediated suppression of p53 activity. The secondary objective of this experiment was to establish whether the RCC1 domain in NEK9, or the phosphorylation activity were integral to the suppression of p53 activation. The introduction of 289R E1A saw a slight decrease in promoter activation, whereas ΔRCC1 caused a significant decrease in cells overexpressing p53. The activity was hampered in cells that overexpressed NEK9 than in those with only the reporter, regardless of the presence of 289R E1A or ΔRCC1. As in the case of the previous experiment (Fig. 8), reporter activation was reduced in cells overexpressing p53 and wild-type NEK9 irrespective of 289R E1A or ΔRCC1.

These results imply p53 activity is negatively affected in HT1080 cells when NEK9 is overexpressed. Furthermore, it seemed that the presence of the RCC1 domain had an effect on the suppression of p53 activity.

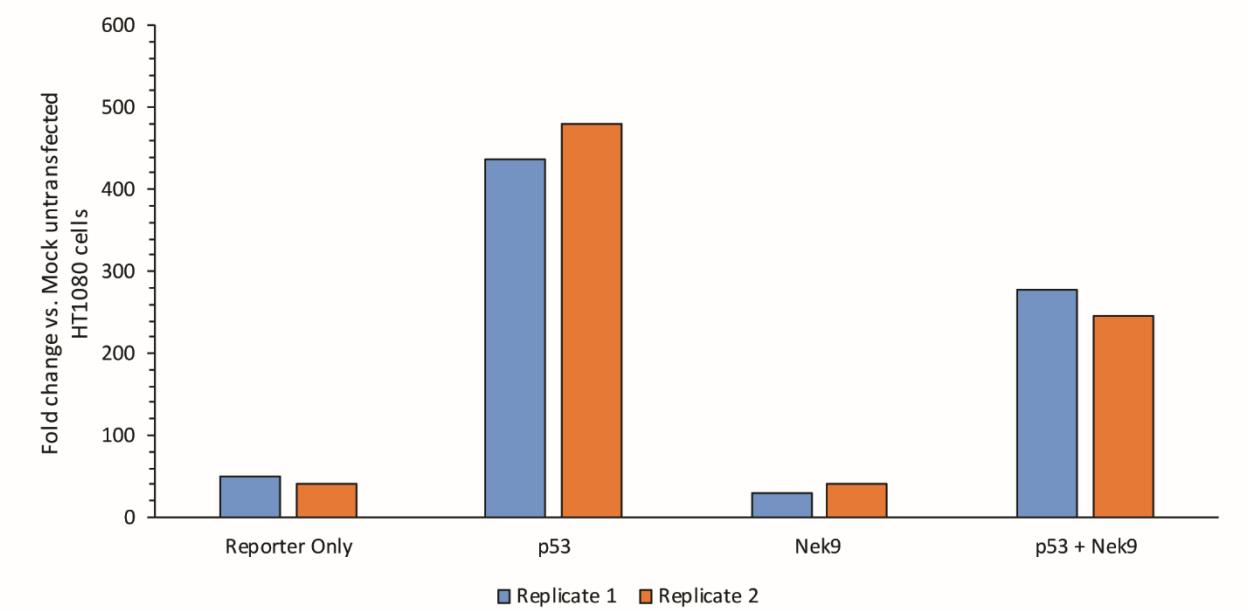

Fig. 8. Luciferase assay shows overexpression of NEK9 suppresses p53-promoter activity

HT1080 cells were transfected with a p53-reporter plasmid to measure p53-transactivation. p53 and NEK9 were overexpressed individually or together in the cells from p53- and NEK9-expressing plasmids. Cells were harvested, lysed and were treated with luciferase substrate, and luminosity was measured using Flexstation 3 Multi-mode Microplate Reader (Molecular Devices). p53 transactivation measured as fold difference between transfected cells (Reporter only, Reporter + p53, Reporter + NEK9, Reporter + p53 + NEK9) against untransfected cells, n = 2.

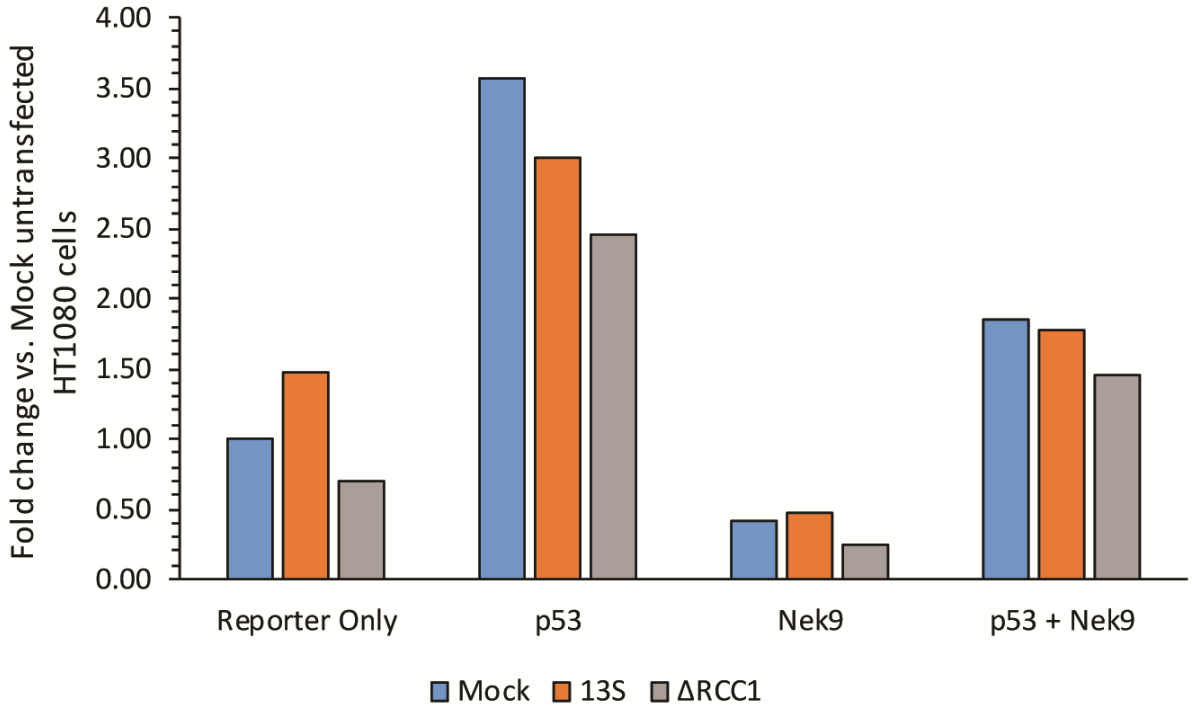

Fig. 9. Luciferase assay shows overexpression of ΔRCC1 also suppresses p53 transactivation
All HT1080 cells were transfected with a p53-reporter plasmid (reporter only). With exception to the Reporter Only, cells were also transfected with a p53 (p53), or a NEK9-expressing plasmid (NEK9) or both (p53 + NEK9). Mock (BLUE) did not have additional transfections. 13S (ORANGE) was also transfected with an E1A-expressing plasmid. ΔRCC1 (GREY) was also transfected with a ΔRCC1-expressing plasmid. 24 h after transfection, cells were harvested, lysed and treated with luciferase substrate prior to measurement of luminosity activity in Flexstation 3 Multi-mode Microplate Reader (Molecular Devices). Data presented as average fold difference between two replicates (n = 2) of transfected cells vs. mock-untransfected cells.

2.3.4. Differential expression in p53-regulated genes based on p53 status

Based on the evidence that NEK9 may play a role in p53 suppression outside of the influence of adenovirus and E1A, it was decided to focus on NEK9's impact on p53-regulated pathways. The Kurioka lab had determined that the proliferation of transformed cell lines was affected by the expression of NEK9 and the wild-type status of p53[78]. Therefore, it was of importance to identify which of the p53-regulated pathways were affected by NEK9. Secondly, we opted to determine whether the wild-type status of p53 affected the activation of these pathways. NEK9 was depleted via siRNA-mediated knockdown in transformed cell lines that were p53 wild-type, such as HT1080 and A549 (Fig. 10) or p53 mutant, such as SW-480 and SK-OV-3 (Fig. 11). The expression of p53-regulated genes responsible for activating cellular arrest (*GADD45α*), promoting apoptosis (*PUMA*, *PIG3*) or regulation of p53 (*MDM2*) was measured using quantitative RT-PCR.

In HT1080 and A549 cells, the relative expression of all the genes tested were similar in the control and knockdown cells. The depletion of NEK9 did not influence the expression of genes involved in several p53-regulated pathways.

These results were in stark contrast to the expression in SW-480 and SK-OV-3 cells. In SW-480 cells depleted for NEK9, the expression of each p53-regulated gene was significantly enhanced. The highest, PUMA, increased seven-fold compared to control cells. Comparably, SK-OV-3 depleted for NEK9 also saw significant enhancement of *GADD45α*, *MDM2*, *PIG3* and *PUMA* expression, up to three-fold compared to control cells. This supported the notion that NEK9 regulated tumour suppressing genes in p53 mutant cell lines.

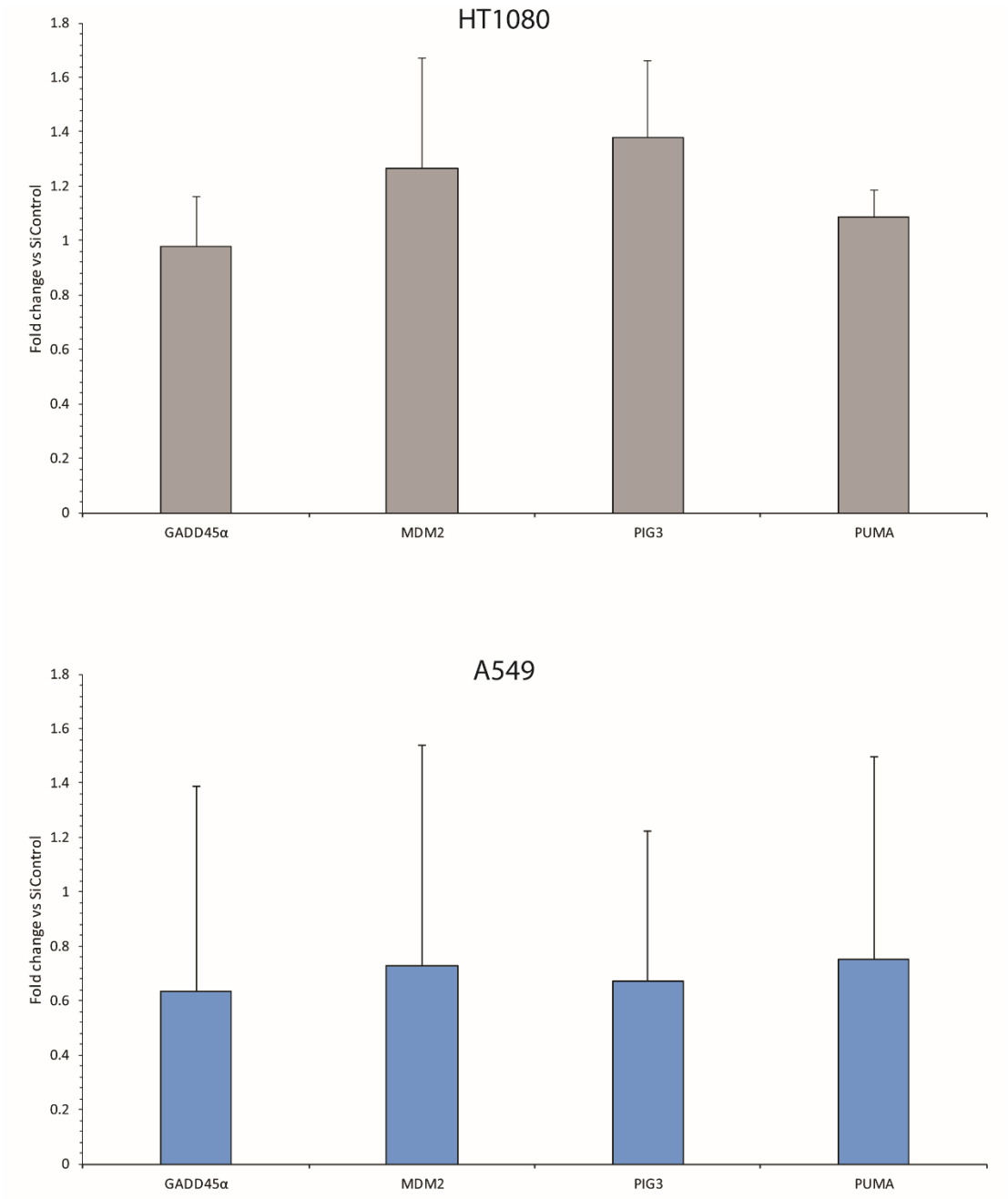

Fig. 10. Gene expression of p53-regulated genes in NEK9-depleted transformed p53^{+} cell lines

p53 wild-type HT1080 (Top) and A549 (Bottom) cells were subjected to siRNA-mediated knockdown of NEK9 for 3 days; control cells were treated with non specific siRNA. Cells then were lysed using nucleoZOL. RNA was purified and used as template for RT-PCR using VILO mastermix along with primers of known p53-regulated genes: *GADD45α*, *MDM2*, *PIG3* and

PUMA. Results are presented as the fold-difference between samples from of depleted and control-knockdown cells. n = 3, error bars represent SD.

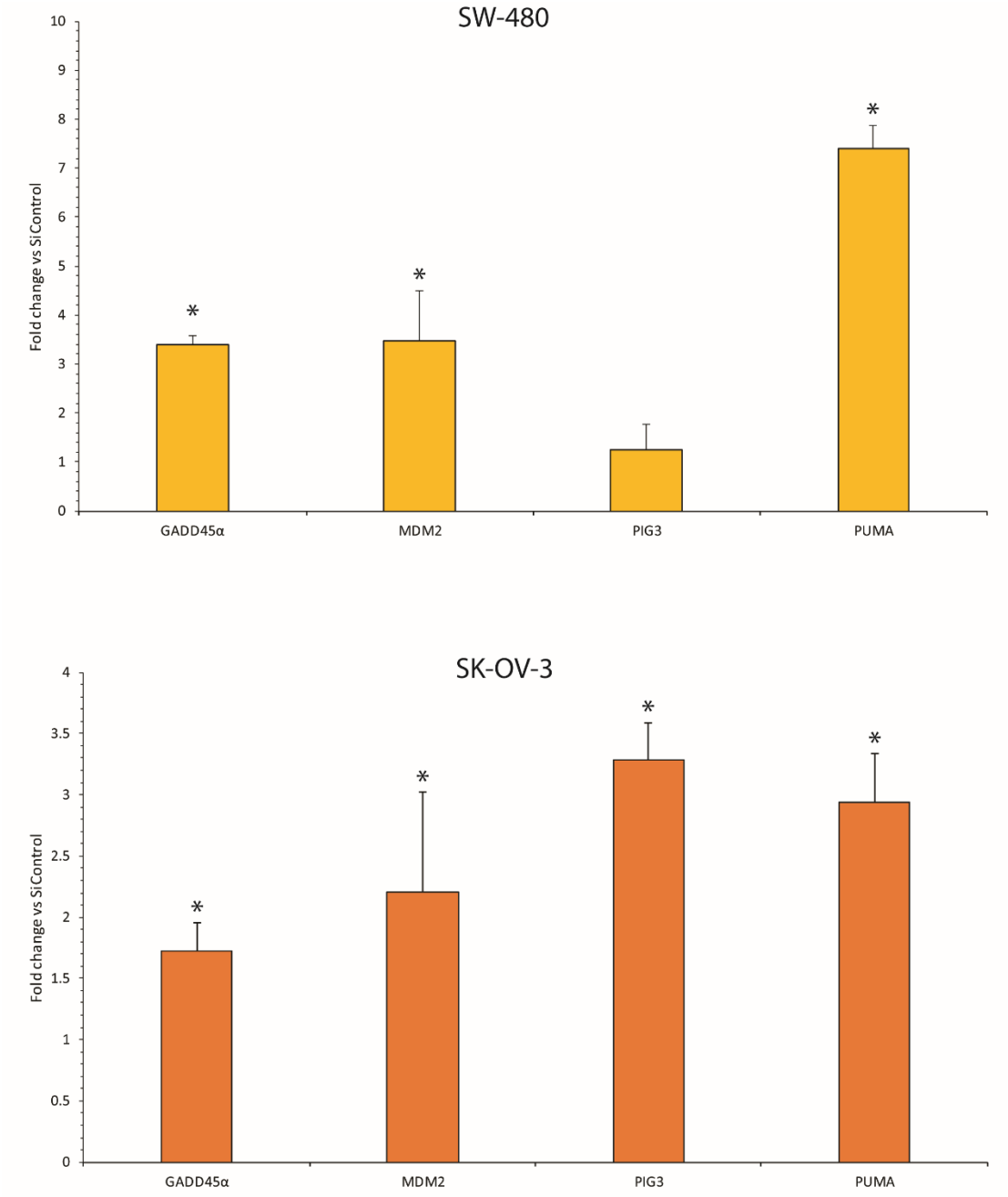

Fig. 11. Gene expression of p53-regulated genes in NEK9-depleted transformed p53$^-$ cell lines

p53 mutant cell lines SW-480 (Top) and SK-OV-3 (Bottom) cells were subjected to siRNA-mediated knockdown of NEK9 for 3 days. Cells were lysed using nucleoZOL. RNA was purified and used as template for RT-qPCR using VILO mastermix along with primers of known p53-regulated genes: *GADD45α*, *MDM2*, *PIG3* and *PUMA*. Results are presented as the fold change

of depleted samples vs. control-knockdown samples. n = 3, error bars represent SD. Significance noted as (*) = $P \leq 0.05$.

2.3.5. Differential stress response of cell lines in siRNA-mediated depletion of NEK9

The enhancement of p53-regulated responses as a consequence of deregulating NEK9 through knockdown prompted the investigation into downstream genes responsible for inducing apoptosis. The expression of the antiapoptotic markers *BCL-2* and *BCL-xL* were measured in A549 (p53 wild-type), HT1080 (p53 wild-type) and SK-OV-3 (p53 mutant) cells to assess the antiapoptotic response when cells were depleted for NEK9 (Fig. 13). HT1080 cells saw little change in expression of these antiapoptotic markers. In contrast, A549 cells had significantly higher expression of these markers compared to HT1080. A549 cells exhibited three-fold the expression of *BCL-2* and *BCL-xL* in cells lacking NEK9 against control-treated cells. In SK-OV-3 cells, *BCL-2* levels were lower upon knockdown of Nek9, while *BCL-xL* levels remained unchanged.

Similarly, expression of proapoptotic markers *BAD* and *BAX* were examined in the same cell lines (Fig. 12). The expression of *BAD* remained relatively unaffected. However, A549 cells exhibited remarkable enhancement of *BAX* expression upon knockdown (10-fold higher), while in HT1080 cells expression increased 3-fold. SK-OV-3 cells displayed decreased expression *BAX* in response to the depletion of NEK9.

These results revealed differences within each respective cell line in terms of the stress-response upon siRNA-mediated knockdown of NEK9. The general increase of proapoptotic and antiapoptotic markers in A549 cells indicated that these cells were particularly sensitive to this treatment. Transcripts for proapoptotic and antiapoptotic markers remained relatively unchanged in HT1080 cells, suggesting that NEK9 did not directly affect BCL-2 mediated stress response in these cells. In contrast, SK-OV-3 cells displayed reduction of both proapoptotic and antiapoptotic markers, implying that the depletion of NEK9 had little effect on the apoptotic pathway and may tighten the regulation of these genes, both in the presence and absence of functional p53.

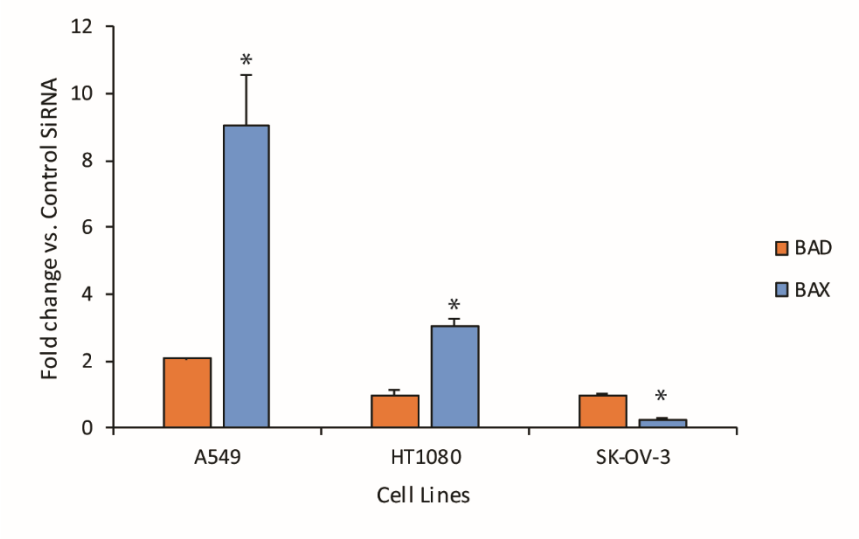

Fig. 12. Expression of proapoptotic gene markers in NEK9-depleted cells

A549, HT1080 and SK-OV-3 cells were subjected to siRNA-mediated depletion of NEK9 for 3 days. Cells were lysed using nucleoZOL. RNA was purified and used as template for RT-qPCR using VILO mastermix along with primers of known proapoptotic gene markers: *BAD* and *BAX*. Results are presented as the fold change of depleted samples vs. control-knockdown samples. n = 3, error bars represent SD. Significance noted as (*) = $P \leq 0.01$.

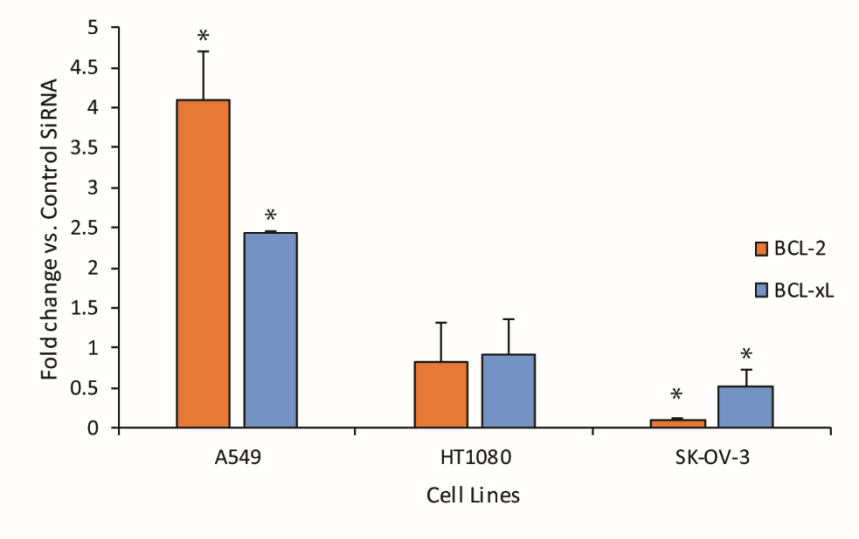

Fig. 13. Expression of antiapoptotic gene markers in NEK9-depleted cells

A549, HT1080 and SK-OV-3 cells were subjected to siRNA-mediated depletion of NEK9 for 3 days. Cells were lysed using nucleoZOL. RNA was purified and used as template for RT-qPCR using VILO mastermix along with primers of known proapoptotic gene markers: *BCL-2* and *BCL-xL*. Results are presented as the fold change of depleted samples vs. control-knockdown samples. n = 3, error bars represent SD. Significance noted as (*) = $P \leq 0.05$.

2.3.6. Observed stress response in HT1080 cells expressing NEK9 variants

Considering the enhanced stress response at the transcriptional level in cells depleted for NEK9, it was in our interest to explore whether this effect was echoed at the protein level. Therefore, HT1080 cells were observed under the microscope for apoptotic morphology 48 h post-infection with viruses overexpressing wild-type NEK9, kinase inactive D194N variant or the truncated ΔRCC1 variant (Fig. 14). Cells were also infected with an Ad-CMV virus that did not express any protein of interest and was used as a background control against the viral expression vectors. The coding sequence for the D194N variant was generated previously[215] by inverse PCR and replacement of the asparagine codon (residue 194) with that of aspartic acid. The ΔRCC1 mutant was generated previously[215] in the same manner and is deleted for the RCC1 domain of NEK9. Cells infected with the virus that expressed wild-type NEK9 did not display apoptotic markers 24 h post infection, but cells infected with virus expressing either the D194N or ΔRCC1 variants displayed lower cell population densities based on the images taken under the microscope 48 h post infection (Fig. 14). The reduction was also evident at 72 h post infection with the D194N or ΔRCC1-expressing viruses, while treatment of the wild-type NEK9 (overexpression) did not lead to this decrease in cell density. This trend was observed 48 h after infection in several cell lines, including A549 (Fig. 15) and SK-OV-3 (Fig. 16) cells. Furthermore, close inspection of cells treated with the NEK9 viruses for 48 h revealed membrane blebbing (indicated by blue arrows) and microtubule spikes (indicated by red arrows) which are indicative of apoptosis.

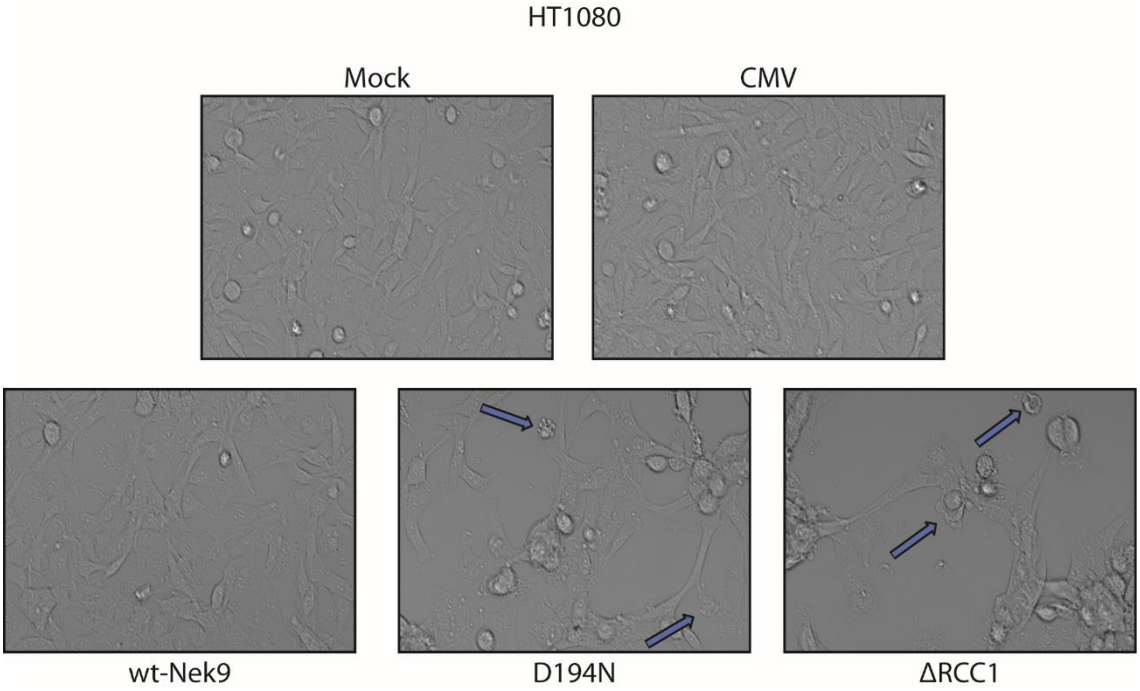

Fig. 14. HT1080 cells ($p53^{+}$) expressing NEK9 variants displaying apoptotic morphology

HT1080 cells were infected with Ad-CMV, wild-type NEK9, D194N and ΔRCC1 viruses at an MOI of 20. Cells were observed with a ZOE microscope and images taken every 24 h. Blue arrows indicate membrane blebbing. Images displayed were taken 48 h post infection.

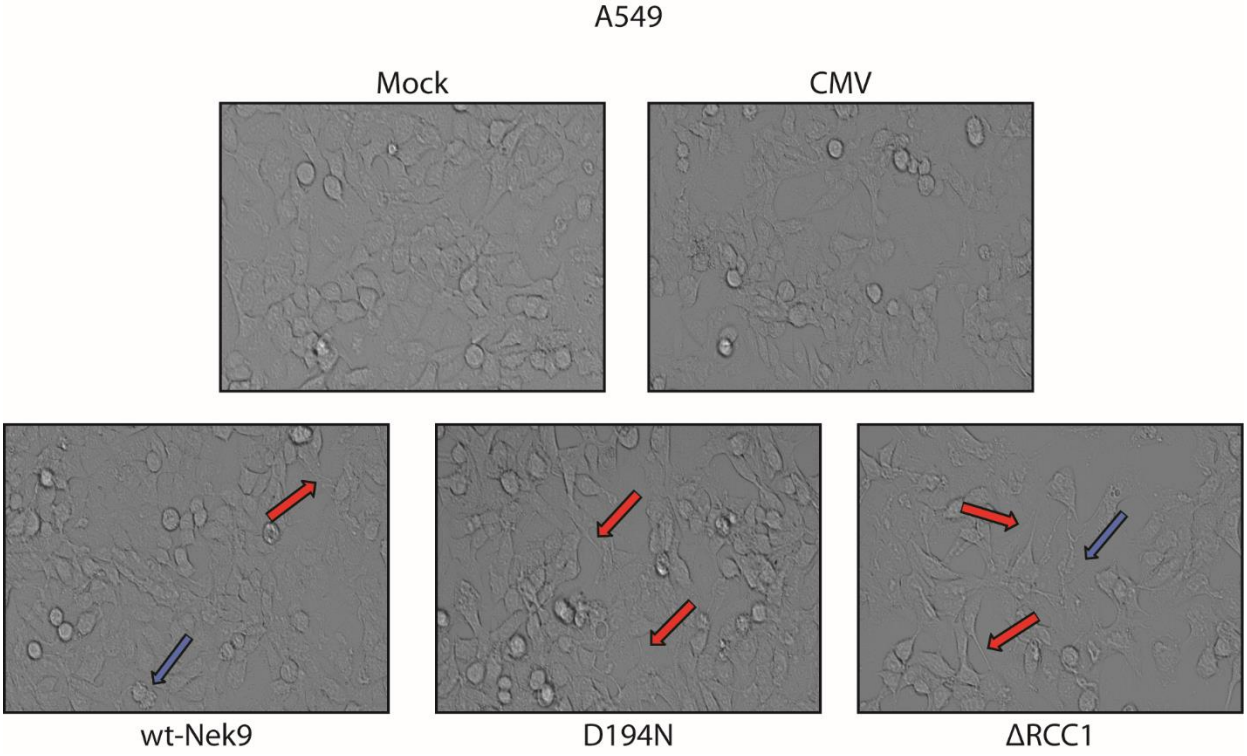

Fig. 15. A549 cells (p53^{+}) expressing NEK9 variants displaying apoptotic morphology

A549 cells were infected with Ad-CMV, wild-type NEK9, D194N and ΔRCC1 viruses at an MOI of 20. Cells were observed with a ZOE microscope and images taken every 24 h. Red arrows indicate microtubule spikes. Blue arrows indicate membrane blebbing. Images displayed were taken 48 h post infection.

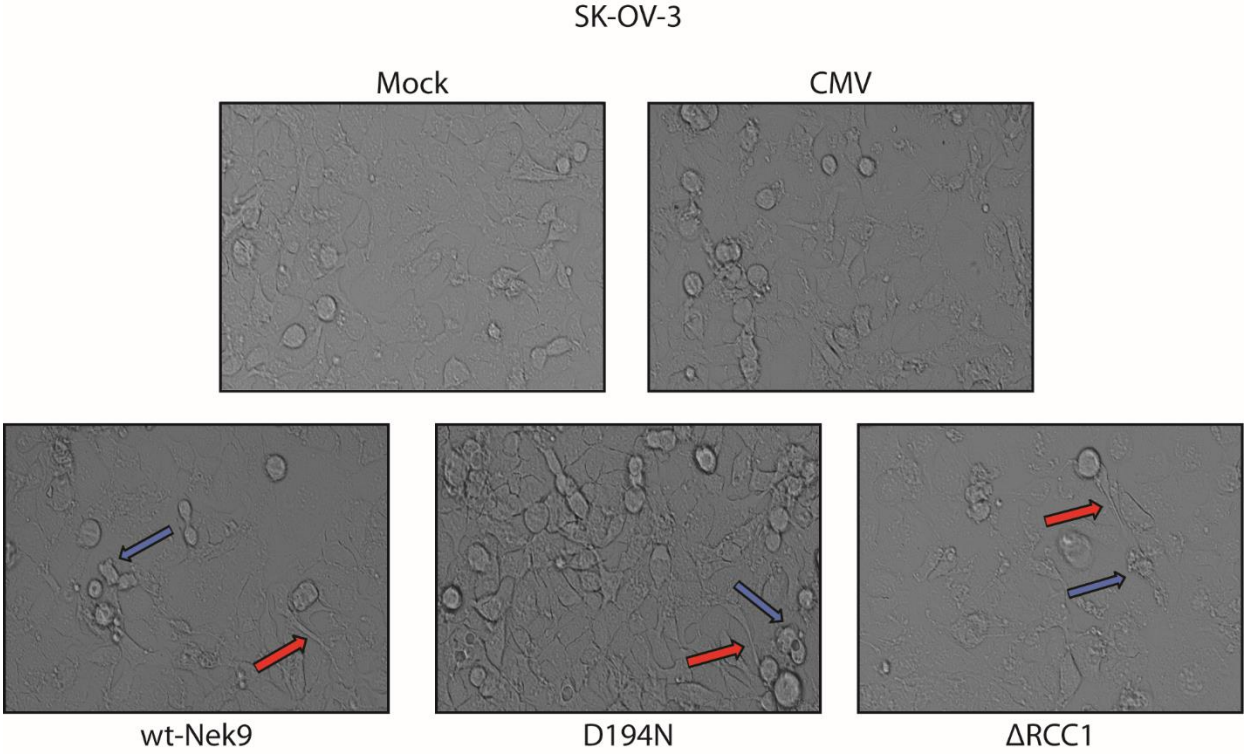

Fig. 16. SK-OV-3 (p53$^-$) cells expressing NEK9 variants displaying apoptotic morphology

SK-OV-3 cells were infected with Ad-CMV, wild-type NEK9, D194N and ΔRCC1 viruses at an MOI of 20. Cells were observed with a ZOE microscope. Red arrows indicate microtubule spikes. Blue arrows indicate membrane blebbing. Images displayed were taken 48 h post infection.

2.3.7. PARP cleavage detected in SK-OV-3 cells overexpressing NEK9 and NEK9 variants

Building on the observation of apoptotic morphology under the microscope, it was important to obtain objective evidence that NEK9 participated in the induction of apoptosis. The cleavage of PARP protein (113 kDa) to generate a C-terminal 89 kDa fragment and a 23 kDa N-terminal fragment, is a clear indicator of apoptosis[40], whereas presence of a 50 kDa fragment would suggest the occurrence of necrosis. SK-OV-3 cells were infected using wild-type NEK9, D194N or ΔRCC1-expressing viruses for 48 and 72 h (Fig. 17). As a positive control, cells were treated with a DNA-intercalating agent, Actinomycin D, which was able to induce apoptosis[221]. Endogenous NEK9 (106 kDa) was detected in all samples. There were two bands detected for the D194N variant. The smaller band may have been a nonspecific band but was observed across all the other conditions. Further investigation is required to determine why this protein was enhanced in samples expressing D194N. The ΔRCC1 variant had a predicted mass of about 75 kDa.

In samples from the control cells, the signal obtained with the α-PARP antibody was relatively weak, and while full length PARP was not detected, bands of ~23, ~50 and ~90 kDa were observed and attributed to the N-terminal, necrotic and C-terminal cleavage fragments of PARP. Additional bands of ~30, ~75 and ~95 kDa were detected but may be the result of nonspecific binding. When cells were treated with Actinomycin D, a remarkably high abundance band at about 90 kDa was observed and likely represented the C-terminal cleavage product. To discount the possibility that the Adeno-vector induced the cleavage of PARP, cells were infected with an empty Adeno-vector (Ad-CMV). Ad-CMV, viral vectors expressing wild-type NEK9, the kinase-inactive D194N variant or the truncated ΔRCC1 variant did not induce high levels of the C-terminal cleavage product 48 h after infection. However, by 72 h, there was an increase of this cleavage product in cells that overexpressed wild-type NEK9, D194N or ΔRCC1, but not at the levels observed following Actinomycin D treatment. Interestingly, a 50 kDa band was detected across all the samples at 48 and 72 h, which suggested that some cleavage of PARP occurred under necrosis. Nonetheless, this observation suggested that NEK9 and the two variants induced a p53-dependent apoptotic pathway.

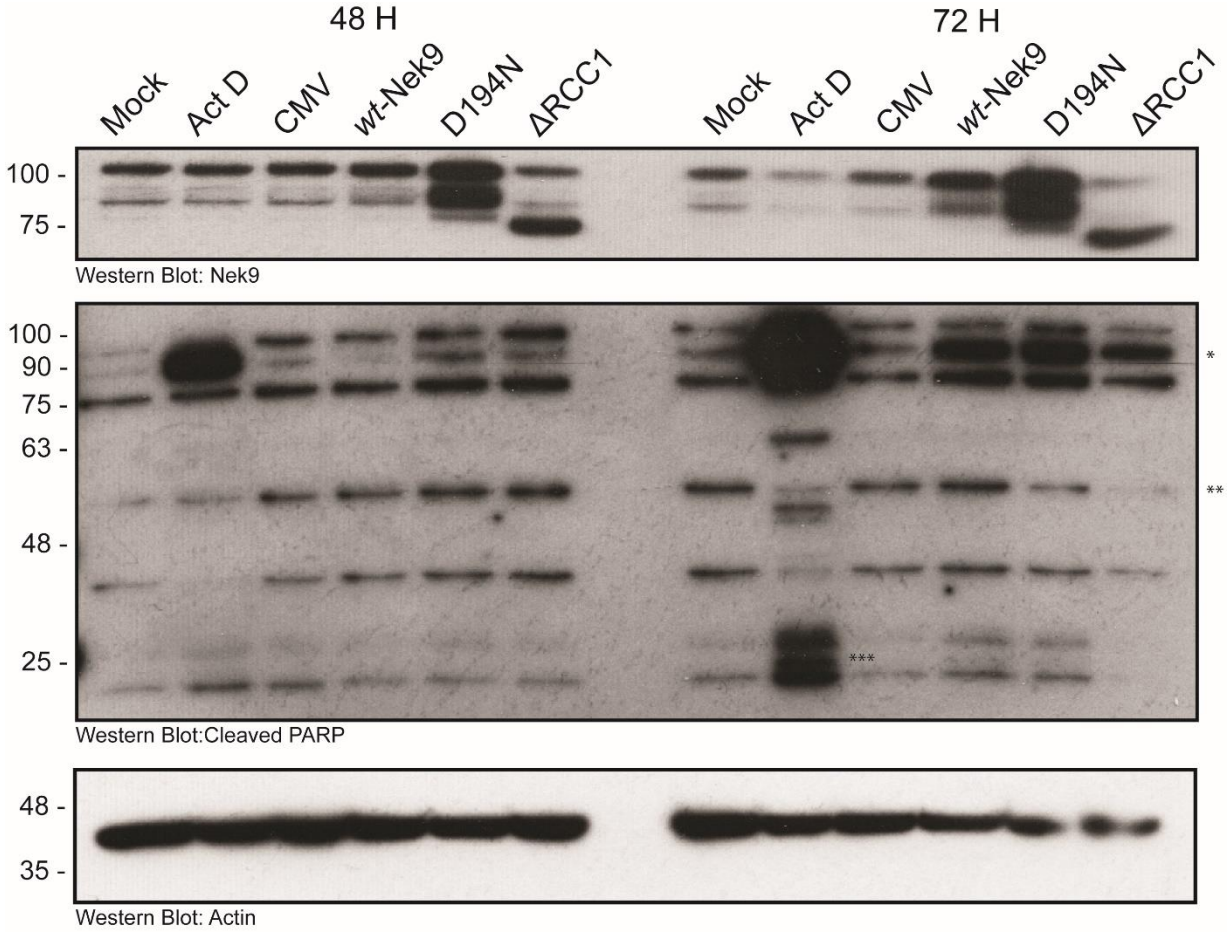

Fig. 17. Cleavage of PARP detected in cells overexpressing NEK9, D194N or ΔRCC1.

SK-OV-3 cells were treated with Actinomycin D or infected with Ad-CMV, wild-type NEK9, D194N or ΔRCC1 at an MOI of 10 for 24 h (data not shown), 48 h and 72 h (shown above). Cell lysates were examined with α-Myc antibody (NEK9, D194N and ΔRCC1) and α-PARP antibody. The cleavage product of PARP is 90 kDa; other bands result from cross-reactivity of the primary antibodies as indicated. (*) = 90 kDa C-terminal cleavage fragment of PARP, (**) = 50 kDa necrotic cleavage fragment of PARP, (***) = 23 kDa N-terminal cleavage fragment of PARP. Actin was used as a loading control.

2.3.8. Cells do not undergo senescence in presence of the NEK9-expressing viruses

In addition to induction of apoptosis, cellular senescence is another possible cause of cell death in NEK9 deregulated cells. The induction of senescence in p53-mutant cell lines upon depletion of NEK9 was first reported by the Kurioka group[78]. We decided to assay β-galactosidase-like activity (β-gal), from an enzyme secreted by cells undergoing cellular senescence. Staining for senescence associated β-gal activity is a gold standard when probing for cells entering a permanent state of arrest[222]. WI-38 cells were infected with the Ad-CMV vector or one of the viruses expressing either wild-type or variant NEK9. These cells, and mock-infected control cells were stained for β-gal (Fig. 18). Other cell lines such as A549, HT1080 and SK-OV-3 were stained for β-gal following treatment of the NEK9 viruses and the results mirrored the observations found with WI-38 cells (data not shown). Cellular senescence does not seem to be a consequence limited to the expression of the D194N or ΔRCC1 variant, as staining was present across each condition.

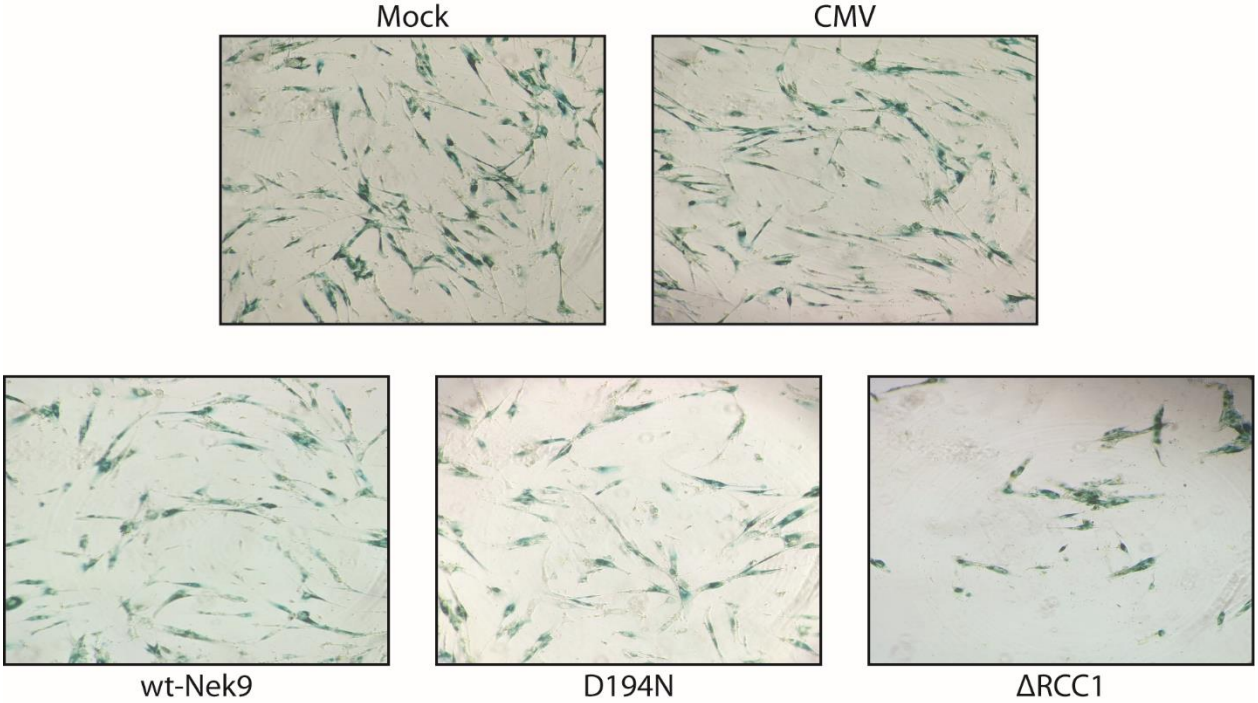

Fig. 18. β-galactosidase senescence assay

Equal amounts of WI-38 cells plated and infected with Ad-CMV, wild-type NEK9, D194N and ΔRCC1 expressing viruses at an MOI of 30. Cells were treated with a β-gal senescence stain overnight as described in chapter 2 (2.2.17. β-galactosidase Senescence Assay), and images were taken using the ZOE microscope.

2.3.9. Cell motility or proliferation is affected upon NEK9 depletion, or expression of NEK9 variants

To further investigate the implication of cells undergoing apoptosis, several assays to measure the proliferation of cells expressing the wild-type or variant NEK9 were conducted. A scratch assay was performed involving SK-OV-3 cells that were depleted or overexpressed for NEK9 or its variants (Fig. 19). Upon infection, a small wound was introduced across the monolayer of cells by scraping the well with a pipette tip, and over the course of a 24 h period, the closure of the gap was measured (Fig. 21). The images in Fig. 20 show the results at the end of the experiment. At 24 h, the gap was closed by the uninfected, control siRNA-treated cells (mock), and those infected with Ad-CMV and the wild-type NEK9-expressing virus. Cells that were depleted for NEK9 or expressed D194N or ΔRCC1 were unable to close the gap by 24 h. The differences between the conditions and closure of the gap can be seen in Fig. 20. The gap in the control treated cells closed within 12 h post infection, followed by control-infected Ad-CMV cells, which had closed the gap by 18 h post infection. The cells depleted for NEK9 had a wound size of about 35% after 24 h of treatment whereas cells overexpressing wild-type NEK9 had completely closed the gap by 18 h post infection, similar to the control-Ad-CMV treatment. The two NEK9 variants, D194N and ΔRCC1, did not see full closure of the gap, with approximately 15% of the wound open for D194N and most surprisingly 80% of the wound unclosed for ΔRCC1. This was by far the largest gap across all of the conditions and is indicative of properties exhibited by the ΔRCC1, that may negatively impact cell proliferation or cell motility. However, due to the nature of the scratch assay, it was unclear whether the expression of the NEK9 variants hampered the motility of the cells, affected the proliferation, or induced apoptosis.

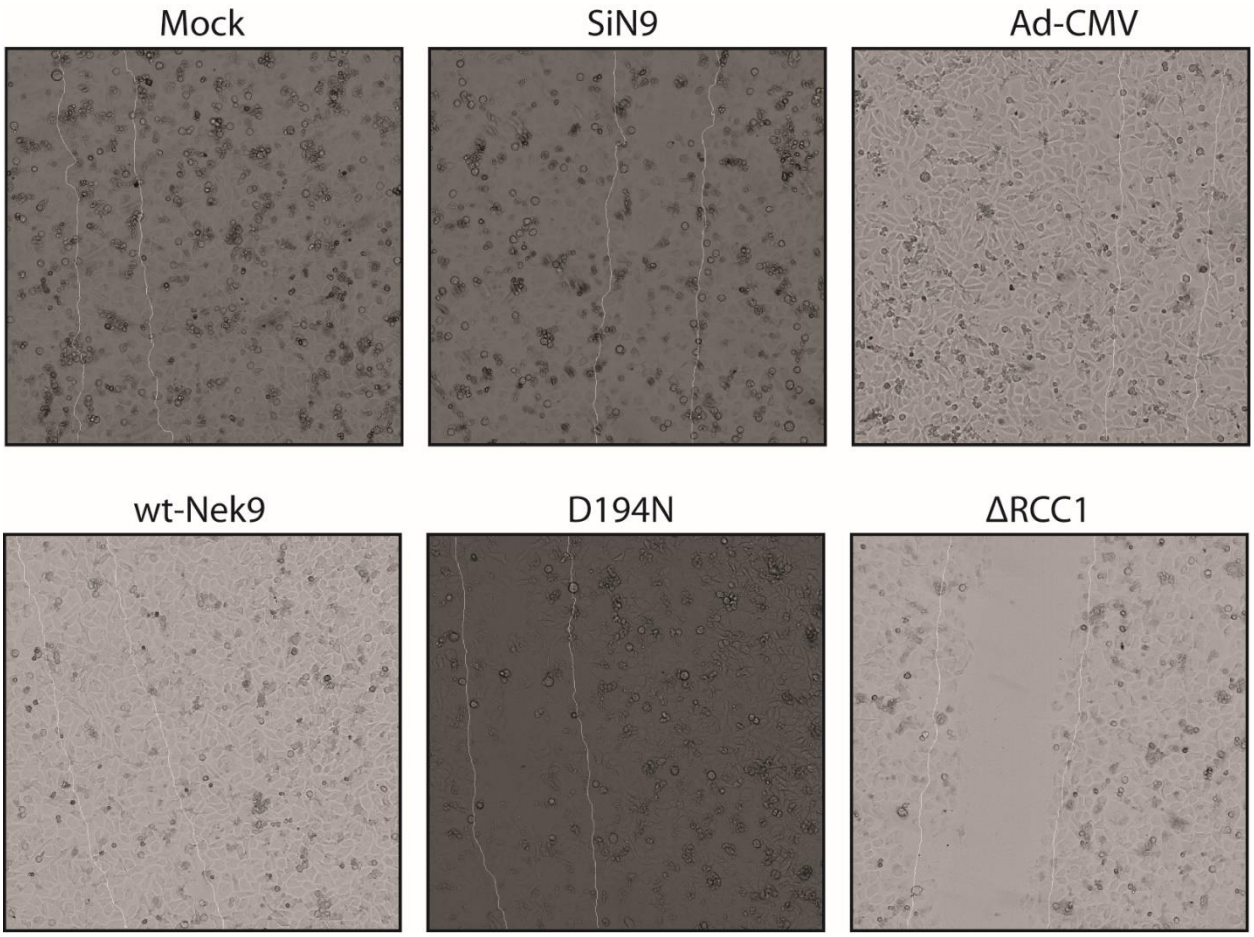

Fig. 19. Scratch assay of SK-OV-3 cells dysregulated for NEK9 expression

SK-OV-3 cells were subjected to siRNA-mediated knockdown of NEK9 or infected with Ad-CMV, wild-type NEK9, D194N or ΔRCC1 for 24 h. A gap was introduced to the monolayer of cells after immediately infection. Closure of the gap was monitored every 6 h for 24 h using the Image Xpress Micro 4 live cell imager. The image (above) was taken 24 h after treatment. White lines indicate the initial borders of the gap.

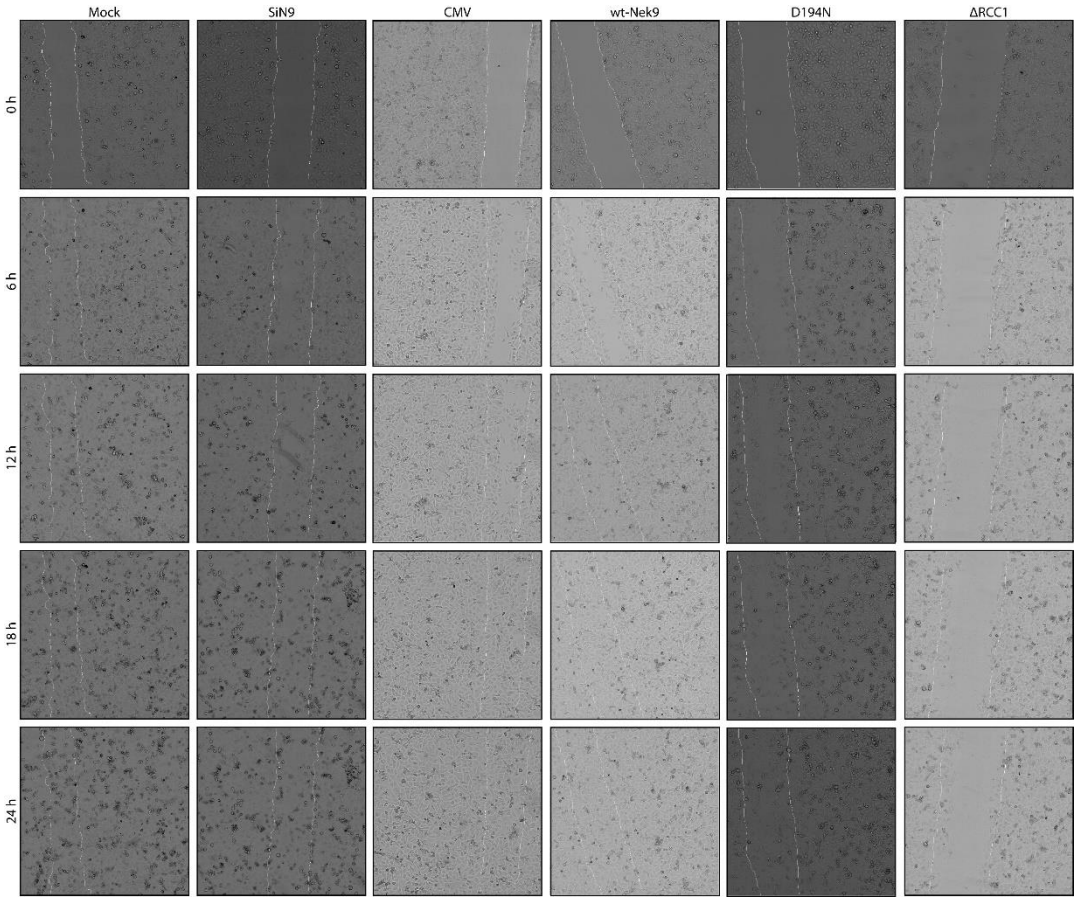

Fig. 20. Scratch assay of SK-OV-3 cells dysregulated for NEK9 expression

SK-OV-3 cells were subjected to siRNA-mediated knockdown of NEK9 or infected with Ad-CMV, wild-type NEK9, D194N or ΔRCC1 for 24 h. A gap was introduced to the monolayer of cells after infection. Closure of the gap was monitored every 6 h for 24 h using the Image Xpress Micro 4 live cell imager. White lines indicate the initial borders of the gap.

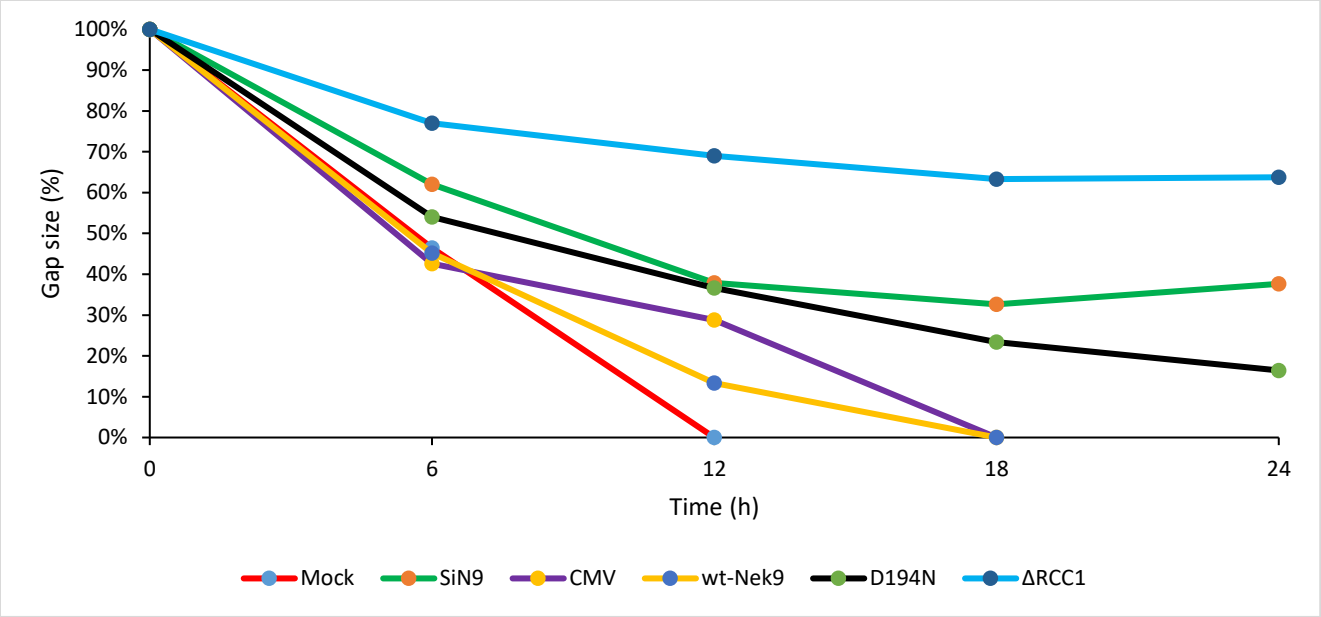

Fig. 21. Dysregulation of NEK9 in SK-OV-3 cells slows the closure of gap in scratch assay

Measurement of the gap size of indicated conditions was taken every 6 h for 24 h. n = 2.

2.3.10. Dysregulation of NEK9 hampers cell viability of HT1080 cells

To accurately interpret the data gathered from the scratch assay, it was important to conduct complementary experiments to distinguish whether our observations supported the notion that the expression of the kinase-inactive D194N or the truncated ΔRCC1 variants affected the proliferation of cells or induced apoptosis. Therefore, an MTT viability assay was conducted involving the infection of HT1080 cells with the NEK9 viruses. The rate of proliferation was measured based on the shift of yellow tetrazole (3-(4,5-dimethylthiazol-2-yl)-2,5-diphenyltetrazolium bromide (MTT)) into insoluble formazan to monitor biomarkers for active growth across a 72-hour period[223]. Infections were based on the titration assay (Fig. 22) and conducted according to the amount of protein expressed rather than MOI. The relative amount of NEK9 protein varied with the volume of lysate used for the infection, and the amount of ΔRCC1 was significantly lower than that of the wild-type or D194N variant. Therefore, the decision to switch the metric for infection was to confirm that the effect on cells was a result of the NEK9 proteins expressed and not due to an anti-viral response to the adenoviral vectors.

Cell viability was measured by infecting HT1080 cells for 24, 48 and 72 h with the wild-type NEK9, D194N or ΔRCC1-expressing viruses. Infection volumes were based on the production of wild-type NEK9 or the NEK9 variant proteins observed in the titration assay (Fig. 22). Therefore, wild-type NEK9 and D194N viruses were infected at a 1:3 ratio to ΔRCC1. Actinomycin D treated samples were used as a negative control and these cells were not viable after 48 h, while Ad-CMV-treated samples was relatively steady over time. At 24 h post infection, the NEK9, D194N and ΔRCC1 treated cells saw a 60% drop in cell viability. By 48 h, there was an observable reduction in cell viability across all the samples, which was due to human error. Therefore, the measurements at 48 h are likely inaccurate and may explain the recovery observed in Ad-CMV and wild-type NEK9 treated samples between 24 h and 72 h. It is worth noting that the D194N and ΔRCC1 treated samples remained unviable after 48 h. Taking errors into account, and with respect to the scratch assay results, the data in Fig. 23 support the hypothesis that the expression of NEK9, D194N and ΔRCC1 may affect the proliferation of the cells and/or induce apoptosis, but not the motility of the cells.

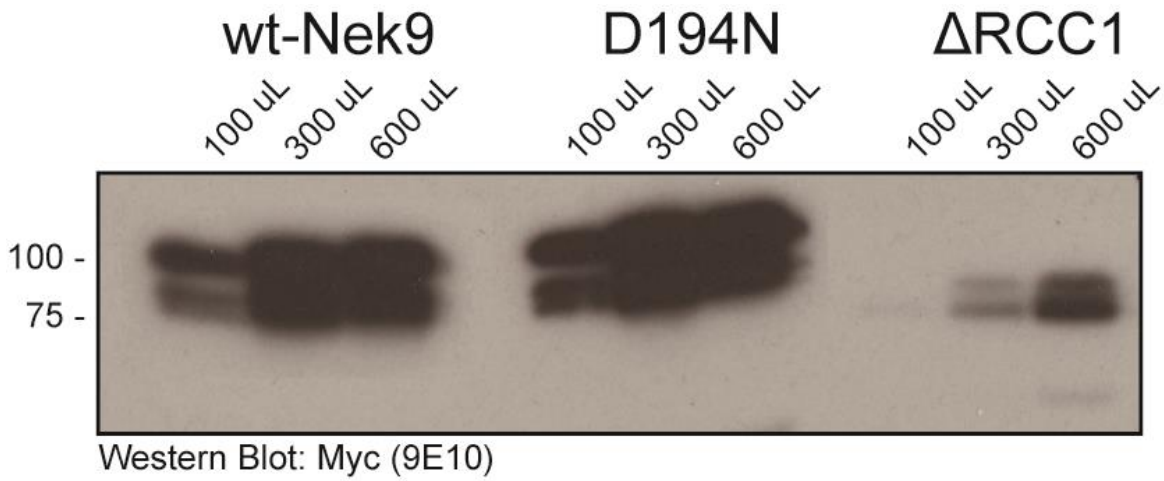

Fig. 22. Titration assay for NEK9 viruses

HT1080 cells were infected with indicated volumes for NEK9 viruses for 24 h, prior to harvest and processing for western blot. Myc-tagged NEK9, D194N and ΔRCC1 were detected using in-house prepared α-Myc antibody (9E10) at a dilution of 1:200. Molecular weight markers are in kDa.

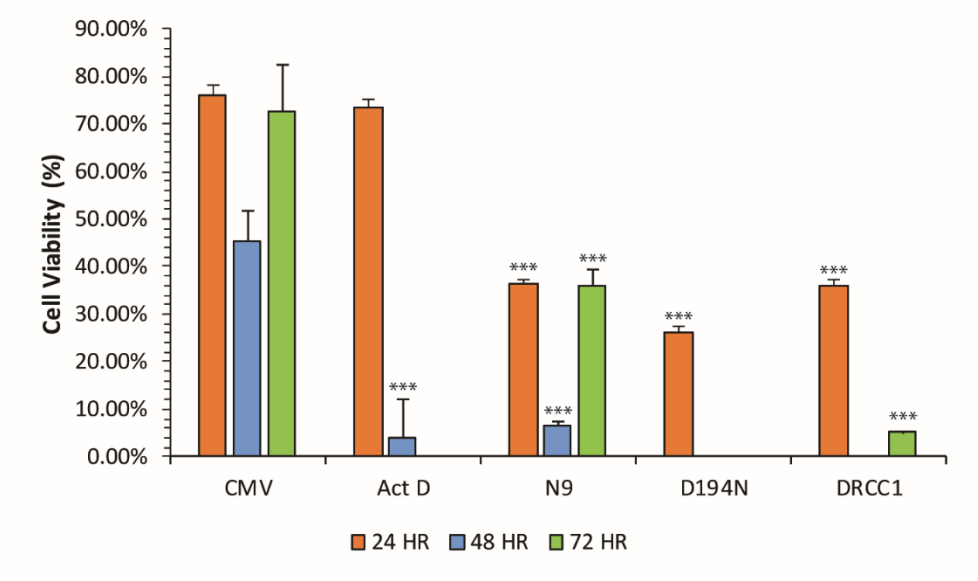

Fig. 23. Cell viability of HT1080 cells expressing NEK9 variants decreases over time

HT1080 cells were treated with Actinomycin D or infected with Ad-CMV, wild-type NEK9, D194N or ΔRCC1 for 24, 48 and 72 h. Cells were treated with MTT solution and the colorimetric shift measured using SpectraMax Multi-mode Microplate Reader (Molecular Devices). n = 3, error bars represent SD. Significance against Ad-CMV treated samples noted as (***) = $P \leq 0.001$.

2.3.11. Depletion of NEK9 reduces S-phase induction in IMR-90 cells

To investigate processes that precede cellular arrest or apoptosis, an EdU incorporation assay was used to investigate the effect of NEK9 on S-phase induction. This experiment involved the incorporation of a thydmidine analogue (5-Ethynyl-2´-deoxyuridine, EdU) into newly synthesized DNA of dividing cells. Measurement of positive cells correlated with the rate of S-phase induction in the respective cell line and growth conditions. For these experiments, IMR-90 cells were analyzed following a three-day arrest in conjunction with siRNA-mediated knockdown of NEK9 (Fig. 24). Cells were stimulated using 20% serum to promote re-entry into the cell cycle and induce S-phase. Arrested cells that were treated with either control siRNA or depleted for NEK9 yielded little difference in terms of the percentage of positive cells, as less than 2% of the population was positive for EdU incorporation (Fig. 24). On the other hand, 10% of IMR-90 cells stimulated using 20% serum and treated with control siRNA were positive. Surprisingly, less than 5% of cells that were stimulated and depleted for NEK9 were positive, which is significantly less than the control treated samples. These results indicated that NEK9 participates in the re-entry of IMR-90 cells into the cell cycle, and the depletion of NEK9 may interfere in the S-phase induction of these cells.

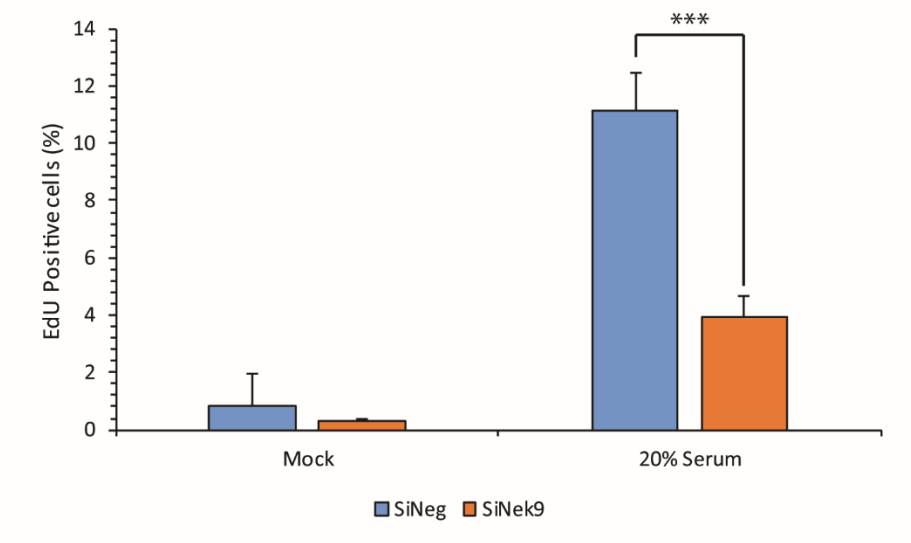

Fig. 24. EdU assay indicates dysregulation of NEK9 attenuates S-phase induction in arrested IMR-90 cells

IMR-90 cells were arrested and simultaneously depleted for NEK9 using siRNA for 3 days. Arrested cells were treated with growth media supplemented with 20% serum to re-stimulate cell growth for 24 h. Depletion of NEK9 in serum-treated cells show a reduced capacity to induce S-phase as compared to mock-depleted cells. n = 5, error bars represent SD. Significance noted as (***) = $P \leq 0.001$.

2.3.12. NEK9 levels affect the S-phase induction in HT1080 cells

Once it was determined that NEK9 effected the induction of S-phase in primary cells following arrest, an investigation whether the knockdown of NEK9, or the expression of D194N or ΔRCC1 would have a similar outcome in a transformed cell line. Therefore, HT1080 cells were monitored for the induction of S-phase by conducting an EdU incorporation assay after siRNA-mediated knockdown of NEK9, or infection of the NEK9 viruses (Fig. 25). HT1080 cells exhibit uncontrolled growth and lack contact inhibition, and therefore had a higher rate of replication as compared to IMR-90 cells. This was noticeable when the baseline percentage of incorporated EdU between the two cell lines was compared. However, as with the case of siRNA-mediated depletion of NEK9 in IMR-90 (Fig. 24), H1080 also displayed a significant reduction in S-phase induction following knockdown of NEK9 (Fig. 25). HT1080 cells that overexpressed wild-type NEK9, D194N or ΔRCC1 had significant reduction in percentage of EdU positive cells compared to mock-infected samples or Ad-CMV infected cells. These results suggested that NEK9 participates in the induction of S-phase. Cells that lacked NEK9 may have been hampered and unable complete the cell cycle. A connection between NEK9 and S-phase induction using primary and transformed cells was observed, indicating this effect was not limited to cell type.

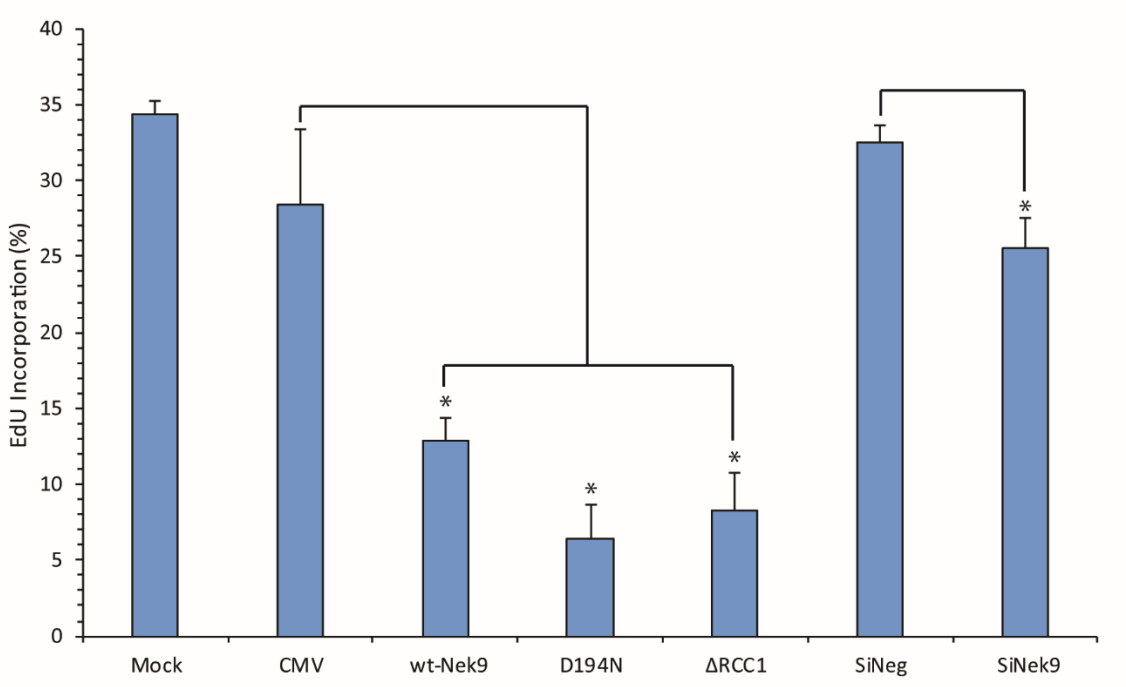

Fig. 25. EdU assay indicates dysregulation of NEK9 attenuates S-phase induction in HT1080 cells

HT1080 cells were subected to siRNA-mediated depletion of NEK9 or infected with Ad-CMV, or viruses overexpressing wild-type NEK9, D194N or ΔRCC1 viruses at an MOI of 10 for 24 h. Cells treated with NEK9 viruses show inability to induce S-phase as compared to control mock-infected and Ad-CMV-infected cells. HT1080 cells depleted for NEK9 are significantly reduced in induction of S-phase as compared to mock-depleted cells. n = 3, error bars represent SD. Significance noted as (*) = $P \leq 0.05$.

2.3.13. Overexpression of wild-type NEK9, D194N and ΔRCC1 causes arrest in S phase

To better understand the effects of NEK9 on the induction of S-phase, flow cytometry was performed using propidium iodide as the primary dye to assess DNA content and sort cells into the respective phases of the cell cycle. Untreated HT1080 cells served as a baseline for normal cell distribution (Fig. 26) in this pilot experiment. About ~50% of the population were in G1 phase, ~30% were in S phase, ~10% in G2 phase and less than 10% in sub G1 phase. Actinomycin D was used as a negative control and displayed the highest percentage of cells in the sub G1 population, indicative of dying/dead cells that have shrunk or possess little DNA present. Cells were infected with an empty viral vector, Ad-CMV, or viruses that expressed wild-type NEK9, or its variants (Fig. 27). Despite slightly lower populations of cells in G1, the Ad-CMV infected sample displayed a similar distribution of cells as the mock treatment. Cells overexpressing wild-type NEK9 and D194N for 24 h remained relatively unchanged. The cells expressing the truncated ΔRCC1 variant displayed a considerable shift in the population of cells in G1 phase (~20%) to S phase (60%), compared to Ad-CMV infected cells (~43% in G1 phase and 39% in S phase) suggesting the introduction of this variant had an effect on the cell cycle.

An expansion of this experiment was conducted to investigate the overexpression of NEK9 in SW-480 cells. These were chosen based on a previous study that reported siRNA-mediated depletion of NEK9 had an effect on G1-S-phase progression[224]. The conditions of the experiment included application of actinomycin D or infection with viruses expressing wild-type NEK9, D194N or ΔRCC1 for 24 (Fig. 29), 48 (Fig. 31) or 72 hours (Fig. 33). The various treatments were compared against a control infection with Ad-CMV for all time points indicated. Cells were harvested and fixed with cold ethanol prior to treatment with propidium iodide. They were then subjected to flow cytometry and analyzed for cell cycle distribution.

During the first 24 h of treatment, cells infected with Ad-CMV had approximately 55% of the population in G1 phase, 30% in S phase, 10% in G2 phase, and 7% in sub G1 (Table 8). Mock samples shared a similar distribution, and as expected, actinomycin D treatment caused a significant reduction in G1 and G2 phases, while exhibiting increases in S and sub G1 phases (Fig. 29). Overexpression of wild-type NEK9 did not cause any observable changes. However, overexpression of the NEK9 variants, D194N and ΔRCC1 resulted in an observable shift in the population of cells in G1 to the S phase.

After 48 h, the Ad-CMV infected cells displayed a similar distribution as the 24 h treatment (Table 9). Based on two replicates, mock-infected samples displayed a similar distribution cells to Ad-CMV-treated samples. Actinomcyin D continued to negatively affect cells, as observed in the continued reduction across every phase and a significant increase of cells in sub G1 (Fig. 31). The overexpression of wild-type NEK9 or NEK9 variants, resulted in a general reduction in G1 populations and an increase in S phase compared to Ad-CMV. Furthermore, little change was observed in G2. There was an increase in the sub G1 phase across each condition which may have been due to over population, as these transformed cells continued to grow despite the lack of space, causing in cell death.

There continued to be little change in the distribution of cells in Ad-CMV infected samples after 72 hours. Approximately 55% of cells were found in G1 phase, 20% in S phase, 4% in G2, and 20% in sub G1 (Table 10). Mock cells remained relatively unchanged compared to the Ad-CMV control. The prolonged treatment of actinomycin D resulted in 70% of the population to shift into the sub G1 category (Fig. 33). Cells that overexpressed wild-type NEK9 were marked with a noticeable decrease as only ~17% of the population remained in G1, while over 60% of cells were found in S phase. Similarly, continued expression of D194N resulted in a drop from ~40% in G1 phase at 48 h, to 15% by 72 h post infection. This led to an increase in the S phase population from ~40% to almost 60%. Cells infected with the ΔRCC1-expresing virus also saw a reduction in G1, and a rise in S phase populations, albeit on a smaller scale as compared to wild-type NEK9 or D194N. The population of G2 were relatively unchanged and there was a marked increase across each condition in sub G1 population.

Through a period of time, we observed a gradual shift of cells found in G1 to S phase. There was little difference between the populations in the G2 phase, suggesting that cells overexpressing wild-type NEK9 or its variants, D194N and ΔRCC1, may induce arrest during the S phase. While these findings support the notion that the dysregulation of NEK9 induces cell cycle arrest, it is worth noting that these experiments were conducted in duplicates and warrant additional trials to confirm our observations.

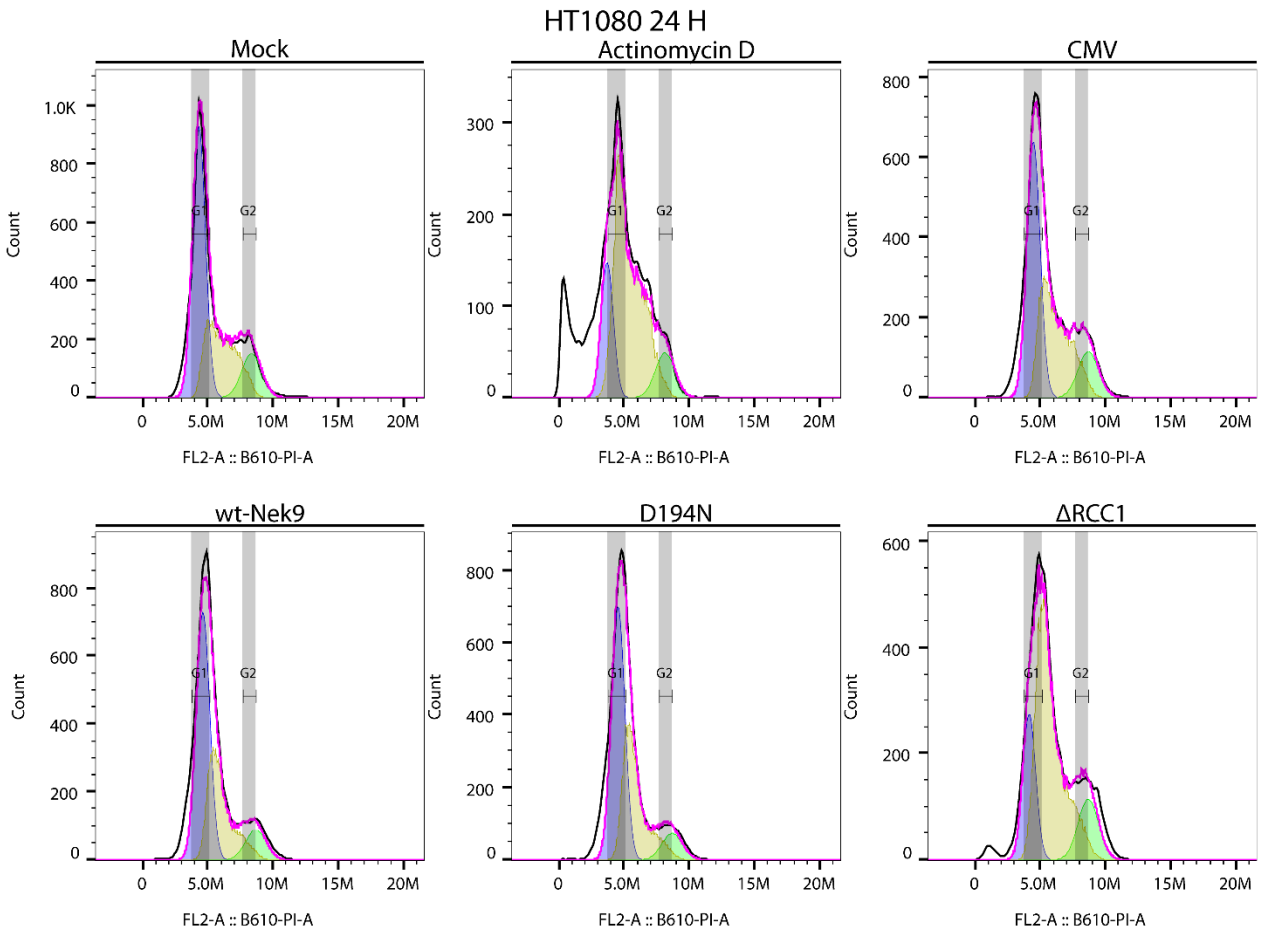

Fig. 26. Cell cycle distribution of HT1080 cells treated with actinomycin D, infected with Ad-CMV or NEK9 viruses for 24 h

HT1080 cells were treated with actinomycin D or infected with Ad-CMV for 24 h. Cells were harvested, fixed with cold ethanol, and stained with PI. The first gate excluded cell debris or aggregates. The second gate excluded doublets. Ancestry of gating is shown in Fig. 44 & Fig. 45. The final population is subjected to cell cycle analysis using the software package from FlowJo (v10.7.1). n = 1.

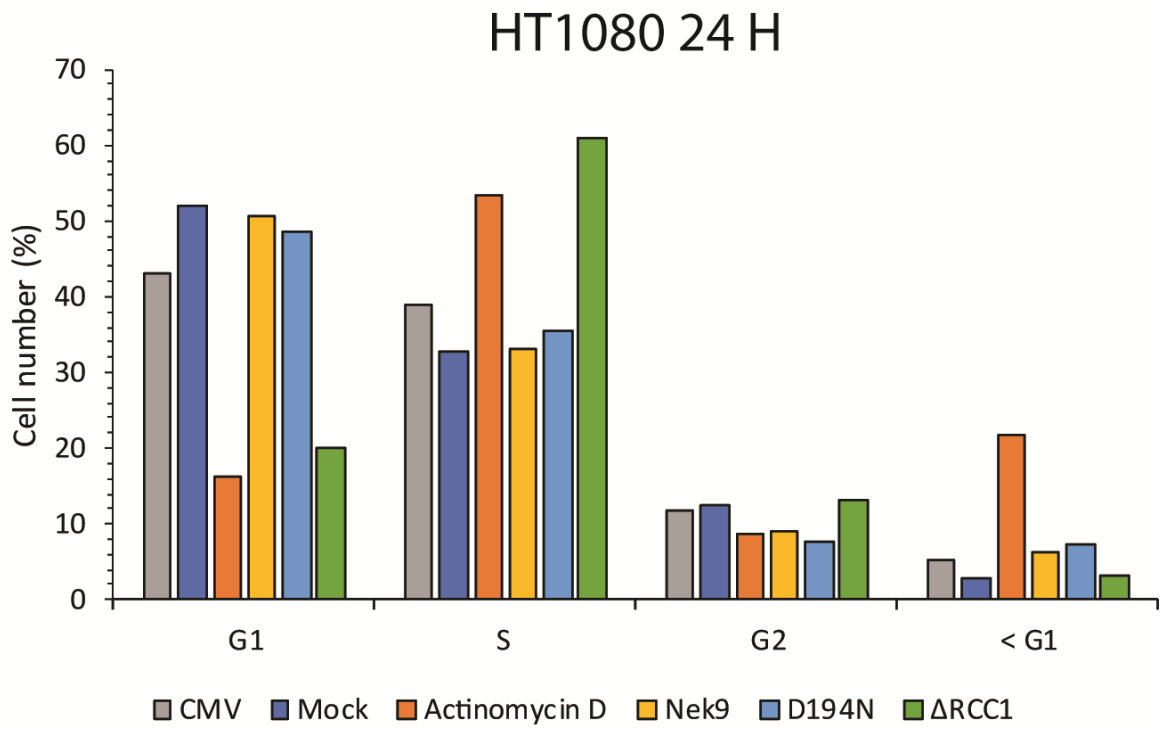

Fig. 27. Cell cycle analysis of HT1080 cells treated with NEK9 viruses for 24 h

HT1080 cells subjected to flow cytometry and cell cycle analysis after 24 h infection with the NEK9 viruses. Cells were treated with Actinomycin D and Ad-CMV to serve as controls. The distribution of cells (events) was analyzed using the cell cycle analysis module from FlowJo version 10.7.1 (BD Biosciences). n = 1.

Table 7. Cell cycle distribution of HT1080 cells treated with NEK9 viruses for 24 h

	% of Population			
	G1	S	G2	< G1
Mock	51.9	32.7	12.6	2.78
Actinomycin D	16.2	53.5	8.57	21.8
CMV	43.1	39	11.8	5.21
NEK9	50.7	33.1	9.18	6.14
D194N	48.5	35.5	7.61	7.17
ΔRCC1	20.1	60.9	13.3	3.34

HT1080 cells were infected with the NEK9 viruses for 24 h and subjected to cell cycle analysis. Cells were treated with Actinomycin D and Ad-CMV to act as controls. The distribution of cells (events) was analyzed using the cell cycle analysis module from FlowJo version 10.7.1 (BD Biosciences). The population of cells expressing the ΔRCC1 display a disrupted cell cycle as compared to D194N and wild-type NEK9 expressing cells, n = 1.

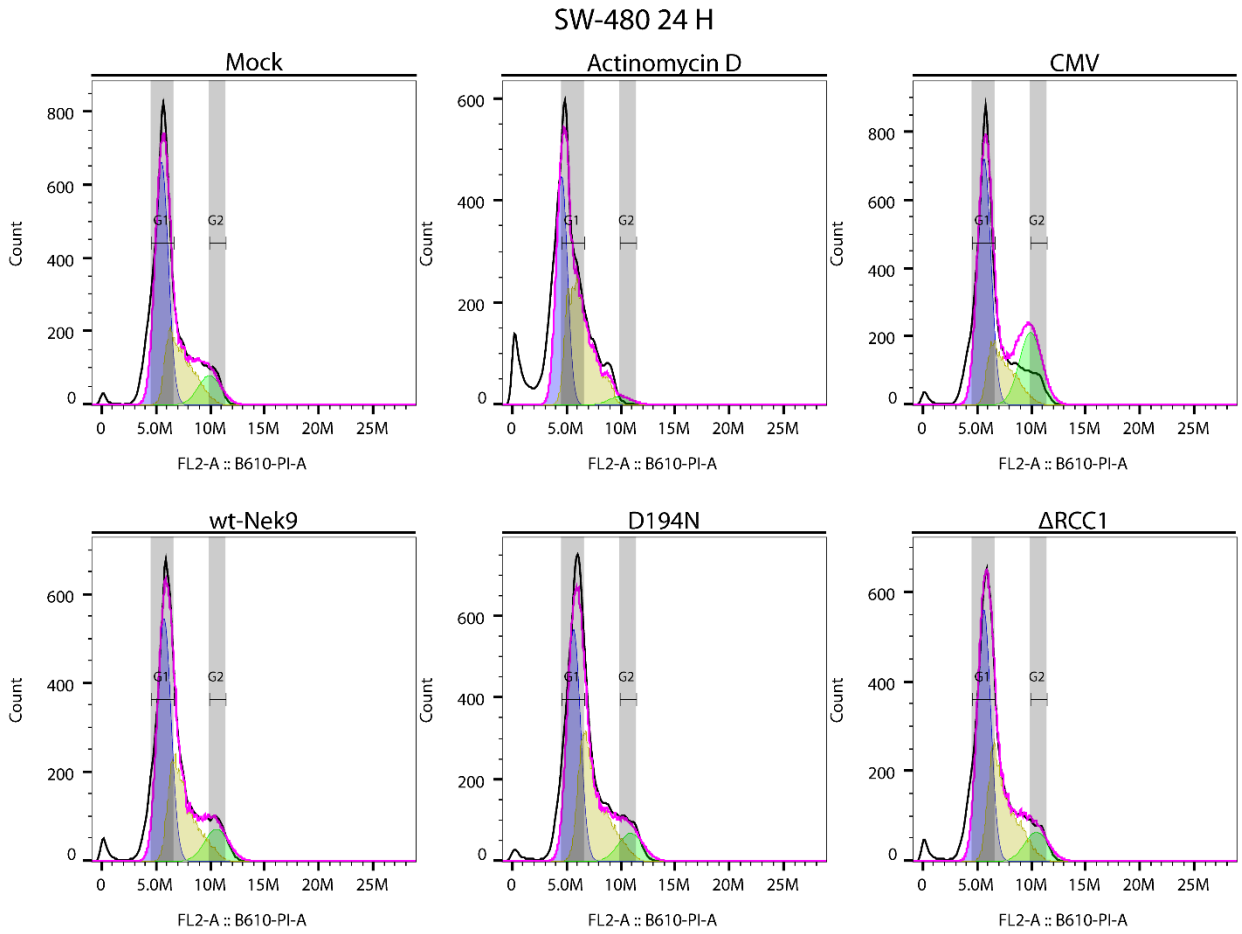

Fig. 28. Cell cycle distribution of SW-480 cells treated with actinomycin D, infected with Ad-CMV or NEK9 viruses for 24 h

SW-480 cells were treated with actinomycin D or infected with Ad-CMV for 24 h. Cells were harvested, fixed with cold ethanol, and stained with PI. The first gate excluded cell debris or aggregates. The second gate excluded doublets. Ancestry of gating is shown in Fig. 46 & Fig. 47. The final population is subjected to cell cycle analysis using the software package from FlowJo (v10.7.1). n = 2.

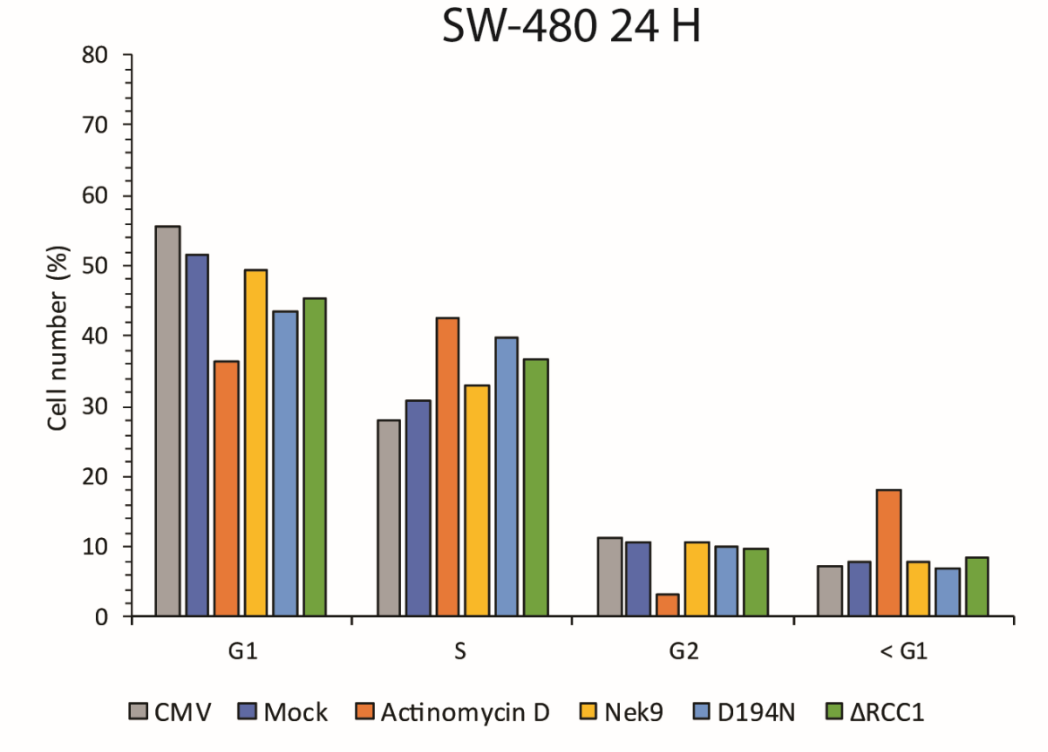

Fig. 29. Cell cycle analysis of SW-480 cells treated with NEK9 viruses for 24 h

SW-480 cells subjected to flow cytometry and cell cycle analysis after 24 h infection with the NEK9 viruses. Cells were treated with Actinomycin D and Ad-CMV to serve as controls. The distribution of cells (events) was analyzed using the cell cycle analysis module from FlowJo version 10.7.1 (BD Biosciences). n = 2, data presented as average of two replicates.

Table 8. Cell cycle analysis of SW-480 cells treated with NEK9 viruses for 24 h

	AVERAGE (% OF POPULATION)			
24 H	G1	S	G2	< G1
CMV	55.55	27.95	11.4	7.375
MOCK	51.55	30.8	10.7	7.925
ACTINOMYCIN D	36.35	42.6	3.11	18
NEK9	49.4	32.9	10.615	7.735
D194N	43.35	39.7	9.915	7.085
ΔRCC1	45.45	36.55	9.8	8.48

SW-480 cells subjected to flow cytometry and cell cycle analysis after 24 h infection with the NEK9 viruses. The distribution of cells (events) was analyzed using the cell cycle analysis module from FlowJo version 10.7.1 (BD Biosciences). Cells were treated with Actinomycin D and Ad-CMV to serve as controls, n = 2.

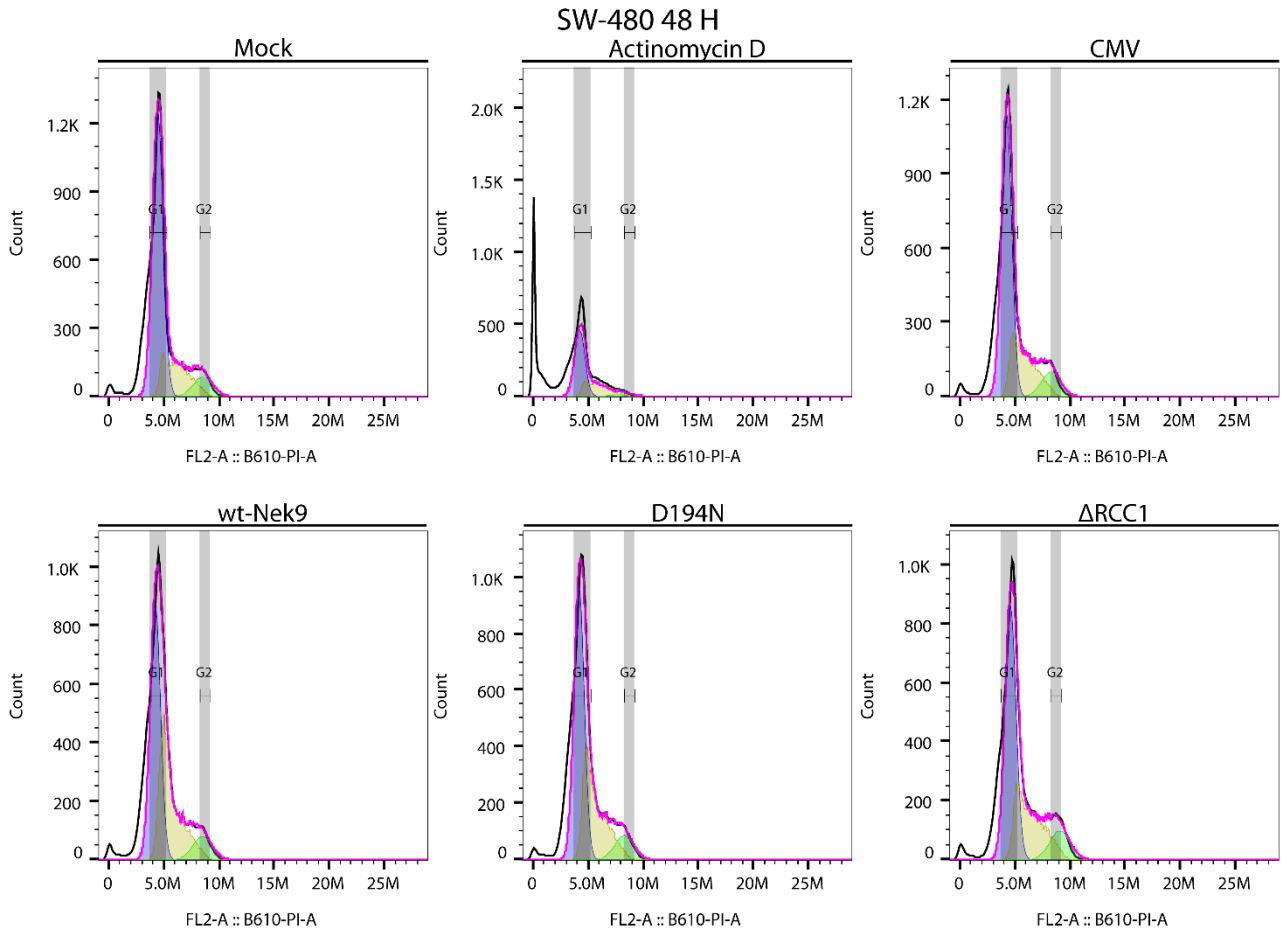

Fig. 30. Cell cycle distribution of SW-480 cells treated with actinomycin D, infected with Ad-CMV or NEK9 viruses for 48 h

SW-480 cells were treated with actinomycin D or infected with Ad-CMV for 48 h. Cells were harvested, fixed with cold ethanol, and stained with PI. The first gate excluded cell debris or aggregates. The second gate excluded doublets. Ancestry of gating is shown in Fig. 48 & Fig. 49. The final population is subjected to cell cycle analysis using the software package from FlowJo (v10.7.1). n = 2.

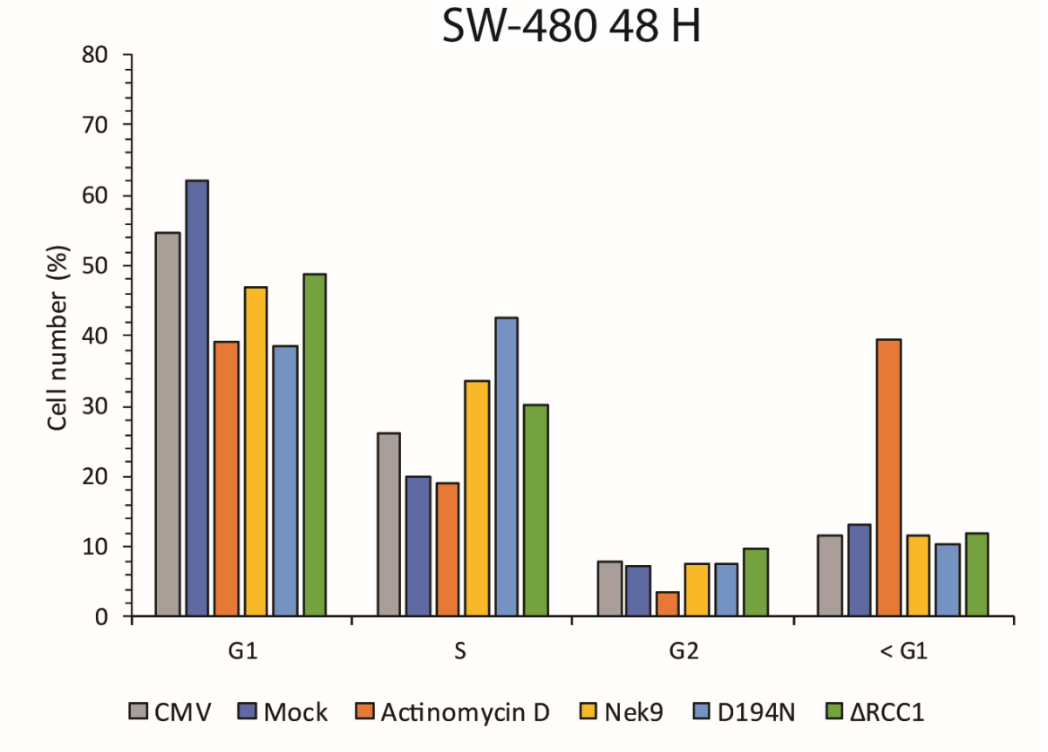

Fig. 31. Cell cycle analysis of SW-480 cells treated with NEK9 viruses for 48 h

SW-480 cells subjected to flow cytometry and cell cycle analysis after 48 h infection with the NEK9 viruses. Cells were treated with Actinomycin D and Ad-CMV to serve as controls. The distribution of cells (events) was analyzed using the cell cycle analysis module from FlowJo version 10.7.1 (BD Biosciences). n = 2, data presented as average of two replicates.

Table 9. Cell cycle analysis of SW-480 cells treated with NEK9 viruses for 48 h

	AVERAGE (% OF POPULATION)			
48 H	G1	S	G2	< G1
CMV	54.7	26.1	8.01	11.75
MOCK	62	19.9	7.335	13.25
ACTINOMYCIN D	39.05	19	3.485	39.55
NEK9	46.8	33.45	7.585	11.55
D194N	38.55	42.7	7.535	10.43
ΔRCC1	48.9	30.1	9.78	11.95

SW-480 cells subjected to flow cytometry and cell cycle analysis after 48 h infection with the NEK9 viruses. The distribution of cells (events) was analyzed using the cell cycle analysis module from FlowJo version 10.7.1 (BD Biosciences). Cells were treated with Actinomycin D and Ad-CMV to serve as controls, n = 2.

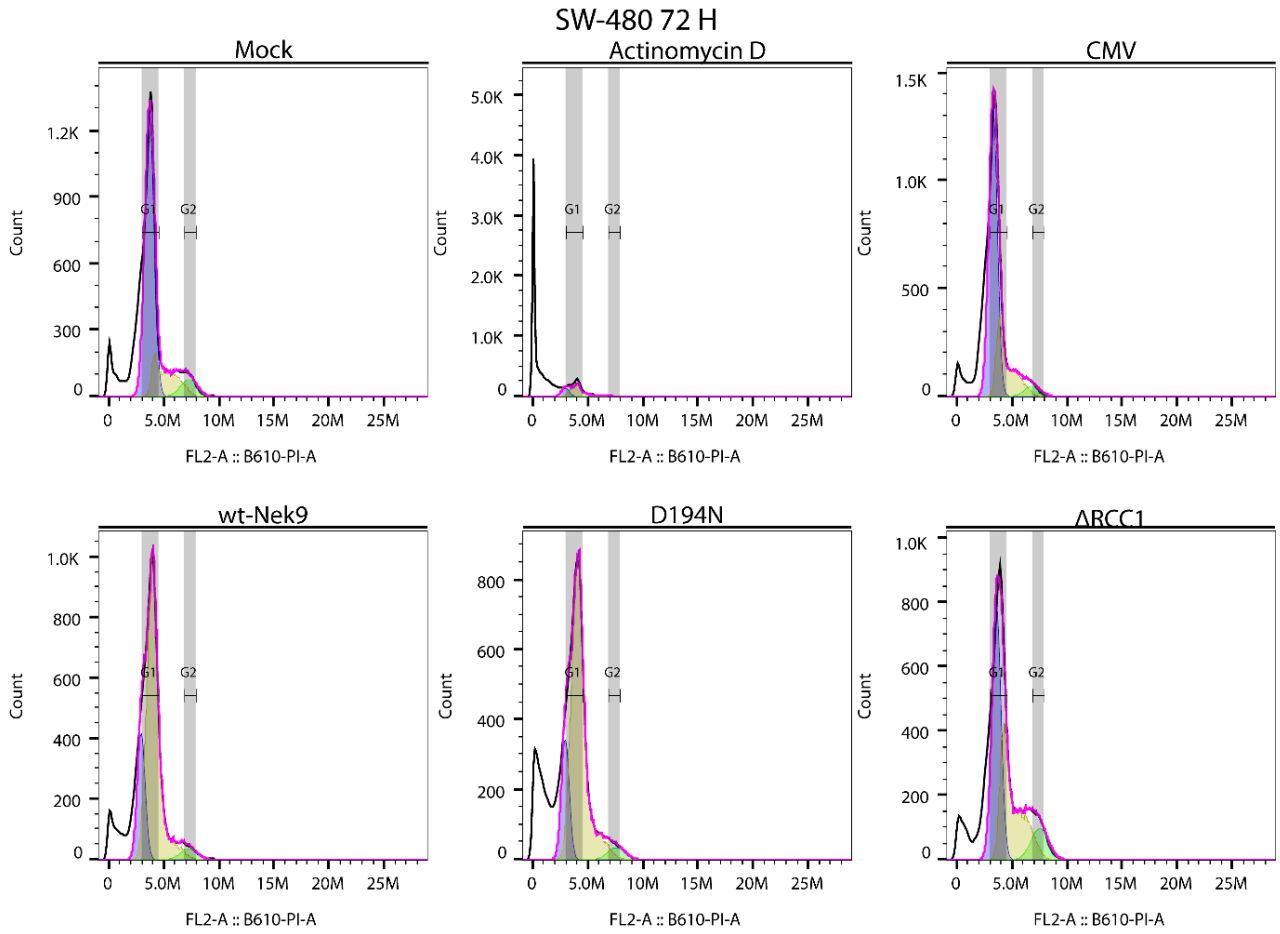

Fig. 32. Cell cycle distribution of SW-480 cells treated with actinomycin D, infected with Ad-CMV or NEK9 viruses for 72 h

SW-480 cells were treated with actinomycin D or infected with Ad-CMV for 72 h. Cells were harvested, fixed with cold ethanol, and stained with PI. The first gate excluded cell debris or aggregates. The second gate excluded doublets. Ancestry of gating is shown in Fig. 50 & Fig. 51. The final population is subjected to cell cycle analysis using the software package from FlowJo (v10.7.1). n = 2.

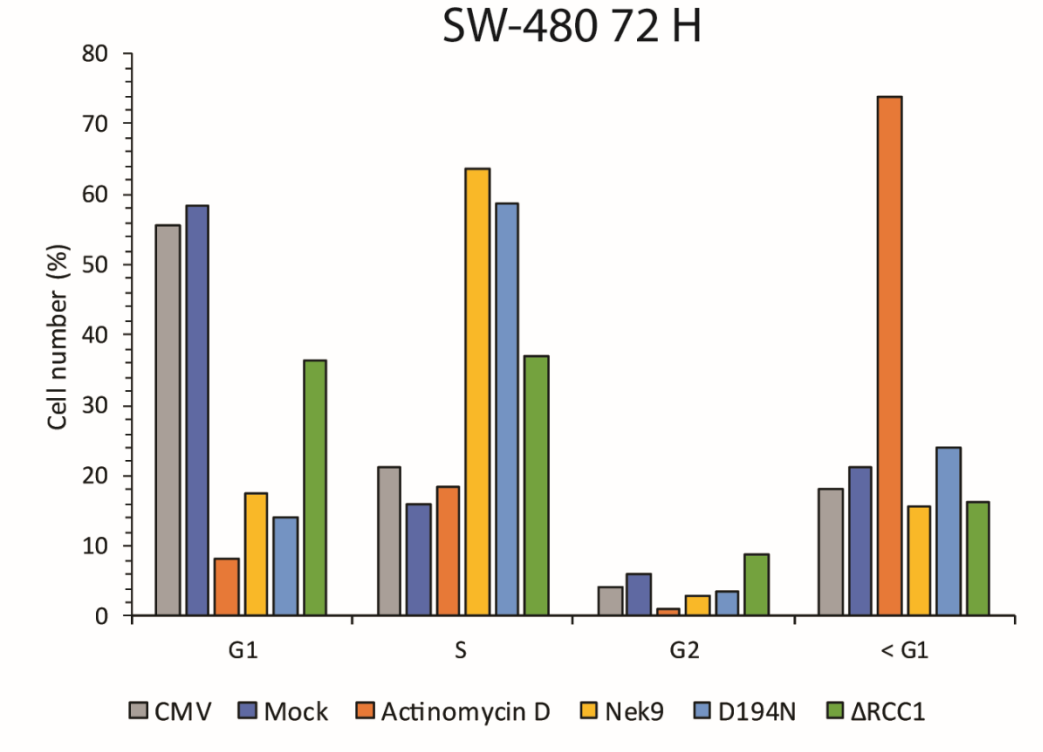

Fig. 33. Cell cycle analysis of SW-480 cells treated with NEK9 viruses for 72 h

SW-480 cells subjected to flow cytometry and cell cycle analysis after 72 h infection with the NEK9 viruses. Cells were treated with Actinomycin D and Ad-CMV to serve as controls. The distribution of cells (events) was analyzed using the cell cycle analysis module from FlowJo version 10.7.1 (BD Biosciences). n = 2, data presented as average of two replicates.

Table 10. Cell cycle analysis of SW-480 cells treated with NEK9 viruses for 72 h

	AVERAGE (% OF POPULATION)			
72 H	G1	S	G2	< G1
CMV	55.5	21.2	4.02	18.05
MOCK	58.35	16	6.135	21.1
ACTINOMYCIN D	8.33	18.45	0.985	73.9
NEK9	17.55	63.75	3.02	15.65
D194N	14.05	58.6	3.435	24
ΔRCC1	36.4	37.1	8.88	16.25

SW-480 cells subjected to flow cytometry and cell cycle analysis after 72 h infection with the NEK9 viruses. The distribution of cells (events) was analyzed using the cell cycle analysis module from FlowJo version 10.7.1 (BD Biosciences). Cells were treated with Actinomycin D and Ad-CMV to serve as controls, n = 2.

2.3.14. HT1080 cells expressing D194N and ΔRCC1 exhibit signs of cell death

Apoptotic morphology in cells that expressed the kinase-inactive variants of NEK9, in addition to the cleavage of PARP pointed towards the possibility that NEK9 was able to trigger apoptosis (Fig. 17). To explore this prospect, HT1080 cells were infected with the control Ad-CMV vector, wild-type NEK9, D194N and ΔRCC1 expressing viruses for 24 h and propidium iodide was used to stain membrane-compromised cells (Fig. 34)[225]. Immediately after infection, propidium iodide was applied and the incorporation of the dye was monitored under a live cell imager. At 24 h post infection, few, if any, cells displayed staining for the propidium iodide-only, Ad-CMV and wild-type NEK9 treated samples. Interestingly, the D194N and ΔRCC1 treated samples exhibited propidium iodide staining, indicative of cells undergoing membrane disruption and were presumably dying. There was also a reduction of cell density in D194N and ΔRCC1 treated samples, compared to wild-type, Ad-CMV and propidium iodide-only treated samples. Furthermore, the effect D194N and ΔRCC1 variants had cells was observed across several other transformed cell lines, regardless of p53 status (Fig. 14, Fig. 15, Fig. 16). These observations support the notion that expression of D194N and ΔRCC1 variants was able to induce or promote cell death.

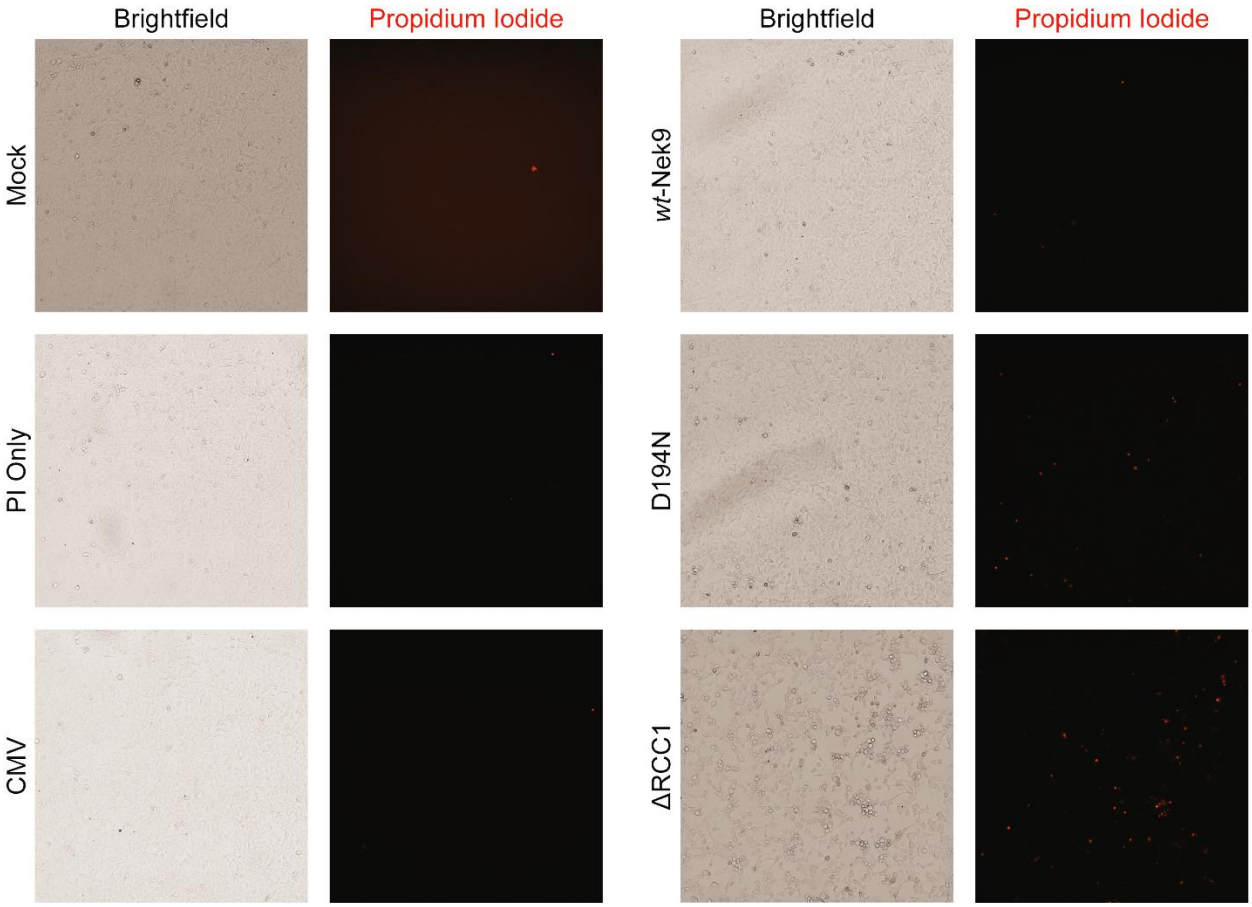

Fig. 34. Propidium iodide exclusion assay

HT1080 cells were infected with Ad-CMV, wild-type NEK9, D194N and ΔRCC1 viruses at an MOI of 20. Cells were treated with propidium iodide and placed in the ImageXpress Micro 4 live cell imager supplied with CO_2. The uptake of propidium iodide was monitored for 24 h. The image displayed is from the endpoint (24 h post infection).

2.4. Discussion

NEK9 was hypothesized to play an active role in the proliferation of transformed cells by acting as a negative regulator to p53-regulated genes involved in cell cycle arrest and apoptosis. Adenoviral vectors were used to overexpress wild-type NEK9, a kinase-inactive variant (D194N) and a RCC1-domain deleted variant (ΔRCC1) to characterize the role of NEK9 in the cell cycle. These roles were first evident when the basal expression of *Nek9* was measured in primary and transformed cells. The levels between two transformed cell lines: ovarian cancer cell line, SK-OV-3 and breast cancer cell line, T47D, expressed *Nek9* mRNA to the highest levels (Fig. 6). Elevated levels of NEK1 and NEK9 have been associated in patients with high-grade serous ovarian cancer (HGSOC)[226], while another study found elevated levels of NEK9 in patients suffering from hormone-receptor (HR) positive breast cancers[130]. In contrast, low expression of NEK9 was common amongst aggressive breast cancer types such as invasive ductal carcinoma (IDC), ductal carcinoma *in situ* (DCIS), usual ductal hyperplasia and atypical ductal hyperplasia. The low expression of NEK9 amongst breast cancer patients also correlated with larger tumour sizes and an overall poorer prognosis[130]. In support of our hypothesis, it seems that dysregulation of NEK9, through enhanced expression or abolishment, promotes abnormal behavior such as causing a delay during G1/S-phase transition[227]. Furthermore, upregulation in breast and ovarian tumour lines is not limited to NEK9 within the NEK family. In fact, NEK2 has also been found to be upregulated in ovarian cancer and breast cancer[97]. In some ovarian cancers, the transcription factor, HIF-1a, upregulates the expression of NEK6, which lead to the activation of genes that promote the inhibition of apoptosis and drug efflux activation[103]. The final NEK protein that has been associated with ovarian cancer is NEK11, which is able to interact with up to 22 proteins and 4 small molecules that aid in drug treatment resistance against ovarian cancer[228]. As previously mentioned, the increased expression of NEK9 does not immediately implicate it as an oncogenic factor. Additionally, high levels of mRNA do not directly translate into high levels of protein. However, given the history of NEK proteins in relation to their promotion of tumour resilience, a closer inspection of NEK9 was warranted.

The results of the transformation assay involving the overexpression in MEF-inducible cell lines infected with wild-type adenovirus (*dl*309) corroborates earlier notions that NEK9 may be a proto-oncogene. Adenovirus has played an essential role as a model of early oncogenesis and has the capability of transformation rodent cells[229]. Ectopic expression of a NEK9 substrate, NEK6,

has been reported to transform rodent cells (JB6 C141) via phosphorylation of a transcription factor; STAT3[230]. In the current study, a large proportion of cells that were infected and induced were transformed and produced foci (*Fig. 7*). While overexpression or infection with adenovirus individually produced foci, it was the combination of these two conditions which enhanced the transformation of MEF cells. This suggested that the deregulation of NEK9 in conjunction with a mutagenic agent (adenovirus) promoted transformation. Speculatively, increased levels of NEK9 may have resulted in enhanced phosphorylation of downstream substrates such as NEK6. In conjunction with the inhibition of tumour-suppressor pathways during adenovirus infection, this may have led to the enhanced transformation of MEF cells. While the link between NEK9, E1A and transformation remains unclear, these observations support our hypothesis, that NEK9 operates not only as a critical factor in the proliferation and survival of tumour cells but is also capable of participating in transformation.

The next objective was to investigate the method by which NEK9 promotes transformation. The results of the luciferase assay indicated that in presence of NEK9, p53 promoter activity was markedly reduced (Fig. 8). Thus, a sufficient quantity of NEK9 may be able to suppress the activity of p53-regulated promoters. Two other members of the NEK family are able to affect p53 activity. NEK2 has been shown to directly inhibit p53 by phosphorylating Ser315, enhancing its sensitivity to degradation[231]. NEK10 can phosphorylate Tyr327 of p53, enhancing the transcription of downstream p53 target genes in presence of DNA damaging agents[232]. Unlike NEK2 and NEK10, NEK9-mediated suppression of p53 activity is likely indirect, as interaction between NEK9 and p53 has not been established[224]. Despite this, the innate ability of NEK9 to suppress p53 activity was further substantiated, when the expression E1A alongside NEK9 did not further reduce p53 activity compared to NEK9 alone. It is possible that NEK9 works in tandem with E1A, or other viral proteins that are known to antagonize the apoptotic or growth-arrest properties of p53, such as the E1B (E1B-19K, E1B-55K) or E4-Orf6 proteins[233]. This provides further insight as to why NEK9 is recruited by E1A during infection.

The research to characterize the relationship between NEK9 and the p53 network continued with a look into the expression of p53-regulated genes. These genes (*MDM2*, *PIG3*, *PUMA*, *GADD45α*) are essential to the tumour suppressing network as they act in concerted effort to prevent the replication of abnormal cells[49]. According to a previous study, the promoter of *GADD45α* was occupied by NEK9 and E1A. As a result, *GADD45α* was inhibited during the

infection of adenovirus[50]. The depletion of NEK9 in transformed cells expressing wild-type p53 did not significantly affect levels of *PIG3*, *PUMA* and *GADD45α* (Fig. 10). In contrast, transformed cells with mutant p53 saw enhanced expression of *MDM2*, *PIG3*, *PUMA* and *GADD45α* when depleted for NEK9. There are several possibilities that may explain these differences. NEK9 may act as a regulator of p53-promoters and work in conjunction with p53 to regulate the expression of *PIG3*, *PUMA* and *GADD45α*. In presence of mutant p53 that is unable to tightly regulate the activity of *PIG3*, *PUMA* and *GADD45α*, transformed cells may opt to enhance and promote the expression of NEK9 to compensate for the lack of functional p53, though further investigation of this relationship is required. Hence, it may prevent the induction of cell cycle arrest or apoptosis, enabling the uncontrolled growth of the mutant-p53 cell lines. Even with these results, the relationship between NEK9 and p53 has yet to be fully elucidated.

An investigation into the expression of stress-related biomarkers in NEK9 depleted cells was conducted. Several members from the BCL-2 family of proteins were chosen. The BCL-2 and BCL-xL proteins are responsible for the prevention of apoptosis, while the BAD and BAX proteins push the cell towards programmed death. Given the upregulation of *PUMA*, *PIG3*, and *GADD45α* upon knockdown of NEK9 in the p53-mutant cell line SK-OV-3, it was surprising to see that the proapoptotic markers were suppressed (Fig. 12). Unexpectedly, in the p53 wild-type cell line, A549, both proapoptotic (Fig. 12) and antiapoptotic (Fig. 13) markers were significantly upregulated in cells lacking Nek9. However, in HT1080 cells, expression of these markers remained largely unaffected. This suggested that the consequence of the depletion of NEK9 was not contingent on the p53 wild-type status of the cell. It is important to note, that the elevated expression of *BAD* or *BAX* does not necessarily translate into elevated protein levels nor induction of apoptosis. According to these results, NEK9 may have an impact on BCL-2 family activation. However, the disparity between these cell lines remains unclear and warrants a future investigation.

To better understand the effects of NEK9 dysregulation, we conducted several assays to determine the outcome of prolonged expression of wild-type NEK9 or its variants in several cell lines. Apoptotic morphology was first observed in HT1080 (Fig. 14), A549 (Fig. 15), and SK-OV-3 (Fig. 16) cells overexpressing wild-type NEK9 or its variants; D194N and ΔRCC1. The cleavage of the poly (ADP-ribose) polymerase (PARP) protein was another indicator of apoptosis. In presence of genomic stress or DNA damage, activated PARP is responsible for the immediate

response by repairing damaged DNA[40]. PARP is inactivated through cleavage by caspase-3 or caspase-7, driving the cell towards death. This serves two main purposes: to maintain genetic integrity of the cell, and to restrict the energy-intensive process of repairing DNA[234]. A western blot of SK-OV-3 cells that expressed either D194N or ΔRCC1 revealed the presence of cleaved PARP, initially at 48 h into infection, and substantially at 72 h (Fig. 17). Overexpression of wild-type NEK9 has been reported to cause toxicity and death in HeLa cells[124]. A mutation that led to the complete loss of NEK9 was marked with a significant reduction in fibroblast cilia length and quantity, along with impaired proliferation[100]. These findings suggest that deregulation of NEK9 has the capacity to induce apoptosis, either through overexpression of wild-type, or its variants.

Cellular senescence, or permanent cell cycle arrest, is a conceivable consequence of aging cells or lack of nutrients. This may also be triggered in presence of mutagenic distresses, as in the case of oncogene-induced senescence (OIS) wherein cells undergo permanent arrest in response to dysregulated oncogene expression[82,235]. According to previous results, NEK9 may be a putative proto-oncogene, so the prospect of cells facilitating OIS was examined. Staining of β-galactosidase-like activity across cells expressing wild-type NEK9, D194N and ΔRCC1 suggested that cells were not undergoing cellular senescence (Fig. 18). Previously, it had been reported that depletion of NEK9 induced senescent-like features in cells[78], which may be explained by the possibility that p21 is regulated by NEK9[50]. CDKN1A, or p21, is a prominent inducer of cell cycle arrest upon activation via p53. Chromatin immunoprecipitation experiments have found that the p53-promoter of p21 is occupied by NEK9[134], and that depletion of NEK9 in p53-mutant cells resulted in enhanced expression of p21[134]. Furthermore, the knockdown of NEK7 (substrate of NEK9) has led to the degradation of telomeres, while overexpression of NEK6 was shown to suppress p53-induced senescence in cancer cells[236–238]. Based on the staining between cells expressing wild-type NEK9 or the variants, it cannot be sufficiently concluded that NEK9 participated in the induction of cellular senescence.

Aside from the canonical function of NEK9 regarding cilia development and spindle formation, NEK9 has been shown to drive cell migration in EML4-ALK cancer patient samples through interaction with NEK7[123,239]. Elevated levels of NEK9 in patients correlated with poorer rates of survival compared to those with low levels of NEK9. Using our highest NEK9-expressing cell line based on mRNA levels (Fig. 6), SK-OV-3, a similar experiment was conducted via the scratch assay. The knockdown of NEK9 mediated by siRNA treatment or expression of the D194N

or ΔRCC1 variants resulted in poor closure of the gap by 24 h (Fig. 21). Based on the cleavage of PARP and apoptotic morphology, it was decided that depletion of NEK9 did not solely impair motility, but also affected cell viability either through hampering cell proliferation or induction of cellular arrest and eventually apoptosis.

It was unclear whether expression of D194N or ΔRCC1 hampered cellular motility, as previously published[123], or if the rate of proliferation had been hindered. The results obtained from the MTT assay regarding the cell viability of HT1080 cells expressing D194N or ΔRCC1 confirmed our hypothesis that these variants impaired the proliferation of the cells. By 72 h, cell viability was significantly reduced compared to mock-infected cells. While the consequence of dysregulating NEK9 using these variants has been examined briefly, the affected pathways remain a mystery.

The work conducted by Sheng-Chung Lee's group characterized NEK9 as a protein that associates with the heterodimeric transcription and replication factor; FACT (SPT16 Homolog, Facilitates chromatin remodeling subunit). They found that the knockdown of NEK9 in HeLa cells triggered a delay during interphase[125]. Prolonged knockdown and multiple passages of HeLa cells lacking NEK9 produced noticeably smaller colonies, which were believed to be the result of slower cell growth. Further inspection revealed that HeLa cells that were depleted for NEK9 experienced stalled progression of the G1 phase and lagged behind control cells when progressing towards S-phase[125]. Another group discovered that Caki12 (kidney) and U1242 (glioblastoma) cells were inhibited for proliferation when subjected to siRNA-mediated depletion of NEK9[240]. These findings differ from the work of Pelka *et al.* in 2007, who reported that siRNA-mediated depletion of NEK9 did not affect cell cycle progression[211]. In the current study, we saw an impact on S-phase progression in cells disrupted for wild-type NEK9 based on flow cytometry data (Fig. 26). The overexpression of the wild-type NEK9, D194N or ΔRCC1 caused delay during the S-phase of the cell cycle as there was a shift of cell populations between the G1 and S-phase populations compared to mock-infected samples (Fig. 27, Fig. 33). Phosphorylated NEK9 had been previously reported to preferentially associate with the FACT complex, and the interaction between these proteins peak at G1/S-phase[125]. The disruption of the Spt16 component of the FACT complex in yeast led to the toxic accumulation of free histones during transcription, resulting in G1 delay[241,242]. It is possible that the expression of kinase-inactive variants may disrupt the association between wild-type NEK9 and the FACT complex, which may lead to a delay during the S-phase. Despite

these reports, it is important to clarify whether the impact on S-phase induction and putative arrest is a result of disrupted phosphorylation between NEK9 and its substrates, NEK6 and NEK7, or is independent of NEK9's kinase activity.

The fate of cells expressing the NEK9 variants, D194N or ΔRCC1 was thoroughly investigated. Based on propidium iodide staining, the cells that expressed the NEK9 variants were subjected to membrane disruption and cell death (Fig. 34). However, propidium iodide is membrane impermeable and is not normally associated with apoptosis. Apoptotic cells retain membrane integrity until they are effectively phagocytosed by leukocytes or other scavenger cells in the body[69]. Propidium iodide is instead known to penetrate and mark necrotic cells, as this endpoint commonly resolves into the disruption of the cell membrane, allowing it to enter the nucleus and stain double-stranded DNA[225]. A close inspection of D194N and ΔRCC1 treated cells revealed cell morphology associated with apoptosis such as membrane blebbing, apoptotic bodies and microtubule spikes (Fig. 14, Fig. 15, and Fig. 16). The western blot assay revealed the cleavage of PARP, resulting in a band at 90 kDa and 23 kDa, which indicated that apoptosis occurring. Protein bands 50 kDa were detected, suggesting necrolytic cleavage of PARP had also occured[234,243]. Taking all of the results into consideration, the D194N or ΔRCC1 variants were likely inducing apoptosis in cells. Due to the nature of the experiments, cells also displayed signs of secondary necrosis. To clarify, the experiments performed to assay apoptosis were conducted on a mono-population of cells that were grown on plastic wells. The experimental environment lacked the dynamic and diverse cast of cells that populate the human body. The endpoint of apoptosis is the phagocytosis of dying cells via scavenger cells, and in the experiments performed in this study, the scavenger cells were simply absent. Therefore, the apoptotic cells may have diverged from the canonic path of apoptosis and underwent secondary necrosis. This end point mirrored that of primary necrosis, which resulted in membrane disruption and leakage of the cytosol into the intermembrane space[69]. It may explain why cells exhibited characteristics of both apoptosis and necrosis.

Altogether, our data support the notion that NEK9 acts as a transcriptional regulator for p53-target genes in transformed cells. We have provided evidence to suggest the overexpression of wild-type NEK9, or NEK9 variants induces apoptosis in some cells. We have shown that factors such as wild-type p53 status, cell-type, and the basal expression of NEK9 influence the outcome of our treatments. This context will be important for any future research that may probe into the

therapeutic potential of NEK9 inhibitors. Previous reports using dabrafenib, a chemotherapy drug, led to the inhibition of NEK9 and CDK16. This was associated with the reduced proliferation of a *BRAF*-mutant melanoma[132]. As with any form of treatment, it is important to note that the therapeutic application of NEK9 may only benefit a subset of patients.

The results of the current study have shown that NEK9 may be a target for cancer research. Elevated levels of NEK9 have the capacity to suppress p53 activity which may aid in transformation during infection of adenovirus in rodent cells. On the other hand, depletion of NEK9 led to the upregulation of tumour suppressor genes in some p53-mutant cell lines. This suggests that cancer cells tolerate the disruption of NEK9 to an extent that permits the progression of mitosis without inducing tumour suppression pathways. In some ways, this draws similarities to genes that maintain physioxic levels and the response to hypoxia. Short periods of exposure to hypoxia are regulated by HIF genes, which prevent the accumulation of ROS, whilst stimulating the formation of new blood vessels[244]. Extensive exposure to hypoxia impairs DNA repair systems, causes extensive DNA damage, and compromises the genomic stability of the cell. As a result, the cell is pushed towards apoptosis to eliminate the affected populations[57]. During oncogenesis, it is believed that tumours are subjected to oscillating periods of hypoxia, wherein ROS cycle between low and high levels to promote mutagenesis through DNA damage but diminish prior to reaching the threshold that activates tumour suppressor networks[57,244]. Like hypoxia, it is important to understand the balance that enables NEK9 to participate in mitosis, without promoting transformation or triggering arrest and apoptosis.

Our research was unable to elucidate the specific pathways mediated by NEK9 that lead to cellular arrest and apoptosis, but we hope that future investigations will elaborate on the relationship between NEK9 and the p53. The earlier findings that describe the disruption of spindle dynamics, induction of cell cycle arrest and repressed centrosome segregation in the absence of NEK9 strongly support the hypothesis that NEK9 is capable of mediating arrest and apoptosis[118,240].

Chapter 3: Identifying NEK9 substrates using an *in vivo* screening assay

3.1. Introduction

This brief section will focus on the development of an assay to identify NEK9 substrates using an *in vivo* screen. Kinase arrays have allowed researchers to determine and generate lists of putative kinases and their respective substrates[245]. Other methods such as kinase microarrays or bioinformatic prediction analysis, have been widely used as high throughput assays, but these methods are limited to *in vitro* or *in silico* studies[246,247]. This is a limitation as kinase-substrate interactions rely on a multitude of factors within the dynamic environment of the cell. For example, temporal expression, localization, abundance, activators, and inhibitors all play an important role in the interaction between a kinase and substrate[92,248,249]. These features cannot generally be simulated in an *in vitro* experiment.

Previous work had generated an assay to visualize the interaction between two proteins *in vivo*[210]. The current study proposes a high throughput *in vivo* assay as a primary screen for kinase-substrate binding. The principle of this assay relies on the co-localization of two proteins: the anchor protein (a fusion protein consisting of the kinase of interest tagged with a fluorescent protein and a LacI binding domain) and the prey protein (a substrate phosphosite tagged with a fluorescent protein). These proteins would be expressed in a CHO cell line that contains LacO arrays inserted into the genome. The anchor protein would bind and localize to the LacO sites. Subsequently the prey would localize alongside the anchored kinase if the phosphosite of the prey protein interacts with the anchored kinase. The result will be an overlap of fluorophore signals, suggesting a positive interaction between the two proteins. In the case of a negative interaction, the prey signal to appear diffuse in the cell, and only the anchor protein will be localized to the LacO sites[210].

3.2. Material and Methods:

3.2.1. Cell lines

CHO Chinese hamster ovarian cells were grown on Ham's F-12 nutrient mixture media supplemented with 10% fetal bovine serum and 1% streptomycin/penicillin (100 µg/mL streptomycin, 100 U/mL penicillin) (Hyclone). Cell culture were kept in T175 flasks (SARSTEDT) at stable temperature of 37°C at 5% CO_2.

3.2.2. Generating fluorophore-tagged constructs

To generate the pCAN-myc-mCherry-LacI plasmid, a LacI insert containing SV40 NLS was cloned into pCAN-myc expression vector using XbaI sites to generate pCan-myc-LacI. Next, the mCherry coding region (with XhoI sites at 5' and 3' end) was PCR amplified from pF9LacI-mCherry using the primers found in Table 11. The mCherry-XhoI insert was treated with T4 Polynucleotide kinase (PNK) to remove 3' phosphoryl groups and enable blunt end cloning into pCAN-myc. Finally, mCherry-XhoI was inserted into the pCAN-myc-LacI to generate pCAN-myc-mCherry-LacI.

To generate the pCAN-myc-NEK9-mCherry-LacI plasmid, the coding region of *Nek9* was amplified using PCR and subcloned into the BAMHI site of pCAN-myc-mCherry-LacI. This process was repeated with the NEK9 mutant D194N to generate pCAN-myc-mCherry-D194N.

To generate the pEGFP-NEK6-Phosphorylation-site plasmid, forward and reverse primers were designed based on the NEK6 phosphosite found through KinaseNET[250]. Forward and reverse primers (Table 11) were PCR amplified and cloned into the BamHI and EcoRI site of the pEGFP expression vector. The NEK9 TYR phosphosite was generated by point mutation (substitution of T210 to Y210).

The remaining phosphosite plasmids were generated as described above.

Table 11. Substrate screen oligo list

Name	**Forward (3'-5')**	**Reverse (5'-3')**

mCherry + XHOI sites	ATCGCTCGAGGTGAGCAAGGGCGAGGAGGAT	ATCGCTCGTAGAAGGCGCGCCCATGCACGTGGAGC
NEK6 Phosphosite	AATTCGGTGGTAGCGAAACCACCGCGGCGCATAGCCTGGTGGGCACCCCGTATTATTAAG	GATCCTTATCGCTTTGGTGGCGCCGCGTATCGGACCACCCGTGGGGCATAATAACCACCG
NEK7 Phosphosite	AATTCGGTGGTAGCAAAACCACCGCGGCGCATAGCCTGGTGGGCACCCCGTATTATTAAG	GATCCTTATCGTTTTGGTGGCGCCGCGTATCGGACCACCCGTGGGGCATAATAAACCACCG
NEK9 Phosphosite	AATTCGGTGGTAGCGAATATAGCATGGCGGAAACCCTGGTGGGCACCCCGTATTATTAAG	GATCCTTATCGCTTATATCGTACCGCCTTTGGGACCACCCGTGGGGCATAATTAACCACCG
NEK9 TYR Phosphosite	AATTCGGTGGTAGCGAATATAGCATGGCGGAATATCTGGTGGGCACCCCGTATTATTAG	GATCCTTATCGCTTATATCGTACCGCCTTATAGACCACCCGTGGGGCATAATAACCACCG
NEK9 Consensus Phosphosite	AATTCGGTGGTAGCGGCCGCGAACGCCGCCTGAGCGTGGTGCCGCGCCCGTATCGCTAAG	GATCCTTAGCGATACGGGCGCGGCACCACGCTCAGGCGGCGTTCGCGGCCGCTACCACCG
CAMK1 Phosphosite	AATTCGGTGGTCGCCCGCTGCGCCGCCGCCTGAGCGAACCGAACCTGCAGGCGAACTAAG	GATCCTTAGCGGGCGACGCGGCGGCGGACTCGCTTGGCTTGGACGTCCGCTTGAACCACCG

3.2.3. Microscopy & Imaging

CHO cells were plated at 40,000 cells per well using a hemocytometer on chamber slides (Thermofisher) and were subsequently transfected by adding a master mix (1 µg of LacI-mCherry-

NEK9, 1 µg of GFP-tagged NEK6 protein expressing plasmid DNA and 5 µL polyethylenimine (PEI) (1 mg/mL)[153]. The LacI-mCherry protein expressing plasmid was used as a negative control. Cells were treated for 24 h to allow uptake of plasmid and subsequent expression of proteins prior to imaging using Zeiss LSM700 confocal laser scanning microscope. Images were analyzed using Zeiss ZEN software package.

Table 12. Kinase assay plasmids

PPB	Name	Features
581	pCAN-myc-mCherry-LacI	Mammalian expression vector for an mCherry-tagged Lac repressor
593	pCAN-myc-NEK9-mCherry-LacI	Mammalian expression vector for an N-terminal myc-tagged NEK9, mCherry tag and Lac repressor
610	pCAN-myc-mCherry-LacI-D194N	Mammalian expression vector for an N-terminal myc-tagged D194N, mCherry tag and Lac repressor
587	pEGFP-NEK6-Phosphorylation site	Expression vector of an N-terminal GFP-tagged NEK6 phosphorylation site
588	pEGFP-NEK7-Phosphorylation site	Expression vector of an N-terminal GFP-tagged NEK7 phosphorylation site
582	pEGFP-NEK9-Phosphorylation site	Expression vector of an N-terminal GFP-tagged NEK9 phosphorylation site
583	pEGFP-NEK9-TYR-Phosphorylation site	Expression vector of an N-terminal GFP-tagged NEK9

		(Tyr substitute for T210) phosphorylation site
585	pEGFP-Consensus-Phosphorylation site	Expression vector of an N-terminal GFP-tagged Consensus phosphorylation site
584	pEGFP-Camk1-Phosphorylation site	Expression vector of an N-terminal GFP-tagged Camk1 phosphorylation site

3.3. Results & Discussion

To test the substrate screen, plasmid expression vectors were constructed based on the established interactions between NEK9 and its known substrates. Wild-type NEK9 and the D194N variant were assessed as anchor proteins against prey that consisted of the NEK6, NEK7, wild-type NEK9 or NEK9 (consensus)-phosphosites. Additionally, plasmids expressing CAMK1 and a NEK9 phosphosite-mutant (NEK9 TYR) were generated to act as negative controls for the anchor proteins. Ideally, each prey, apart from CAMK1 or NEK9 TYR, would have colocalized with the wild-type NEK9 anchor, but not D194N, due to its inactive kinase site.

Primary results have indicated the successful expression of LacI-mCherry, LacI-mCherry-NEK9 and LacI-mCherry-D194N in CHO cells. Each fusion protein localized to the expected LacO sites within CHO cells. Furthermore, the expression of GFP-tagged NEK6, NEK7 NEK8, wild-type NEK9, NEK9 consensus site, NEK9 Tyr, and CAMK1-phosphosites were successful in CHO cells.

Initial microscopic observations revealed colocalization between the GFP-tagged NEK6-phosphosite and the LacI-mCherry-tagged wild-type NEK9 in CHO cells, as seen in the top row of Fig. 35, suggesting an interaction between wild-type NEK9 and the phosphosite of NEK6. However, expression of the empty fusion protein, LacI-mCherry, alongside GFP-tagged NEK6-phosphosite, also displayed localization (bottom row of Fig. 35). This implied that the previous interaction between GFP-tagged NEK6-phosphosite and the LacI-mCherry-tagged wild-type NEK9 was nonspecific. It was worth noting that GFP-tagged NEK6-phosphosite was dispersed evenly throughout the cell when expressed alone, indicating that it did not have an affinity towards the LacO sites.

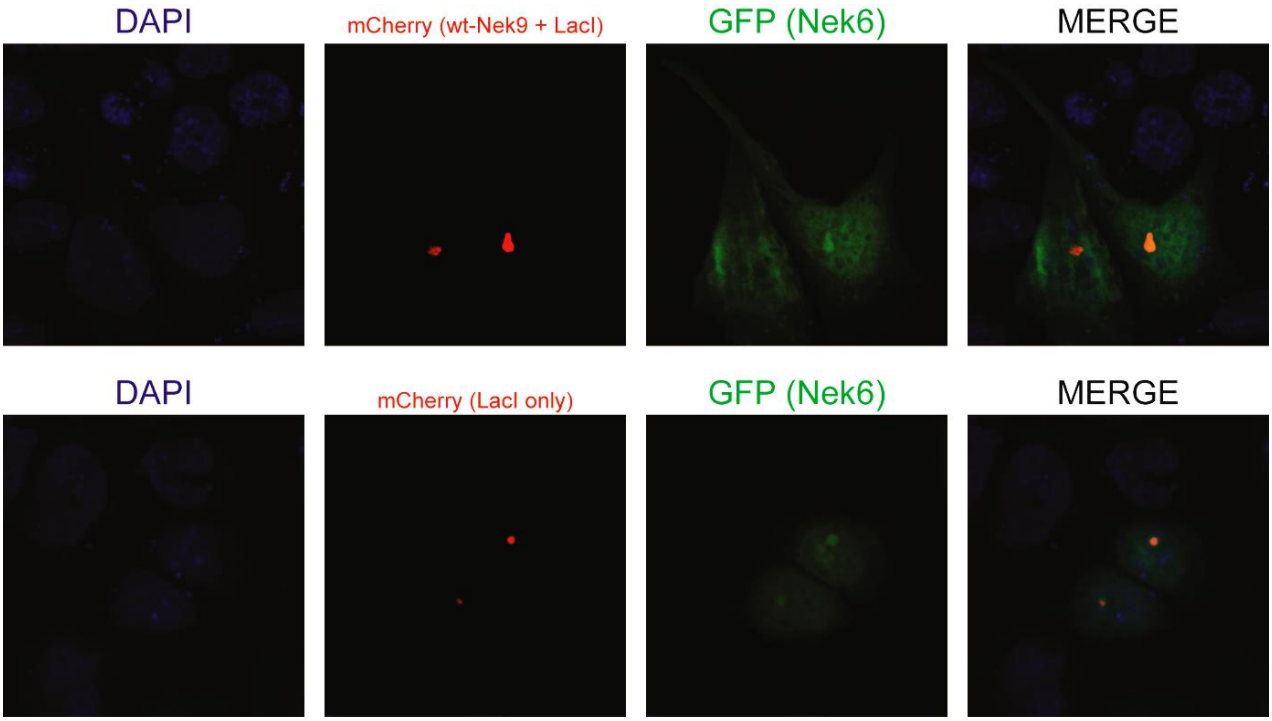

Fig. 35. CHO cells expressing fluorescent NEK9 kinase and NEK6 substrate

CHO cells transfected with plasmids expressing mCherry NEK9-LacI (RED) or mCherry LacI only (RED) and GFP-tagged NEK6 (GREEN). Nucleus of the cell is stained with DAPI (BLUE). Colocalization may be observed in both conditions under the MERGE column.

Previous studies have revealed two possible mechanisms by which NEK9 is able to activate NEK6. The first mechanism is through direct phosphorylation of Ser206 in the activation loop[251]. The second mechanism that has been proposed, based on experiments with NEK7 which shares 87% amino acid identity with NEK6, is an interaction with a noncatalytic domain of NEK9 that causes a structural shift in NEK6 into an active state[116,220,252]. As it currently stands, the GFP-tagged NEK6 expresses the phosphosite (15 amino acids) of NEK6, instead of the full-length protein (313 amino acids). It is possible that secondary features absent from the active site, such as additional binding sites or structures, are important to the interaction between NEK9 and NEK6.

Overall, these findings are indicative of the complex nature of kinase-substrate interactions, and additional work must be completed to optimize the *in vivo* assay. Based on the current state of the assay, we cannot draw any appropriate conclusions to support or reject our hypothesis. Ideally, this screen would offer valuable insight to the transient interactions between kinases and substrates, while simultaneously providing a platform to research kinase-inhibitors in a suitable environment.

Chapter 4: Temporal dynamics of adenovirus 5 gene expression in normal human cells

Co-Authorship Statement

Chapter 3 (section 4.1 – section 4.3) was published in PLOS ONE and accepted on January 9th, 2019 as referenced in Crisostomo *et al.* 2019[254]. Dr. Peter Pelka designed the experiments and composed the manuscript. I was involved in infecting, harvesting, and processing samples with the help of Andrea Soriano, Drayson Graves and Megan Mendez. Additionally, Megan Mendez performed the experiments involving the digital droplet PCR instrument. I participated in designing the figures and conducted the statistical analysis of the data sets.

4.1. Introduction

This section will focus on the step-wise activation of viral genes during the infection of normal human cells using human adenovirus 5 (HAdV5). Mapping the temporal expression of adenovirus genes has been reviewed extensively by other groups in the past[155,156,194,255,256]. The aim of this study was to provide new insight into this topic by using the most current technology available to detect the presence of RNA transcripts as soon as they are expressed. Additionally, previous reports had mainly revolved around the use of a cervical transformed cell line (HeLa)[155,156,257] which may not be as biologically relevant when compared to a study using a primary cell line. Our investigation into the chronological expression of HAdV5 genes using digital droplet PCR and arrested primary lung fibroblasts will be detailed below.

4.2. Temporal Materials and Methods:

4.2.1. Cell culture

IMR-90 human lung fibroblast cells were grown on Dulbecco's modified Eagle's medium (DMEM) (Hyclone) supplemented with either 10% or 5% fetal bovine serum and 1% streptomycin/penicillin (100 µg/mL streptomycin, 100 U/mL penicillin) (Hyclone). Cell culture kept in T175 flasks (SARSTEDT) at stable temperature of 37°C at 5% CO_2.

4.2.2. Infection

IMR-90 cells were plated at 425,000 cells per well in a 6-well plate. The cells were subjected to arrest by incubation in conditioned media for 3 days prior to infection. Infection was carried out by first washing the cells with SF-media and the infection mixture (*dl*309 adenovirus at an MOI of 100, topped to 500 µL of SF-media) was subsequently added directly unto the cells. Cells were rocked gently every 15 minutes for 1 h at 37°C. Subsequently, conditioned media was added to top up each well. Infection was carried for time points indicated per experiment and samples were harvest for processing or kept in -80°C freezer for storage.

Table 13. Adenovirus Primers and Probes

Primer	Forward (3'-5')	Probe	Reverse (5'-3')
GAPDH (qPCR)	GAGTCAACGGATTTGGTCGT	-	TTGATTTTGGAGGGATCTCG
E4-Orf3 (qPCR)	GCACAATGGCTTCCAAAAGG	-	ACTGACCTCGAGTTCCAAAAGATTATCCAAAA
VAII	TTTTCCAAGGGTTGAGTCGC	TCGAGTCTCGGACCGGCCGGAC	AATTTGCAAGCGGGGTCTTG
E1A	TGTGTCTGAACCTGAGCCTG	AGCCCGAGCCAGAACCGGAGCCTGCAA	ATAGCAGGCGCCATTTTAGG
E1B-19K	TTCTGCTGTGCGTAACTTGC	TGGAACAGAGCTCTAACAGTACCTCTTGGTTTTGGAG	ACTAACTTTGCCTGGGATGAGC
E1B-55K	AACTGTCACCTGCTGAAGACC	ACGTAGCCAGCCACTCTCGCAAGGCCTGG	ACCCAAATGCAAGGAACAGC
DNA-POL	ACCATGGTGTCATAGTCCAGC	AGCTTGCCCTTGGAGGAGGCGCCGCA	AGCTCTACGCCCTCAAAAGTC
DNA Binding Protein	TTTCTTCTTGGGCGCAATGG	AGGTCGATGGCCGCGGGCTGGGTGT	AAGACTCATCACAAGACGCG
E3	TTGTTGCCATCTCTGTGCTG	ACGCCACCGTCTTCACCCGCCCAAGCAA	AAAGTACCAGGTAAGGTTCGCC
E4-Orf3	GCACAATGGCTTCCAAAAGG	ACGGCCCTCACGTCCAAGTGGACG	TTTGGGCATGGTTGAAGGTG
E4-6/7	AAGTTCATGTCGCTGTCCAG	AGCCACAGGCTGCTGTCCAACTTGCG	GTGGACTTCTCCTTCGCCG
52k Encapsidation protein (EP)	ATCCTGCAGAGCATAGTGGTG	AGCCTGGCTGACAAGGTGGCCGCCA	TCTTGCGGGCGTAAAACTTG
pIIIa	TCCATGGTTGCACTAAACGC	AGTACACAGCCCGCCAACGTGCCGCG	CGCTCACAAAGTTGGTGTAGTC
III (Penton Base, Capsid Protein III)	AGCAATGACAGCACCTTCAC	ACGGCGACCCTCAGACCGGAATCCGCT	TTACGTCAGGAGTGCAAAGC
Hexon	AGCATTTGCCTTTACGCCAC	TGGCCCACAACACCGCCTCCACGCTT	TGTCGTTTCTAAGCATGGCC
100K (L4 Hexon Assembly Protein)	TCTGCAACAGGAAAACAGCG	AGGGTGACAACGCGCGCCTAGCCGT	ACCTCGATGCTGCGTTTTAG
Fiber (L5)	ATGCTTGCGCTCAAAATGGG	TCTGGACGAGGCCGGCAACCTTACCTCCCA	TTTTTGAGAGGTGGGCTCAC

Probes were produced by Integrated DNA Technologies (IDT, Coralville, Iowa, United States). The probes enclosed a FAM fluorophore with double quenchers; ZEN and Iowa Black.

4.2.3. Gene expression

Arrested and infected IMR-90 cells were harvested every h for 24 h, every two h between 24 h and 36 h. After harvest, cells lysed and total RNA was extracted using NucleoZOL (Machery Nagel, Düren, Germany). Cells were placed into microfuge tubes and 500 µL of NucleoZOL was added per sample. Subsequently, 100 µL of NucleoZOL of RNA-free water was added to the sample, shook vigorously for 15 seconds and incubated for 15 minutes at room temperature. Samples were centrifuged at 12,000 x g for 15 minutes at 4°C. The supernatant (500-600 µL) was transferred into a fresh tube and kept on ice. The RNA was precipitated by adding 250 µisopropanol per 500 µL of supernatant, invert and incubate for 10 minutes on ice. The samples were centrifuged at 4°C for 10 minutes. The supernatant was aspirated, leaving a small white pellet of RNA. The pellet was washed with 500 µL of ethanol by inversion at room temperature. The samples were spun at 12,000 x g for 5 minutes to settle pellet. The ethanol was aspirated, leaving the RNA pellet. The samples were placed in the biosafety cabinet for 2-5 minutes to allow the ethanol to evaporate. Once the pellet became clear, 50 µL of double-distilled syringe-filtered (0.22 µm filter) H_2O (ddH_2O) was added per sample. The RNA pellet was allowed dissolve into ddH_2O on ice for 30 minutes. Once dissolved, 6.6 µL of DNAse I master mix (1 µL DNAse 1 (2,000 units/mL) per 5.6 uL DNAse 1 Buffer (10X reaction buffer)) (New England Biolabs, Ipswich, Massachusetts, United States) was pipetted per sample, vortexed vigorously and centrifuged briefly to spin down sample. The samples were placed in a 37°C water bath for 30 minutes.

Afterwards, 0.7 µL of EDTA (10% (w/v) EDTA, pH 8) was added to each sample, vortexed and spun down. The samples were placed into a 75°C heat block for 10 minutes, and subsequently placed on ice. Complementary DNA (cDNA) was generated by adding total RNA (up to 2.5 µg) with 2 µL of SuperScript VILO Reverse Transcriptase Master Mix (Thermofisher) for a total volume of 10 µL. The samples were vortex, spun down and incubated at 42°C for 1 h. The samples were diluted by adding 90 µL of ddH_2O per tube and kept on ice. Real-time expression analysis was conducted using the ddPCR Probe Master Mix (BioRad) in conjunction with the QX200 Digital Droplet PCR (BioRad) or the SsoAdvanced Master Mix (BioRad) alongside the CFX96 real-time thermocycler (BioRad) (Reaction steps detailed below) after 17 h. Gene expression was normalized relative to the percentage of GAPDH (glyceraldehyde 3-phosphate dehydrogenase) mRNA levels. Data generated from the digital droplet PCR was analyzed using QuantaSoft version 1.7 (BioRad) and data generated from the qRT-PCR was analyzed using CFX Maestro version 1.1 (BioRad) software package.

Table 14. Reaction steps for PCR (QX200 – ddPCR Probe Master Mix)

Cycling Step	Temperature	Duration	Cycles
Enzyme Activation	95°C	10 minutes	1
Denaturation	94°C	30 seconds	40x
Annealing/Extension	60°C	1 min	40x
Enzyme Deactivation	98°C	10 minutes	1
End	4°C	-	Hold

Reaction steps as described from ddPCR Probe Master mix manual[258].

Table 15. Reactions steps for PCR (CFX96 - SsoAdvanced Master Mix)

Cycling Step	Temperature	Duration	Cycles
Enzyme Activation	95°C	30 seconds	1
Denaturation	95°C	5-15 seconds	40x
Annealing/Extension	60°C	5-15 seconds	40x
End	4°C	-	Hold

Reaction steps as described from SsoAdvanced Master mix manual[259].

4.2.4. Viral genome quantification

IMR-90 cells were plated at 425,000 cells per well in a 6-well plate (SARSTEDT). Cells were arrested for 3-days prior to infection with *dl*309. Cells were harvested every h for the first 36 h and a final set at 48 h. The cells were lysed using lysis buffer (50 mM Tris pH 8.1, 10mM EDTA and 1% SDS) for 10 minutes in ice. Samples were sonicated using the 500 Bp fragmentation setting on the M220 Focused Ultrasonicator (Covaris, Woburn, Massachusetts, United States). Samples were then treated with Proteinase K (NEB) for 10 minutes on ice. Subsequently, DNA was extracted and purified using EZ-10 Gel Extraction Kit (Bio Basic). Viral genomes were quantified using the samples, E4Orf3 primers, and Evagreen QX200 ddPCR EvaGreen Supermix (BioRad)for use on the QX200 Digital Droplet PCR. Data was analyzed using QuantaSoft version 1.7 (BioRad) software package.

4.2.5. Western Blot

IMR-90 cells plated at 425,000 cells per well in a 6-well plate. Samples were scraped into microfuge tubes and lysed using NP-40 lysis buffer (150 mM NaCl, 1% NP-40, 50 mM Tris-Cl at 8 pH) (NP-40 lysis buffer, 2006). Samples were centrifuged at 13,000 RPM (Sorvall Lynx 4000 centrifuge) for 10 minutes at 4°C. A Bradford assay was conducted to determine and normalize protein concentrations. Supernatant was transferred into a separate microfuge tube and 2X Sample Buffer (2 mL Tris (1M, pH 6.8), 4.6 mL glycerol (50% w/v), 1.6 mL SDS (10% w/v), 0.4 mL bromphenol blue (0.5% w/v), 0.4 mL β -mercaptoethanol) was added[156]. Samples were boiled for 10 minutes at 100°C. Samples were placed in an ice bucket to cool and was subsequently ran on 4-12% Novex Bolt Gradient gel (Thermofisher). Once separated, the proteins were transferred unto PDVF membrane using the eBlot L1 transfer system (Genscript, Piscataway, New Jersey, United States). The PVDF membrane was placed into a container with Blocking Buffer (5% skim milk powder dissolved in TBS-T solution) and gently rocked for 1 h. Primary antibodies were applied as follows: E1A primary mouse monoclonal antibodies: M2, M37, M58, M73 was applied at 1:10 dilution, 72k E2 DNA Binding Protein antibody was applied at 1:400 dilution and adenovirus type-5 primary antibody was applied at 1:5000 dilution (Primary antibodies were diluted in 3% BSA solution, or Blocking Buffer (5% skim milk diluted in TBS solution) overnight, rocking at 4°C. The respective primary antibody was removed and the membrane was washed using ~30 mL of TBS-T solution (100 mL TBS solution, 900 mL of dd H_2O, 1 mL Tween 20) and rocked at room temperature for 10 minutes. This wash step was repeated three times. After the

third wash, a secondary antibody is applied to the membrane for 30 minutes, gently rocking at room temperature. Subsequently, the membrane is washed several times with TBS-T. Immobilon Forte Western HRP Substrate (Horseradish peroxidase) (Millipore) is applied to the membrane for 5 minutes and film is used to detect protein bands.

4.2.6. Statistical analysis

Data was analyzed using one-way analysis of variance (ANOVA) and a post hoc comparison of the Tukey test comparing *dl*309-infected samples to mock-infected samples. The P-value was two-tailed for the gene expression and genome quantification data and P-values of <0.05 were considered significant.

4.3. Results

4.3.1. Expression of viral early genes in arrested lung fibroblasts

As the master regulator of early viral protein production during adenovirus infection, the activation of Early Region 1A gene, or *E1A*, marked the initiation of early viral gene expression of adenovirus. The first task was to monitor the expression of early viral genes at every hour for the first 24 h, and every 2 hours subsequently up to 36 h post infection (Fig. 36). To replicate normal conditions for adenovirus infection, human fibroblast cells from the respiratory system were chosen. IMR-90 cells were arrested through contact inhibition in conditioned media for 3 days prior to infection with the wild-type strain of adenovirus 5 (HAdV5), *dl*309.

Expression of *E1A* was observed as early as 6 h into infection and increased steadily over time until the last reported time point (36 h post infection). Viral transcripts of *E1B-19K* and *E1B-55K* were both detected approximately 13 h into infection. Both transcripts had increased suddenly (10-fold increase) between 12 h and 13 h into infection and displayed a steady rise throughout the rest of infection. Similarly, *DBP* was readily detected 13 h into infection, rising steadily until 22 h post infection where *DBP* levels displayed a mild plateau before rising again approximately 28 h into infection (Fig. 37). Viral *DNA Pol* gene expression was observed at 13 h post infection and, despite a steady increase, displayed similar plateauing as *DBP* at 22 h post infection before resuming a steady increase in levels until the last reported time point. The gene expression of *E3* displayed increasing levels of expression throughout the first 36 h of infection, initially detected at 12 h into infection. Interestingly, the two the *E4* transcripts, *E4Orf3* and *E4Orf6/7* were detected as early as *E1A* (6 h into infection). Levels of *E4Orf3* and *E4Orf6/7* appeared to undulate, rising, and dropping throughout the early stages of infection. Expression of these early viral genes may be viewed on a linear scale in Fig. 38.

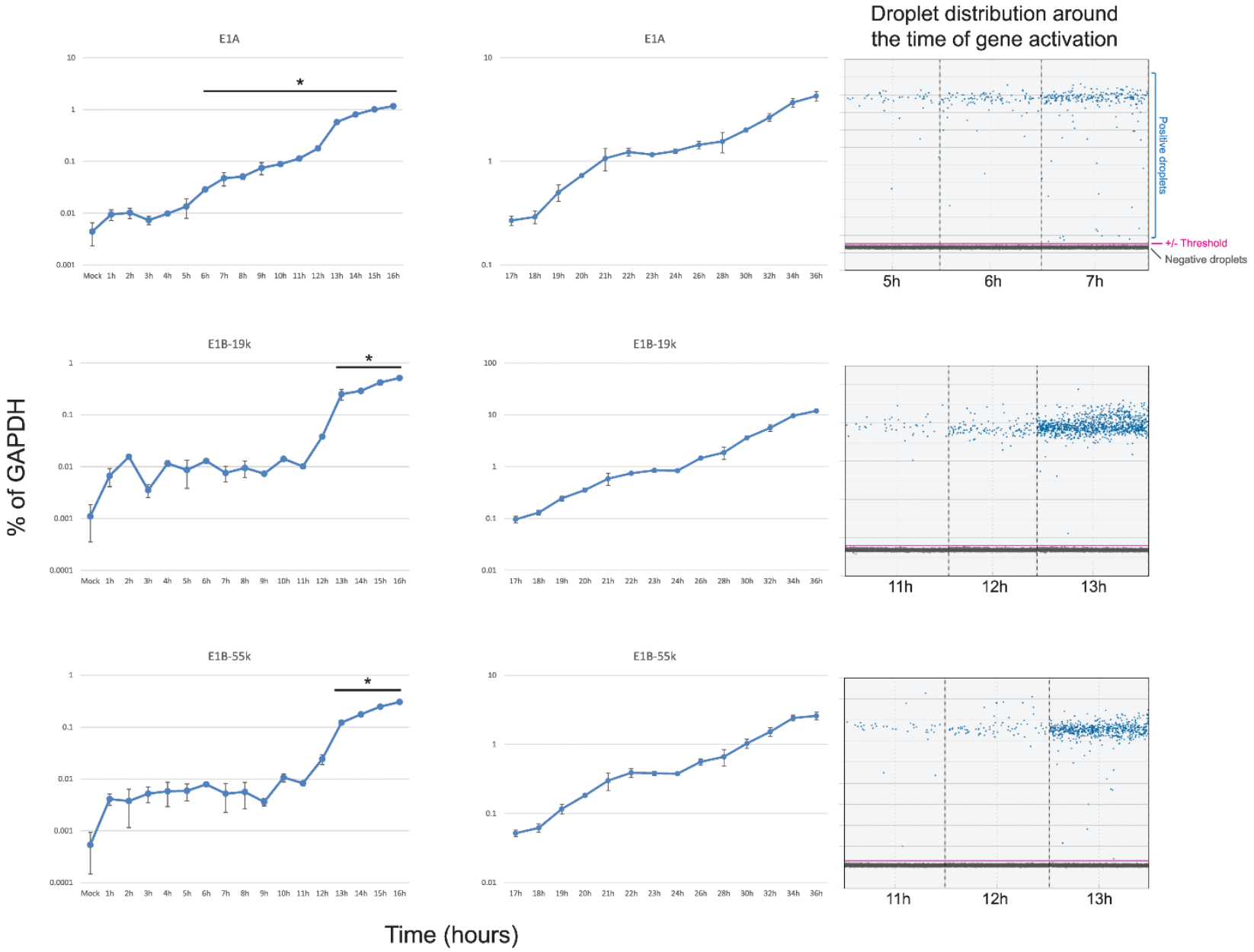
E1A
E1A
Droplet distribution around the time of gene activation
E1B-19k
E1B-19k
E1B-55k
E1B-55k
% of GAPDH
Time (hours)
Positive droplets
+/- Threshold
Negative droplets
5h
6h
7h
11h
12h
13h

Fig. 36. Expression of early adenoviral genes

IMR-90 cells were infected with adenovirus at a MOI of 50 following arrest for 3 days. Cells were harvested at indicated time points and subsequently extracted for mRNA. Early viral gene primers (E1A, E1B-19K, E1B-55K) were used in conjunction with sample cDNA and run on BioRad QX200 Digital Droplet PCR system. Results analyzed on Quantsoft version 1.7 (BioRad) and presented as % of GAPDH alongside visualization of droplet distribution at initial point of detection. n = 3, error bars represent SD. Significance noted as (*) = $P \leq 0.0001$. Obtained from Crisostomo *et al.* 2019[254].

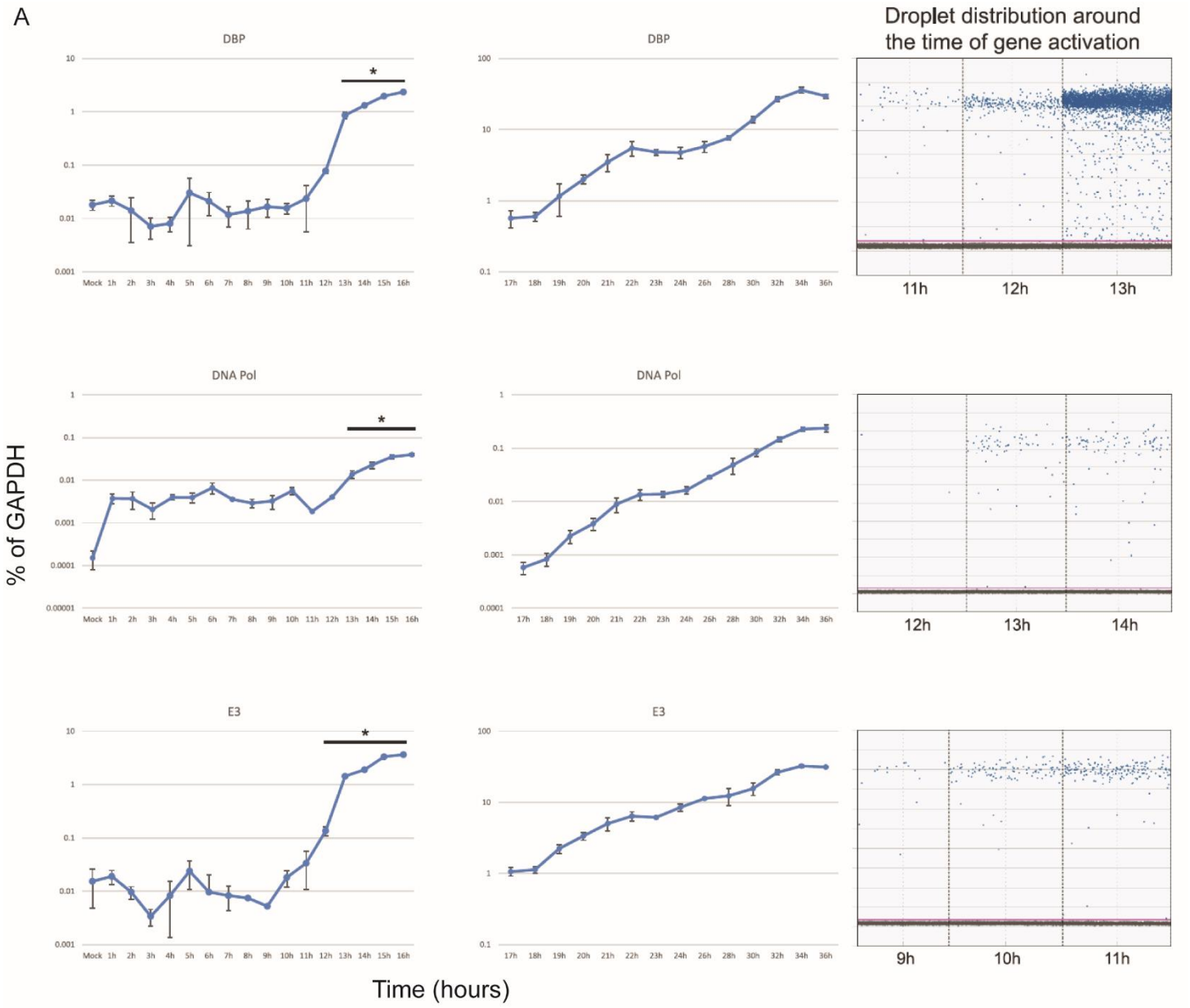
A
DBP
DBP
Droplet distribution around the time of gene activation
DNA Pol
DNA Pol
E3
E3
% of GAPDH
Time (hours)
Mock 1h 2h 3h 4h 5h 6h 7h 8h 9h 10h 11h 12h 13h 14h 15h 16h
17h 18h 19h 20h 21h 22h 23h 24h 26h 28h 30h 32h 34h 36h
11h 12h 13h
12h 13h 14h
9h 10h 11h

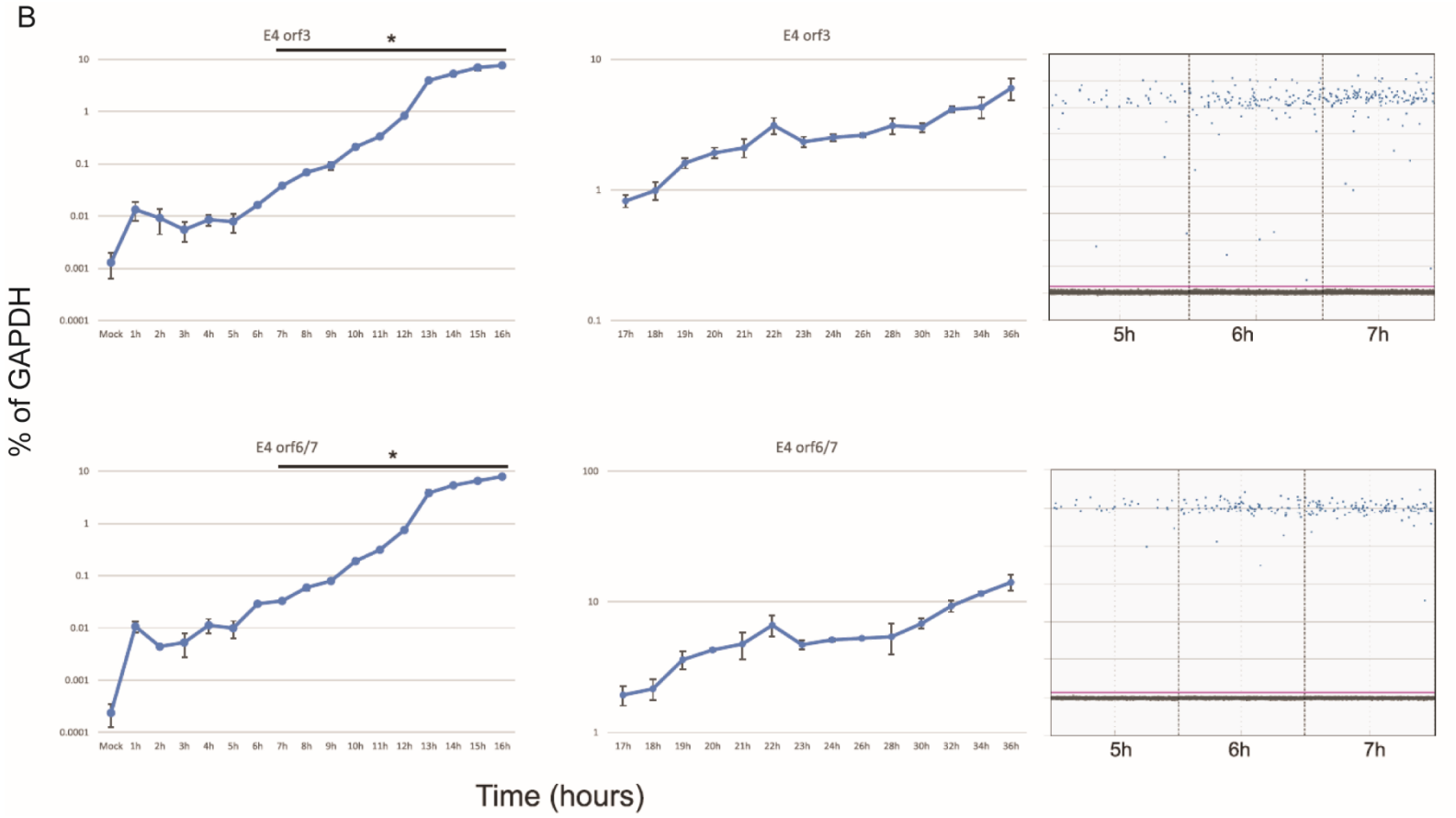

Fig. 37. Expression of early adenoviral genes (cont.)

IMR-90 cells were infected with adenovirus at a MOI of 50 following arrest for 3 days. Cells were harvested at indicated time points and subsequently extracted for mRNA. Early viral gene primers A) DBP, DNA Pol, E3 and B) E4 orf3, E4 orf6/7 was used in conjunction with sample cDNA and run on BioRad QX200 Digital Droplet PCR system. Results analyzed on Quantasoft version 1.7 (BioRad) and presented as % of GAPDH alongside visualization of droplet distribution at initial point of detection. n = 3, error bars represent SD. Significance noted as (*) = $P \leq 0.001$. Obtained from Crisostomo *et al.* 2019[254].

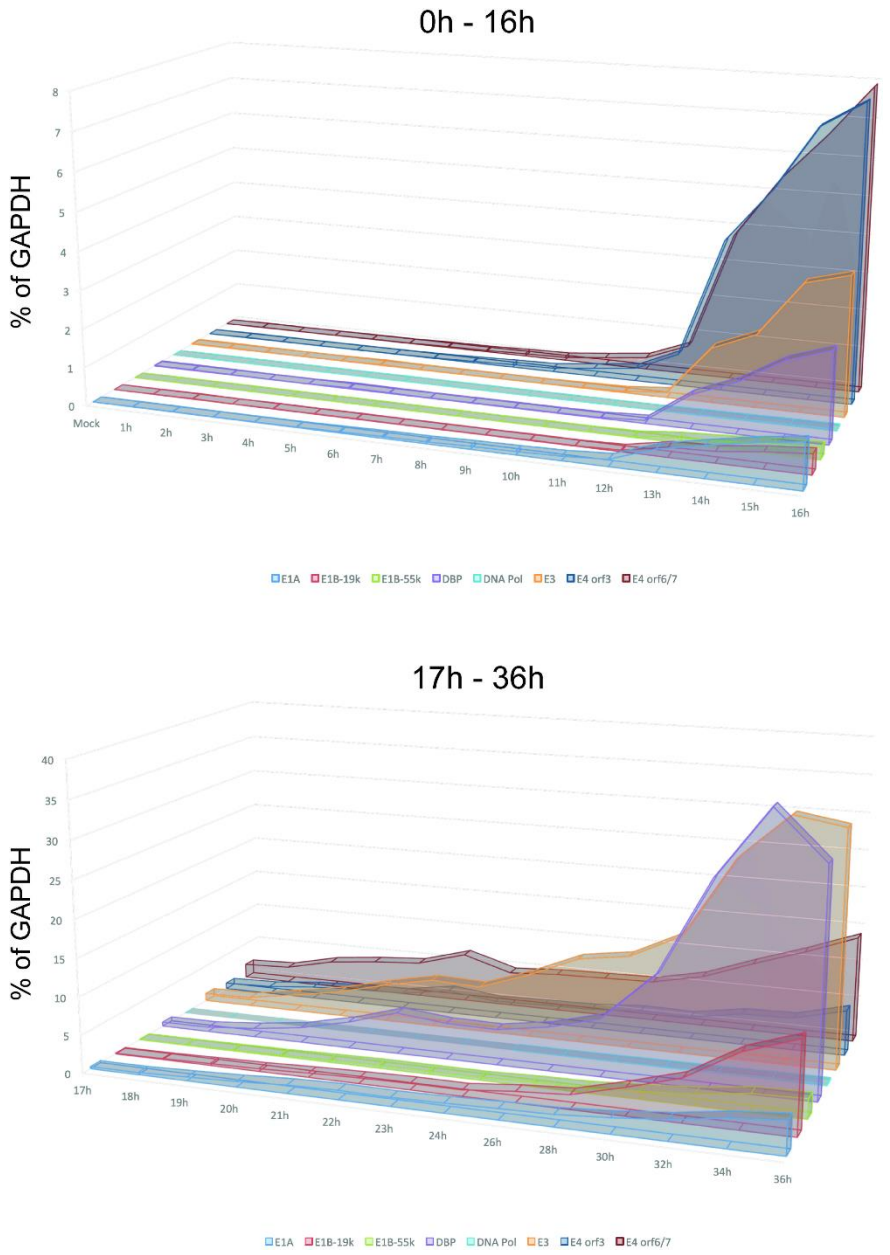

Fig. 38. Expression of early adenoviral genes (Linear graph)

Linear scale of early adenoviral gene expression as % of GAPDH. Obtained from Crisostomo *et al.* 2019[254].

4.3.2. Expression of virus associated RNA II

In addition to the early viral genes, the virus-associated RNA II (*VAII*) gene was also evaluated. Its counterpart, the virus-associated RNA I (*VAI*) acts to suppress Protein Kinase R (PKR) activation[260]. On the other hand, the function of *VAII* has yet to be clearly understood. Surprisingly, the expression of *VAII* was detected 4 h post infection (Fig. 39). Contrary to earlier findings, the expression of *VAII* marked the first transcript detected, as it was expressed 2 h prior to any other viral gene. This was the first time *VAII* had been reported as the first detectable viral gene expressed in adenovirus infection. The *VAII* levels remained relatively steady until 24 h post infection when it increased in expression until the last reported time point at 36 h post infection. Similarly, the *VAII* of human adenovirus 2 (HAdV2) was also detected during the early phase of infection, but gradually decreased as *VAI* levels rose[261].

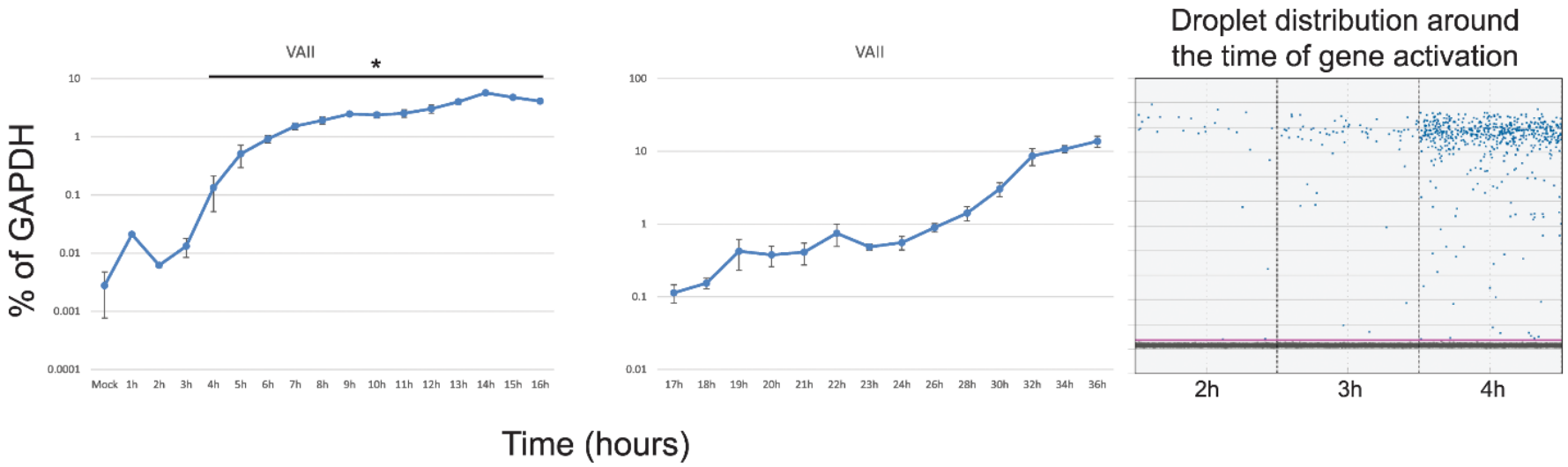

Fig. 39. Expression of virus-associated RNA II gene

IMR-90 cells were infected with adenovirus at a MOI of 50 following arrest for 3 days. Cells were harvested at indicated time points and subsequently extracted for mRNA. Early viral gene primer (VAII) was used in conjunction with sample cDNA and run on BioRad QX200 Digital Droplet PCR system. Results analyzed on Quantasoft version 1.7 (BioRad) and presented as % of GAPDH alongside visualization of droplet distribution at initial point of detection. n = 3, error bars represent SD. Significance noted as (*) = $P \leq 0.01$. Obtained from Crisostomo *et al.* 2019[254].

4.3.3. Expression of viral late genes

Following the transcription of early viral genes, the expression of viral genes associated with the late stages of infection of adenovirus was determined (Fig. 40). The late viral genes were measured using the same samples on the digital droplet PCR system as the early viral genes and may be observed on a linear scale in Fig. 41. The viral structural genes: 52K encapsidation protein (*EP*), PIIIa, Penton base, Hexon, 100K HAP and Fiber transcripts were detectable at approximately 13 h into infection. The expression of each structural gene displayed a steady increase throughout the initial 36 h of infection.

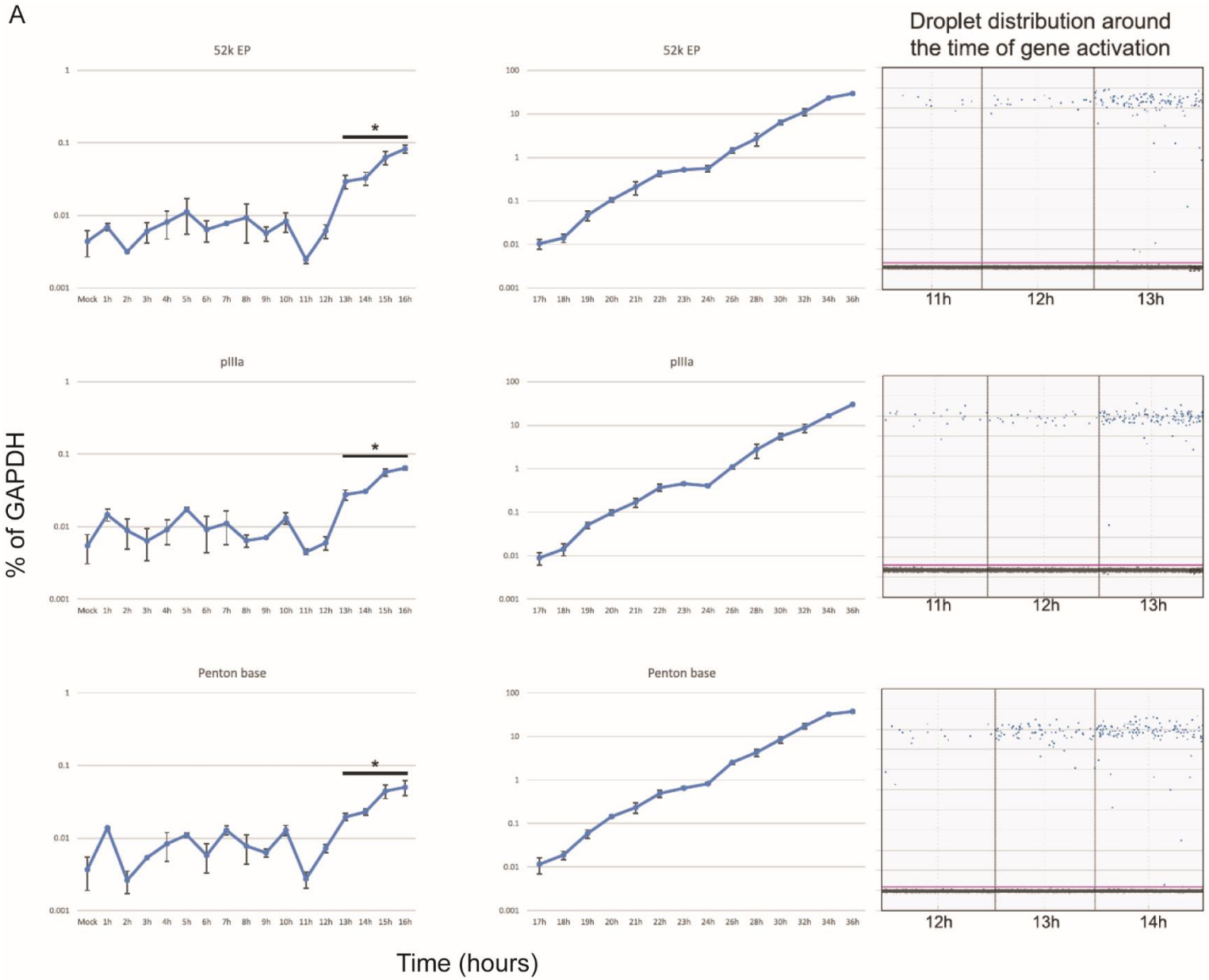
A
Droplet distribution around the time of gene activation
52k EP
52k EP
pIIIa
pIIIa
Penton base
Penton base
% of GAPDH
Time (hours)
Mock 1h 2h 3h 4h 5h 6h 7h 8h 9h 10h 11h 12h 13h 14h 15h 16h
17h 18h 19h 20h 21h 22h 23h 24h 26h 28h 30h 32h 34h 36h
11h 12h 13h
12h 13h 14h
*

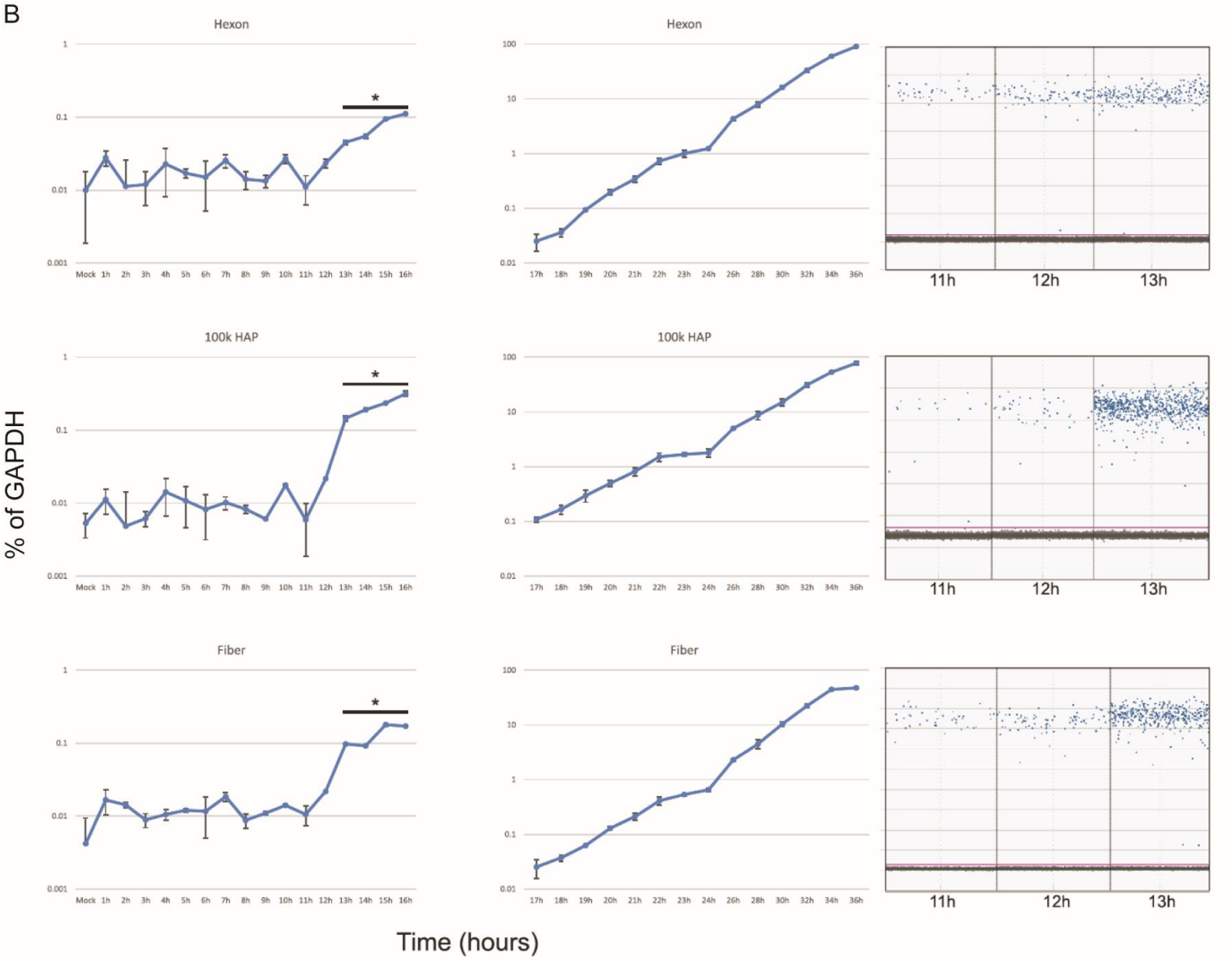
B
Hexon
Hexon
100k HAP
100k HAP
Fiber
Fiber
% of GAPDH
Time (hours)
Mock 1h 2h 3h 4h 5h 6h 7h 8h 9h 10h 11h 12h 13h 14h 15h 16h
17h 18h 19h 20h 21h 22h 23h 24h 26h 28h 30h 32h 34h 36h
11h
12h
13h
*

Fig. 40. Expression of late adenoviral genes

IMR-90 cells were infected with adenovirus at a MOI of 50 following arrest for 3 days. Cells were harvested at indicated time points and subsequently extracted for mRNA. A) Late viral gene primers 52K EP, pIIa and B) Penton base, Hexon, 100K HAP, Fiber was used in conjunction with sample cDNA and run on BioRad QX200 Digital Droplet PCR system. Results analyzed on Quantasoft version 1.7 (BioRad) and presented as % of GAPDH alongside visualization of droplet distribution at initial point of detection. n = 3, error bars represent SD. Significance noted as (*) = $P \leq 0.001$. Obtained from Crisostomo *et al.* 2019[254].

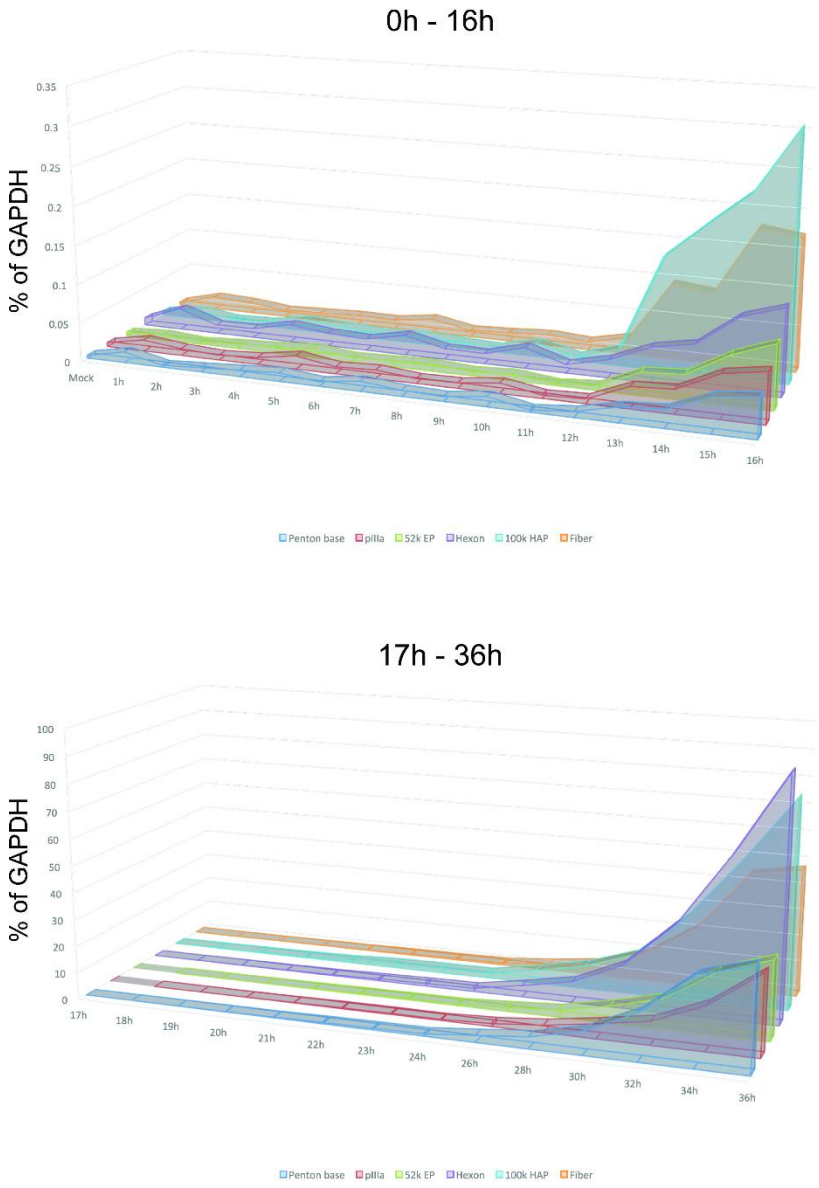

Fig. 41. Expression of late adenoviral genes (Linear)

Linear scale of late adenoviral gene expression as % of GAPDH. Obtained from Crisostomo *et al.* 2019[254].

4.3.3. Initiation of viral genome replication

In addition to mapping the temporal expression of viral genes, the point at which adenovirus initiated viral genome replication was established. IMR-90 cells were arrested and subsequently infected with *dl*309. Samples were harvested every hour for the first 30 h, and every 2 h subsequently until 36 h post infection. The viral gene *E4Orf3* acted as a marker for the presence of viral genomes. Between the initial time point at 2 h post infection until 28 h post infection, the detectable levels of genomes per cell remained unchanged at approximately 100 viral genomes per cell (Fig. 42). The presence of these genomes represented the infectious particles introduced at the beginning of the experiment. At approximately 29 h post infection, there was a significant increase, with 1,000 genomes per cell detected by 30 h post infection. This amount continued to climb until the last reported time point (48 h post infection). There was a 10-fold increase between 29 h, and 30 h post infection, which suggested that there was a rapid switch into viral genome replication, rather than a gradual accumulation of viral genomes.

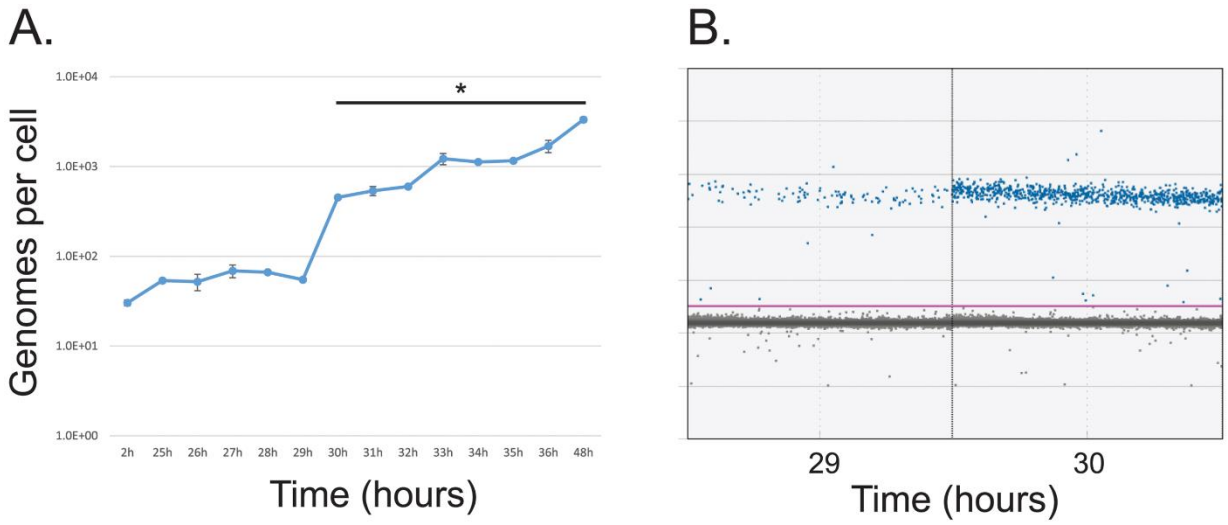

Fig. 42. Detection of viral genome replication

IMR-90 cells were infected with adenovirus at a MOI of 50 following arrest for 3 days. Cells were harvested at indicated time points and subsequently extracted for viral DNA. Purified viral DNA was run alongside E4 primers on BioRad QX200 Digital Droplet PCR system to detect presence of viral genomes. Results analyzed on Quantasoft 1.7 (BioRad) and represented as viral genomes per cell. A) Number of viral genomes per cell graphed according to indicated time points. B) Sample of the droplet distribution as positive (above threshold of purple line) or negative (below threshold of purple line). n = 2, error bars represent SD. Significance noted as (*) = $P \leq 0.0001$. Obtained from Crisostomo *et al.* 2019[254].

4.3.4. Analysis of viral protein expression

To examine whether our observations with viral gene expression reflected levels of viral protein expression, infected IMR-90 cells were harvested at indicated time points and processed for western blot assays. The largest E1A isoforms were readily detectable in film two minutes after exposure. The 243R and 289R isoforms had bands in samples harvested at 18, 24 and 36 h post infection (Fig. 43). At 36 h post infection, there was an observable band between 22 kDa and 30 kDa. The 55R, 171R and 217R isoforms were visible on film after 90 minutes of exposure. Furthermore, 243R and 289R isoforms were faint but discernable 12 h post infection. The expression of the largest isoform (289R E1A) seemed to peak at 24 h post infection, and levels decreased by 36 h post infection. This reflected an independent study that was conducted on the temporal expression of viral proteins during HAdV2 infection[262]. The viral protein DBP was indicated by a faint 72 kDa band 18 h post infection and gradually increased until the last reported time point at 36 h post infection. Accumulation of structural viral genes was believed to coincide with the decrease of early viral genes, as suggested by previous work[146,262].

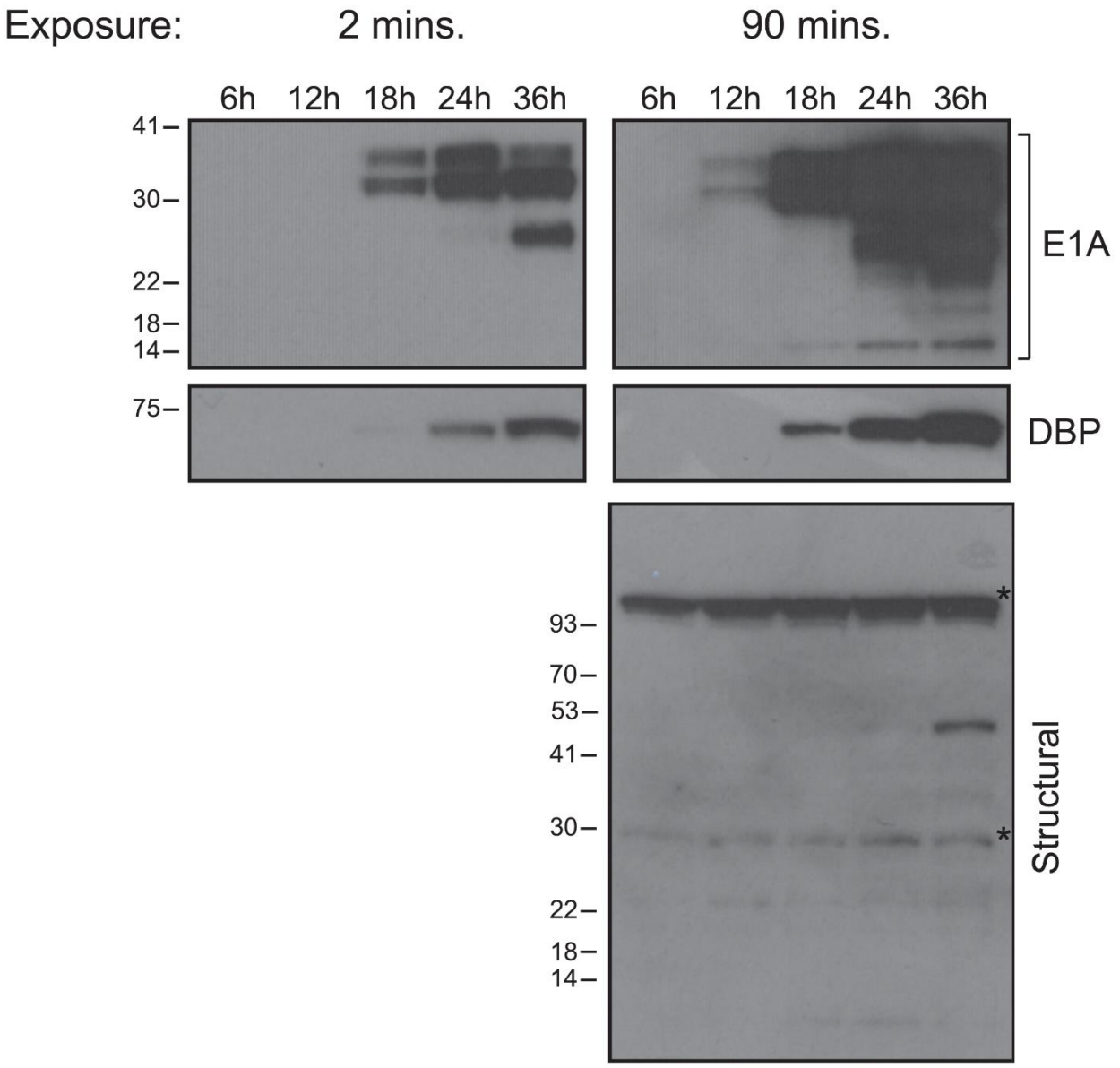

Fig. 43. Western blot analysis of viral protein expression during adenovirus infection

Arrested IMR-90 cells were infected with *dl*309 at a MOI of 50 and harvested at indicated time points. Harvested cells were lysed in NP-40 Lysis buffer and spun down to separate cell debris. Supernatant was boiled in 2X Sample Buffer and subsequently ran through SDS-PAGE system. Protein samples were transferred unto PVDF membrane and probed using M2, M37, M58, M73 was applied at 1:10 dilution to detect E1A, 72k E2 DNA Binding Protein antibody was applied at 1:400 dilution to detect DBP, and adenovirus type-5 primary antibody was applied at 1:5000 dilution to detect structural proteins. Viral protein bands were visualized using film and size represented as kDa. (*) indicate background bands. Obtained from Crisostomo *et al.* 2019[254].

Table 16. Temporal adenovirus gene expression in IMR-90 cells vs. HeLa cells

Gene	IMR-90[a]	HeLa[b]
E1A	6h	1.5—2h
E1B-19k	12h	8h
E1B-55k	12h	3.5h
52k EP	13h	7—8.5h
E2A	12—13h	2—3h
E3	12h	3h
E4	6—7h	3h
VAII	4h	~3h

Modified chart representation of the expression of early adenovirus genes in the current study compared to previous studies using HeLa cells[155,156,257]. [a] This current study. [b] Based on previous studies[155,156,257]. Table obtained from Crisostomo *et al.* 2019[254].

4.4. Discussion

The early gene expression of *E1A* comes as no surprise, as it has been shown to act as a trans-activator protein responsible for the initiation of downstream viral genes. *E1A* transcripts were first detected 6 h post infection in arrested IMR-90 cells. Comparatively, *E1A* was also observed within the early stage of infection (approximately 0 – 4 h post infection) in HeLa cells (Table 16)[256]. There was a gap between the expression of *E1A* and the activation of other viral genes such as *E1B*, *E2*, and *E3* between our study and published reports from other groups. A difference between the current study and the experiments conducted by previous groups would the cell lines used during infection. Arrested IMR-90 cells were used in this study, whilst other reports utilized HeLa cells. The enhanced metabolism and oncogenic properties of HeLa cells do not appropriately reproduce natural infection conditions of adenovirus in normal human cells[209,263]. Our investigation did not distinguish between the five known isoforms of *E1A* (*9S*, *10S*, *11S*, *12S* and *13S*). Earlier work suggested that the transcripts detected during the early phase of infection (< 2 – 2.5 h post infection in HeLa cells) was composed of the largest isoforms of *E1A*, which was the *13S* and *12S* isoforms[155]. Recently, the expression between these two isoforms has been disputed, and the authors suggested that the accumulation of 13S and 12S was dependent on viral DNA levels in individual cells. Curiously, they did not detect presence of 13S or 12S E1A between 1 and 13 h post infection of HeLa cells, contradicting earlier reports[155,264]. During the late stages of infection, the *9S* mRNA is reported to be the most abundant and first detected during the "intermediate" phase of the infection[155,265]. To support the observations regarding the early transcription of *E1A*, the expression of the two largest isoforms of E1A as early as 12 h post infection was detected (Fig. 43). Moreover, smaller isoforms of E1A protein were detected at 18 h into infection and these accumulated as infection progressed. This observation is in-line with previous reports that described the shift in E1A species in relation to the phase of infection[153].

The levels of the two *E1B* transcripts share similar points of initial expression between 12 h and 13 h post infection. The *E1B-19K* and *E1B-55K* transcripts increased steadily until 22 h post infection before rising at 26 h into the infection (Fig. 36). There was a deviation between the two transcripts, as the *E1B-19K* unit continued to steadily rise and became the most abundant in the later stages of infection compared to the *E1B-55K* transcript. This supported earlier evidence reported by Ricciardi *et. al*, in that the smaller *E1B* transcript [19K] is less abundant during early

phases of infection, but eventually increased at later stages of infection before passing the larger *E1B* unit [55K] in terms of relative abundance[155].

A possible explanation of the sudden downshift in *E4* transcript levels at 13 h could be due to the emergence of DBP at the same time point. The viral protein DBP is believed to down-regulate the expression of the *E4* transcripts (*E4Orf3* and *E4Orf6/7*)[155]. Admittedly, the DBP band was not visible on western blot until 18 h post infection (Fig. 43). However, *E4Orf3* and *E4Orf6/7* transcript levels decreased alongside the appearance of DBP. This suggested the downregulation of *E4* genes by DBP. The presence of DBP and DNA pol at these time points also suggest the slow climb towards the initiation of viral replication.

This study found the viral gene, *VAII*, is the earliest transcript detected during infection with adenovirus. Previous publications have suggested that *VAII* acts in similar fashion to its counterpart, *VAI* to suppress the PKR pathway, albeit at a reduced capacity[260]. The *VAII* gene is conserved across the majority of adenovirus serotypes[266]. *VAII* is also highly expressed during infection and the growth of a virus double-mutant lacking *VAI* and *VAII* is significantly worse compared to a VAI-mutant virus alone. Furthermore, the expression of *VAII* increased throughout infection, which reinforced previous findings that described the expression of *VAII* late into infection[190] (Fig. 39). These observations, along with the early detection of *VAII* during infection, supported the notion that it may play an important role in the viral life cycle, that has yet to be fully understood. It is imperative, then, that characterization of *VAII* be at the forefront of future work.

The activation of late viral genes in arrested IMR-90 cells appeared earlier than expected. The transcripts of late viral genes were detected approximately 13 h into infection (Fig. 41). These observations placed the expression of late viral transcripts in line with the expression of early viral genes. A steady increase of the late viral genes throughout the entire infection was also noted. The expression of the *L1* (late gene transcribed from the Major Late Promoter) was observed as early as 1 h into the infection of HeLa cells and steadily accumulated throughout the entire infection. Two other late transcripts; *L2* and *L3* were detected towards the late phase of infection (6 – 15 h post infection), increasing until they had matched levels of *L1*[256]. However, a later study was unable to detect *L1* earlier than 10 h post infection. These authors posited the difference that the difference in the detection of *L1* transcripts may be due to the use of cycloheximide in the earlier study as it has been shown to alter mRNA stability and enhance the accumulation of early viral

transcripts[156,267,268]. The transcription of intermediate-late structural viral genes was also observed quite early during infection and accumulated until the virus transitioned into the later stages of infection in later studies[155,156]. Reports that described the activation of the MLP (Major late promoter) of HAdV2 during the early phase of infection and the conditional expression of the *L1* transcripts support these claims[269]. However, levels of viral mRNA did not correlate to protein levels observed in the western blot. The earliest bands of structural proteins were observed 36 h into infection, following genome replication observed at approximately 29- and 30-h into infection. This timeline followed similar patterns as previously published data[194], with the rapid production of late viral proteins following the activation of the MLP and viral genome replication.

Replication of the viral genome was initiated suddenly between 29- and 30-h into infection (Fig. 42). The replication of the adenovirus genome is primarily governed by three viral proteins: pre-terminal protein (pTP), DNA pol and DBP[163]. Based on these findings, the expression of DBP was observed as early as 18 h post infection and levels increased throughout the infection. It was also important to note that the expression of DBP followed the initial detection of E1A at 12 h post infection (Fig. 43). The accumulation of E1A during the early stages of infection is crucial to effective growth of the virus, as E1A acts as a regulator of downstream viral genes, including the E2 genes, which are responsible for viral DNA synthesis. These findings supported the early work published by Yamashita *et. al* (1974), that described the necessity of early viral protein production in viral DNA synthesis. Canonically, replication of the adenovirus genome is believed to occur between 24 h and 48 h post infection[153,209,270]. There was also a window between the transcription of early viral genes and initiation of viral genome replication. Groups in the past have suggested that adenoviral replication centers (AdRCs), which are essential for efficient viral genome production, are assembled during this time. AdRCs provide compartments wherein viral and cellular factors are concentrated[271–273]. These areas are free of anti-viral factors, such as Daxx or Mre11, that may suppress DNA replication[274]. The assemblage of these centers may explain the gap between early viral gene expression and initiation of viral genome replication. Using the droplet technology, this study was able to pinpoint the initiation of viral genome replication of HAdV5 to within an hour in IMR-90 cells.

The advent of new technology capable of detecting minute quantities of genetic material will be crucial to many aspects in the field of microbiology. This study took advantage of this equipment by constructing a temporal map of adenovirus gene expression. Taken together, these

findings corroborated previous results, but also provided insight into the stepwise activation of viral genes during infection. Subsequently, the synthesis of viral genomes between 29 and 30 h into infection followed by the early development of late-structural viral proteins was observed. In support of our hypothesis, we found the activation of viral genes to be delayed in primary cells as compared to earlier work using transformed cells. Despite the temporal differences in gene expression (Table 16), we maintain that the order in which viral genes are expressed in HAdV5-infected IMR-90 cells support the findings of previous publications involving HAdV2-infected HeLa cells[155,156,257]. Moreover, our current study provided biologically relevant data concerning normal human cells that were more likely to be targeted by adenovirus. It is with hope that this research will pave the path for other groups to utilize this technology to provide a better understanding of the mechanisms behind viral infections.

Chapter 5: Conclusions

5.1. Thesis conclusions and observations

The work described in this thesis, alongside ongoing research presented by other groups, has led to our hypothesis that NEK9 antagonizes p53 to cause differential regulation of specific promoters, thereby leading to the suppression of pathways involved in cellular arrest or induction of apoptosis. In this section, a summary of our findings and overall conclusions will be detailed.

The first goal of this thesis was to investigate the relationship between NEK9 and E1A with respect to oncogenesis. Based on an earlier study regarding the importance of NEK9 to the effective growth of adenovirus[134], we posited that NEK9 may participate in viral processes such as transformation. We report that the overexpression of NEK9 in adenovirus-infected rodent cells enhanced their transformation. Increased expression of NEK9 also had a negative impact on p53-promoter activation. However, the expression of the ΔRCC1 variant or 289R E1A did not significantly affect the activation of p53-promoters in cells overexpressing NEK9. The disruption of p53 transactivation, which is mediated by the E1B-55K protein of adenovirus during infection, has been reported to be an essential factor that drives the transformation of rodent cells[159]. These observations provide evidence to support our initial hypothesis wherein elevated levels of NEK9 suppresses p53 promoter activity.

The second goal was to characterize the role of NEK9 in the suppression of p53-regulated genes. The depletion of NEK9 enhanced the expression of tumour suppressor genes such as *GADD45α, PIG3,* and *PUMA* in p53-mutant cells, but not in the wild-type. In contrast, the expression of *BCL-2, BCL-xL, BAD,* and *BAX* varied amongst the cell lines depleted for NEK9, independent of their status of p53. Additional factors may participate in the regulation of these apoptotic markers between each cell line, and future investigations will be required to identify these elements. Despite this, we have provided evidence that corroborates NEK9 as a transcriptional regulator of p53 activated genes.

The next goal was to examine the NEK9 variants, D194N and ΔRCC1, and investigate the impact of their expression on the cell cycle. Cellular senescence was not observed in cells overexpressing wild-type NEK9 or its variants. However, there was strong evidence to support our initial hypothesis that the expression of the NEK9 variants would push cells towards arrest or apoptosis. This was based on our observations of apoptotic morphology (Fig. 14), detection of PARP cleavage (Fig. 17), and uptake of propidium iodide (Fig. 34). These results support data

from other groups who have shown that the absence of NEK9 promotes apoptosis[240], and contributes to prolonged G1 phase and S-phase induction[78].

Altogether, the results highlighted in chapter two provide support that NEK9 could be a potential target for cancer therapy. Our work may act as a small steppingstone towards research into NEK9 as a candidate for tumour inhibitors.

The third chapter of this thesis described the development of an *in vivo* NEK9-kinase substrate screen. The constructs were successfully created for the screen and the initial experiments showed an interaction between the mCherry-NEK9-LacI fusion protein and a GFP-tagged NEK6 consensus site. However, the GFP-tagged NEK6 consensus site also co-localized with the negative control, the mCherry-LacI fusion protein, which suggested that nonspecific binding had occurred between our constructs. The binding affinity between kinases and substrates may rely on the combination of several factors such as the phosphorylation and docking sites, and other binding motifs[275]. Therefore, the absence of secondary or tertiary structures in the GFP-tagged NEK6 consensus site could have reduced its specificity towards NEK9 and enhanced the probability for promiscuous interactions to occur. This may explain why the GFP-tagged NEK6 consensus site co-localized with the negative control. We speculate that the generation of full-length substrates may supply the molecular features that would promote the specificity between the mCherry-NEK9-LacI fusion protein and the GFP-tagged substrates. The establishment of this assay would provide an *in vivo* approach to identify kinase-substrate interactions. *In vitro* models are unable to reliably replicate protein folding, glycosylation and other post-translational modifications on kinases and/or substrates that may be important. This assay may offer an alternative platform to *in vitro* methods for high throughput identification of substrates, or other protein-protein interactions.

The final goal of this thesis was to generate a temporal map of adenovirus gene expression during the infection of normal human cells. The expression of early viral genes was determined to occur within the first hour of activation. The initial viral RNA detected was *VAII*, several hours prior to the detection of *E1A* transcripts. *VAII* was also found to steadily accumulate throughout the infection. Despite its early appearance and stable presence, our understanding of its role is limited. Does the role of *VAII* change throughout the course of infection? Depletion of *VAII* along with *VAI*, significantly impacts viral growth which suggests that *VAII* may have an important role during infection[276]. In the absence of *VAI*, *VAII* is upregulated but cannot compensate for the weak inhibition of PKR activation that normally results from interaction with *VAI*[277]. Dissection of

various viral processes would provide a foundation to understand the impact of *VAII* to the viral fitness of adenovirus. A study into the growth dynamics, viral gene expression and protein production of a VAII-deletion mutant virus may provide clues as to the function of *VAII*. A thorough investigation is required to better understand the significance of this viral gene.

E1A transcripts were first detected 6 h post infection and preceded the expression of most genes. It was followed shortly by expression of *E4* transcripts (6 – 7 h post infection), and eventually by the rest of the early viral transcripts. Effective transcription from the *E2* promoter is reliant on the binding of E2F transcription factors, which is enhanced when both E1A and E4 products are present[278]. This may explain the detection of *E4* transcripts immediately after those of *E1A*. The late viral transcripts were readily detected around 13 h post infection. Our study successfully mapped the initiation of viral genome replication between 29 and 30 h after infection. This sudden switch into genome replication may be a result of the shift from early AdRCs, which is believed to generate genomes for transcription, to late AdRCs, which produce genomes for packaging[271,279,280]. We detected the E1A protein as early as 12 h, DBP by 18 h and structural proteins by 36 h post infection. A study involving HAdV5 and human foreskin fibroblasts (HFFs) reported similar times for viral protein expression[209].

We elected to conduct experiments using normal human lung fibroblasts (IMR-90), as compared to previous temporal models utilizing cervical cancer cells (HeLa)[155,156,257]. The differences between the two cell lines during infection are highlighted in chapter four (Table 16). There is strong evidence to support our hypothesis in that the temporal activation of viral genes is delayed during the infection of normal human fibroblasts as compared to HeLa cells. This allowed a clear analysis of key molecular events and phases of infection. Our study took advantage of the most current technology available to detect minute quantities of viral transcripts, allowing the precise mapping of viral gene activation. Thus, the current model provides an appropriate biological representation of adenovirus gene expression in normal human cells.

Overall, the work completed in this thesis supports the hypothesis that NEK9 acts as a transcriptional regulator of specific p53-activated genes, which are responsible for the induction of cellular arrest, or apoptosis. The development of an *in vivo* assay to identify substrates of NEK9 was also described. Finally, the temporal expression of early, intermediate, and late viral genes of adenovirus was investigated in normal human cells.

5.2. Future directions

Despite the observations of the current study, the exact relationship between NEK9 and p53 remains unclear. We succeeded in describing the consequences of dysregulating NEK9 through depletion, overexpression, or expression of its variants. However, we did not establish the process by which NEK9 suppresses p53 activity. A previous study reported the presence of NEK9 along the promoters of suppressed p53-regulated genes[134], suggesting that these effects could be due to competitive inhibition of p53 by NEK9. Identifying a NEK9 mutant that is unable to suppress p53 activity would be beneficial for future experiments. This may be accomplished by screening NEK9 deletion mutants in the luciferase assay mentioned previously in chapter two. This would help determine whether the enhanced transformation in the presence of NEK9 was driven by the suppression of p53 activity, or by another means.

Characterizing the various domains of NEK9 would provide useful information regarding its kinase activity, regulatory properties, and protein-protein interactions. In chapter two, we found that the expression of the ΔRCC1 variant did not lead to the same level of reduction as the overexpression of wild-type NEK9 on the activation of p53 promoters (Fig. 9). But to what extent does the deletion of the RCC1 region affect NEK9's ability to regulate the transcription of p53-activated genes? It would be of interest to compare the relative occupancy levels of the ΔRCC1 variant and wild-type NEK9 on the promoters of p53-regulated genes in p53-mutant and p53-wild-type cell lines. Conducting a chromatin immunoprecipitation (ChIP) assay, combined with RNA-SEQ analysis, would offer an insight into changes in transcription regulation that occur in the presence of the ΔRCC1 variant. In addition to the RCC1 domain, future investigations could include experiments involving the coiled-coil (CC) domain. The removal of the CC domain may inhibit autophosphorylation[126], and we speculate that this could lead to a decrease in kinase activity. However, more data is required to fully investigate this hypothesis.

5.3. Supplementary Data

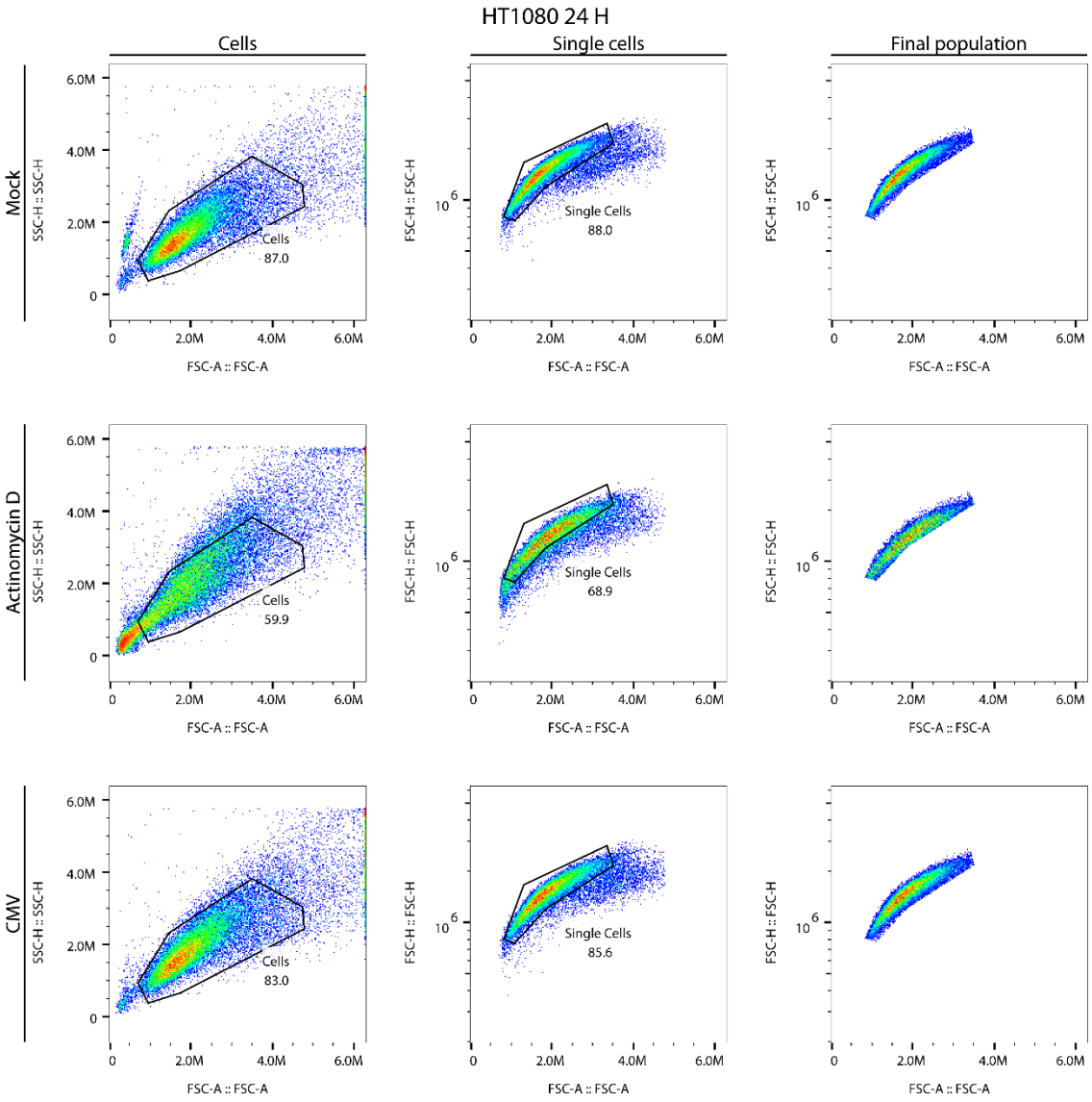

Fig. 44. HT1080 cells treated with actinomycin D or infected with Ad-CMV for 24 h subjected to flow cytometry analysis

HT1080 cells were treated with actinomycin D or infected with Ad-CMV for 24 h. Cells were harvested, fixed with cold ethanol, and stained with PI. A region has been drawn around cells to exclude possible debris or aggregated cells during cell cycle analysis. A second gate was used to exclude doublet cells.

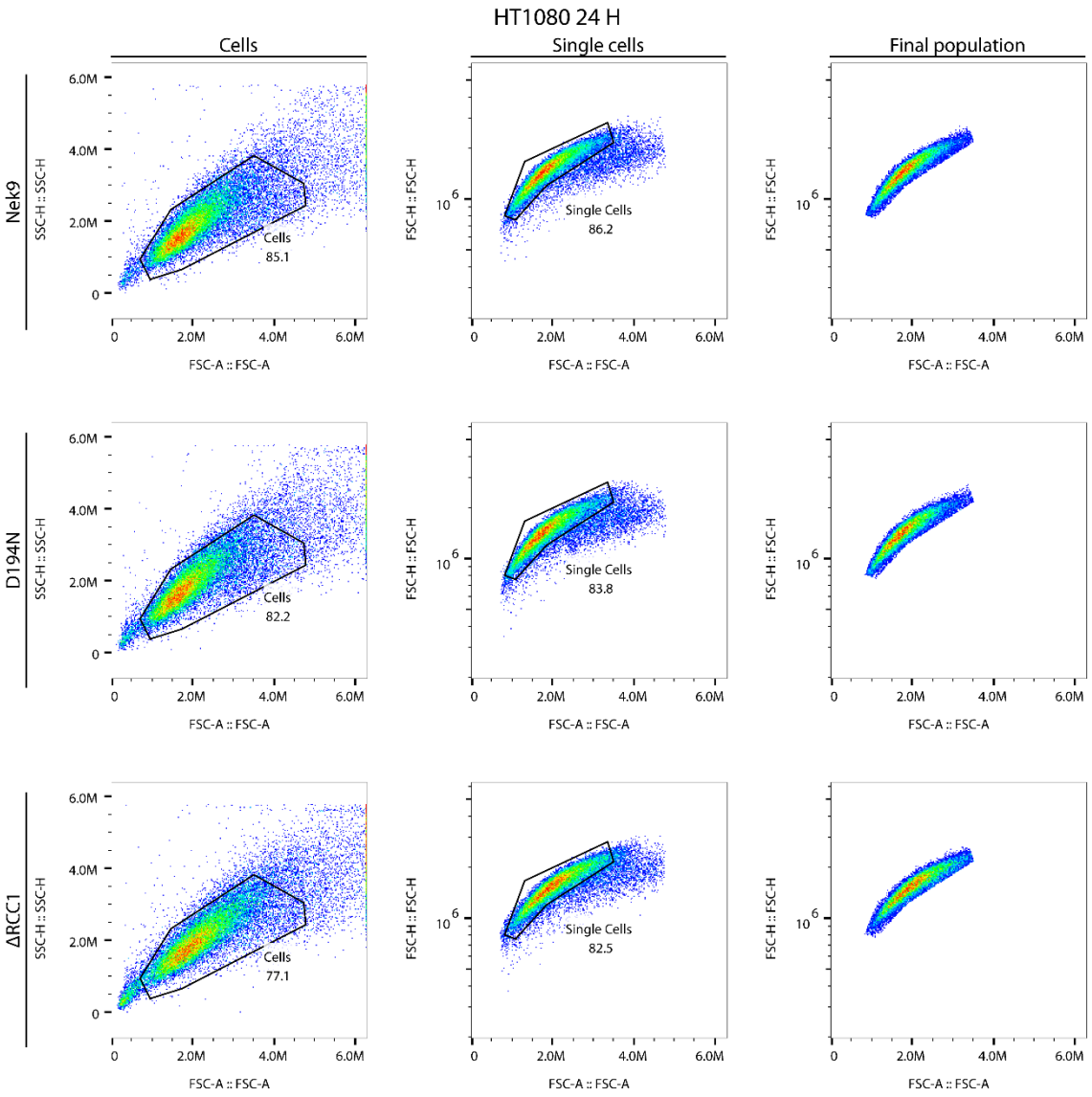

Fig. 45. HT1080 cells infected with wild-type NEK9, D194N or ΔRCC1-expressing viruses for 24 h and subjected to flow cytometry analysis

HT1080 cells were infected with wild-type NEK9, D194N or ΔRCC1-expressing viruses for 24 h. Cells were harvested, fixed with cold ethanol, and stained with PI. A region has been drawn around cells to exclude possible debris or aggregated cells during cell cycle analysis. A second gate was used to exclude doublet cells.

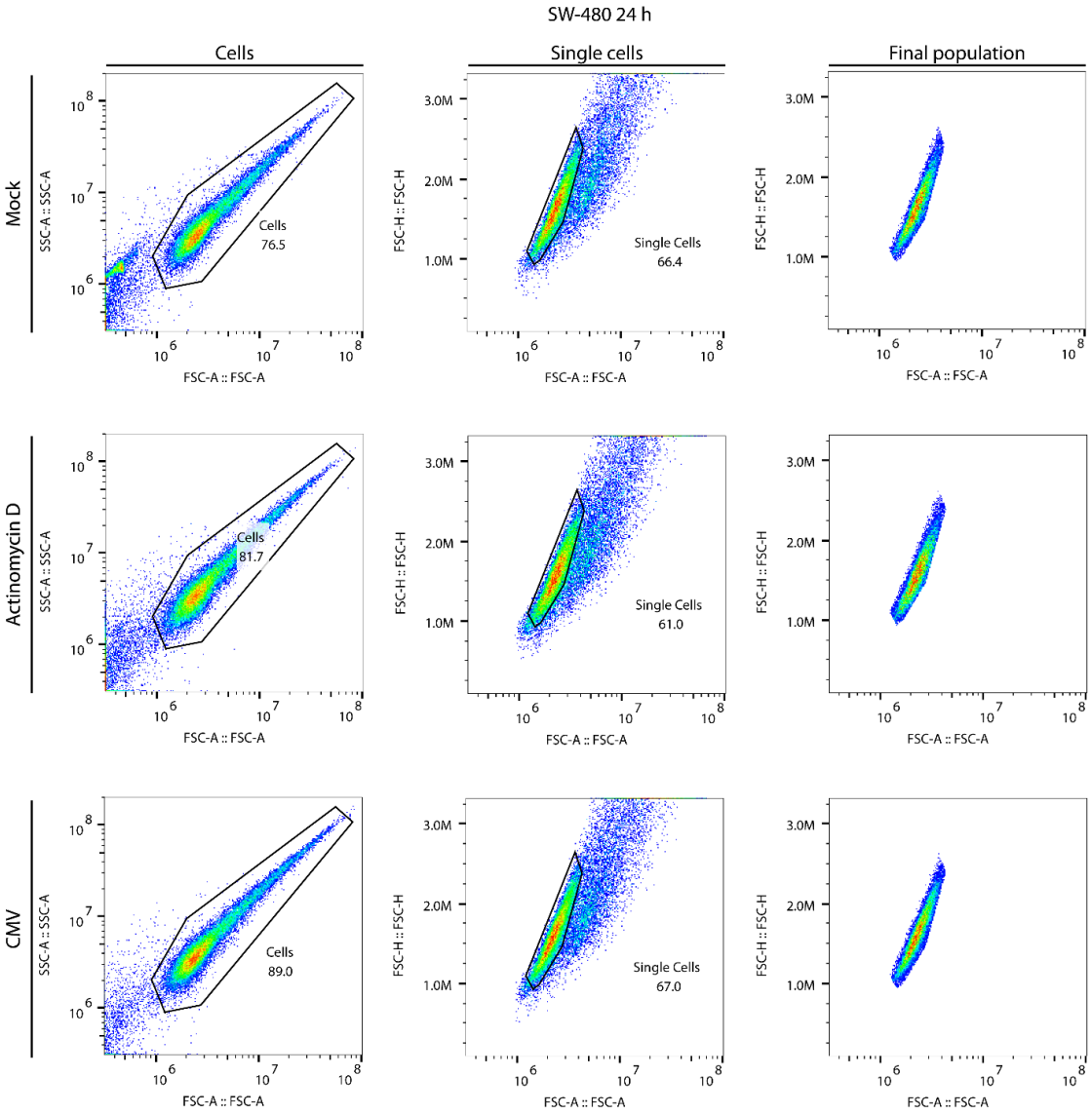

Fig. 46. SW-480 cells treated with actinomycin D or infected with Ad-CMV for 24 h subjected to flow cytometry analysis

SW-480 cells were treated with actinomycin D or infected with Ad-CMV for 24 h. Cells were harvested, fixed with cold ethanol, and stained with PI. A region has been drawn around cells to exclude possible debris or aggregated cells during cell cycle analysis. A second gate was used to exclude doublet cells.

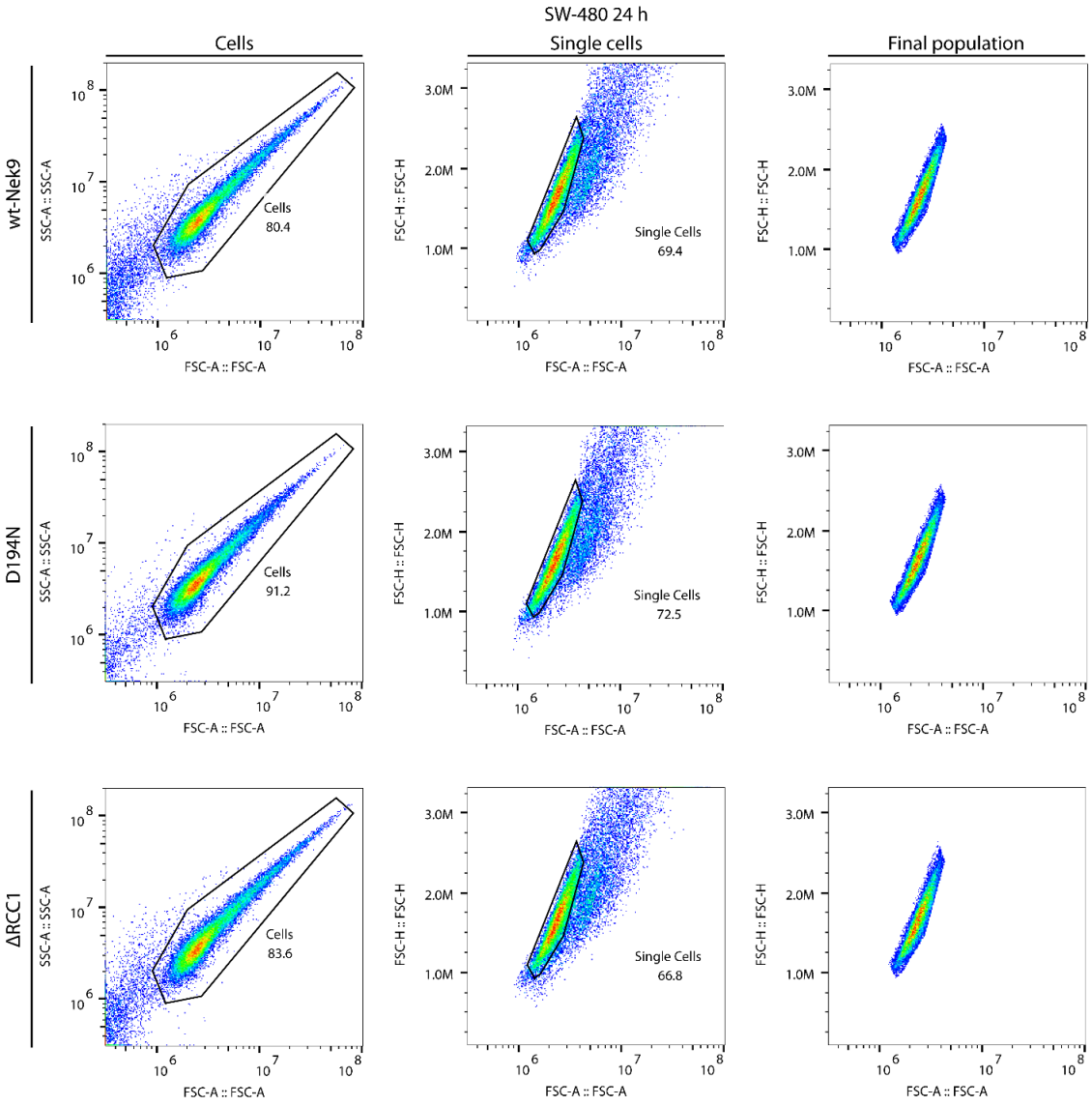

Fig. 47. SW-480 cells infected with wild-type NEK9, D194N or ΔRCC1-expressing viruses for 24 h and subjected to flow cytometry analysis

SW-480 cells were infected with wild-type NEK9, D194N or ΔRCC1-expressing viruses for 24 h. Cells were harvested, fixed with cold ethanol, and stained with PI. A region has been drawn around cells to exclude possible debris or aggregated cells during cell cycle analysis. A second gate was used to exclude doublet cells.

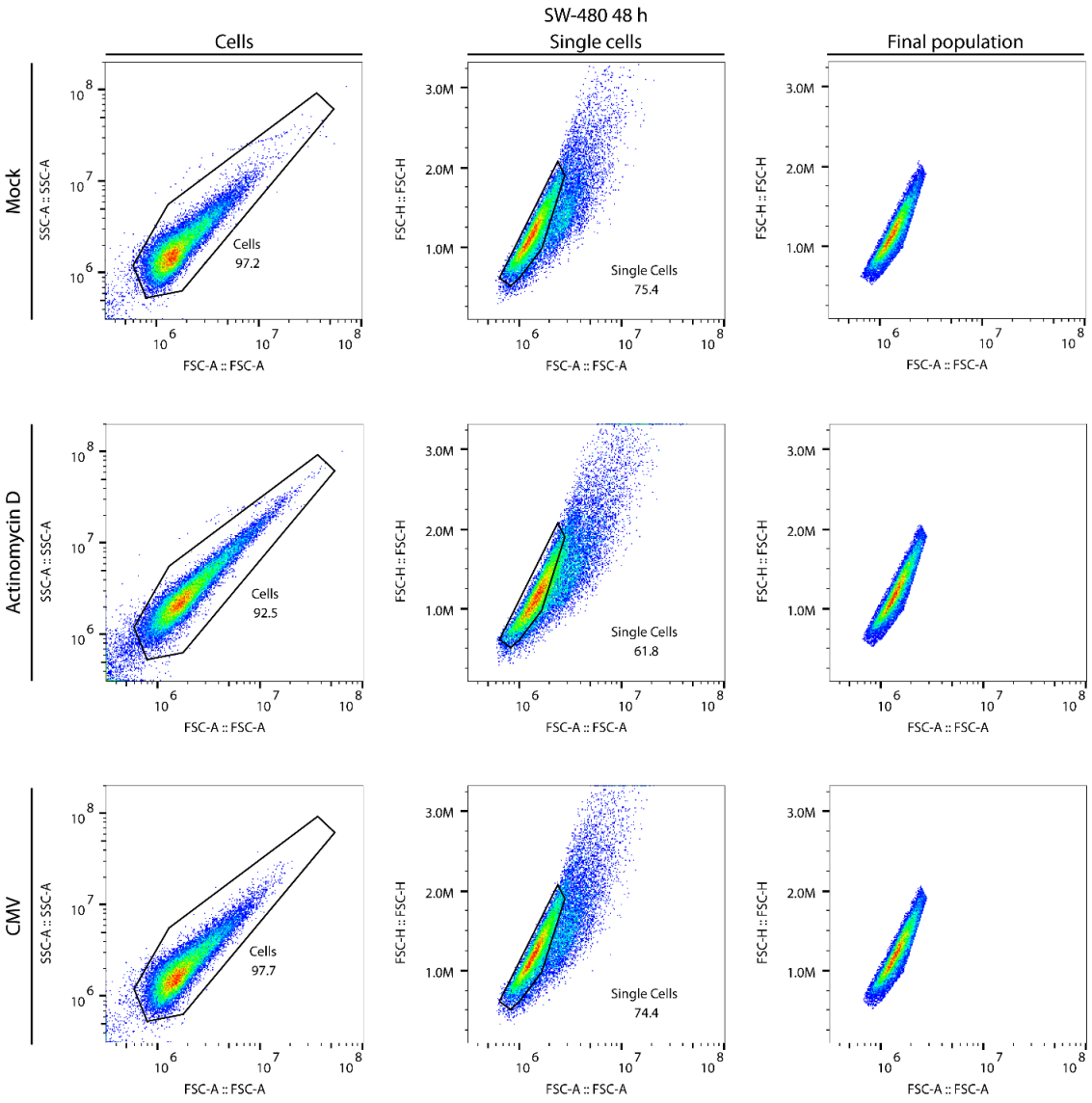

Fig. 48. SW-480 cells treated with actinomycin D or infected with Ad-CMV for 48 h subjected to flow cytometry analysis

SW-480 cells were infected with wild-type NEK9, D194N or ΔRCC1-expressing viruses for 48 h. Cells were harvested, fixed with cold ethanol, and stained with PI. A region has been drawn around cells to exclude possible debris or aggregated cells during cell cycle analysis. A second gate was used to exclude doublet cells.

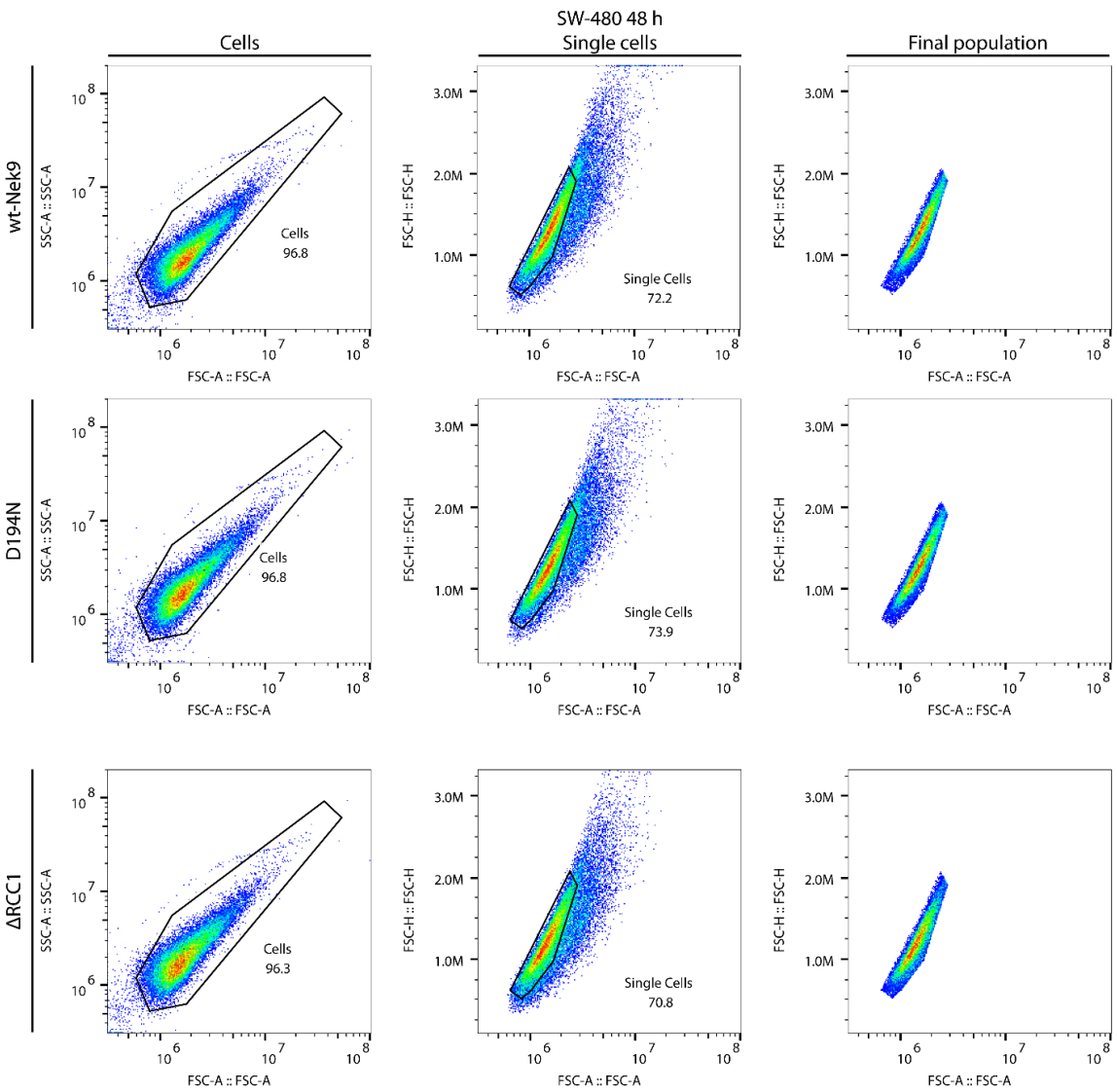

Fig. 49. SW-480 cells infected with wild-type NEK9, D194N or ΔRCC1-expressing viruses for 48 h and subjected to flow cytometry analysis

SW-480 cells were infected with wild-type NEK9, D194N or ΔRCC1-expressing viruses for 48 h. Cells were harvested, fixed with cold ethanol, and stained with PI. A region has been drawn around cells to exclude possible debris or aggregated cells during cell cycle analysis. A second gate was used to exclude doublet cells.

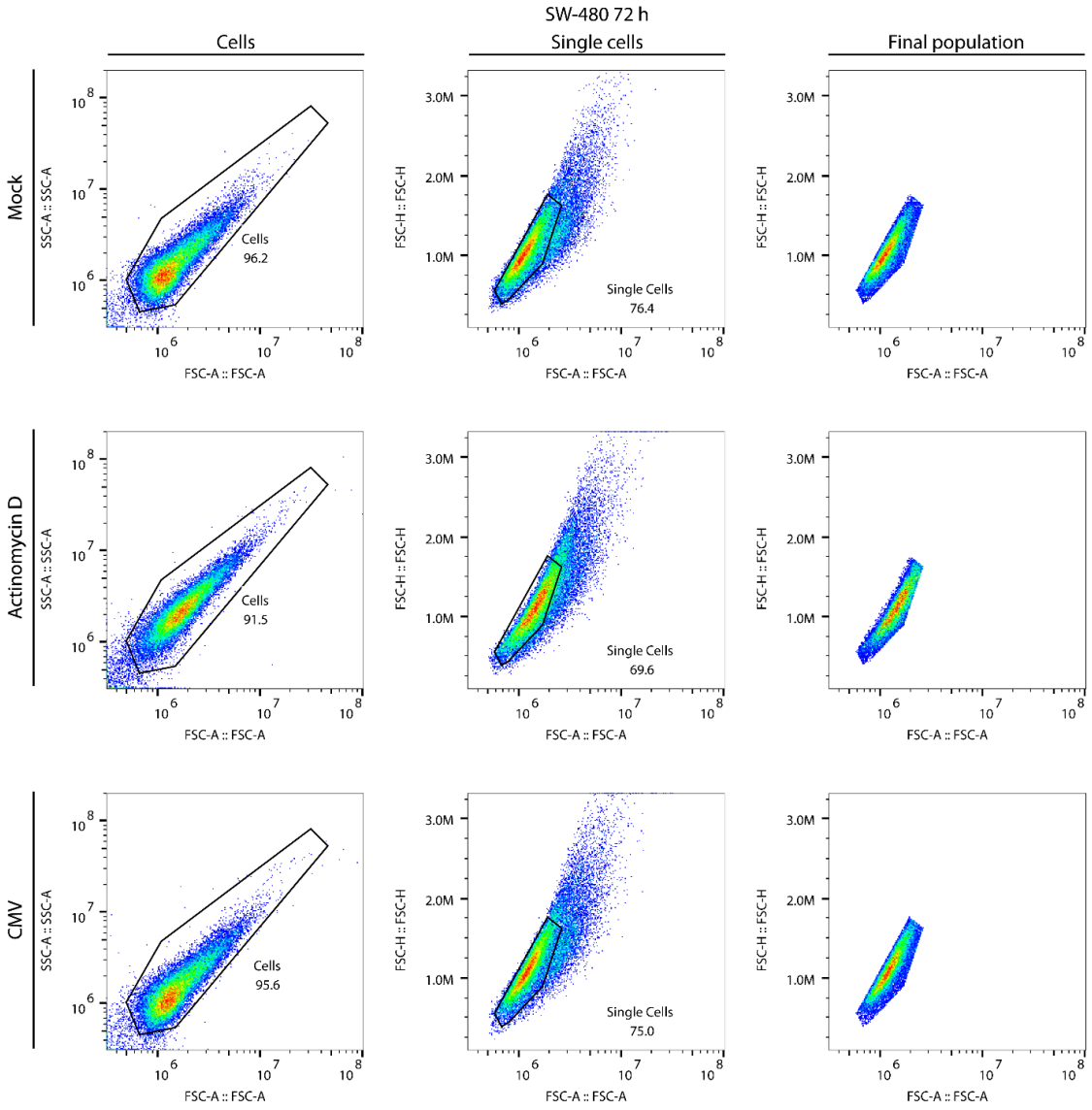

Fig. 50. SW-480 cells treated with actinomycin D or infected with Ad-CMV for 72 h subjected to flow cytometry analysis

SW-480 cells were treated with actinomycin D or infected with Ad-CMV for 72 h. Cells were harvested, fixed with cold ethanol, and stained with PI. A region has been drawn around cells to exclude possible debris or aggregated cells during cell cycle analysis. A second gate was used to exclude doublet cells.

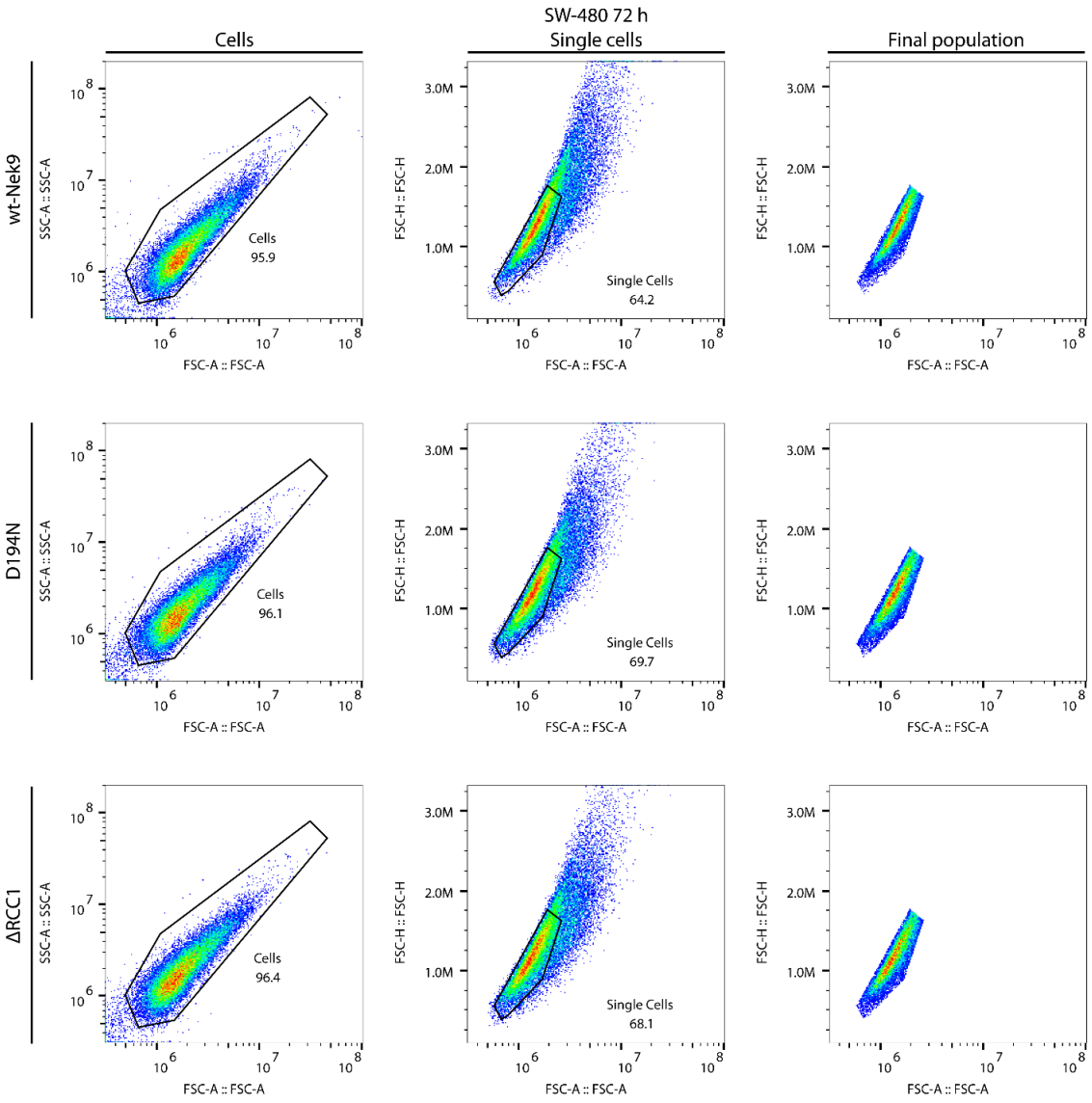

Fig. 51. SW-480 cells infected with wild-type NEK9, D194N or ΔRCC1-expressing viruses for 72 h and subjected to flow cytometry analysis

SW-480 cells were infected with wild-type NEK9, D194N or ΔRCC1-expressing viruses for 72 h. Cells were harvested, fixed with cold ethanol, and stained with PI. A region has been drawn around cells to exclude possible debris or aggregated cells during cell cycle analysis. A second gate was used to exclude doublet cells.

5.4. References:

1. Doronin, K. *et al.* Tumor-Specific, Replication-Competent Adenovirus Vectors Overexpressing the Adenovirus Death Protein. *J. Virol.* (2000). doi:10.1128/jvi.74.13.6147-6155.2000
2. Schafer, K. A. The Cell Cycle: A Review. *Veterinary Pathology* (1998). doi:10.1177/030098589803500601
3. Alberts, B. *et al.* DNA replication mechanisms. in *Molecular Biology of the Cell* (2002).
4. Liskay, R. M. Absence of a measurable G2 phase in two Chinese hamster cell lines. *Proc. Natl. Acad. Sci. U. S. A.* (1977). doi:10.1073/pnas.74.4.1622
5. Robbins, E. & Scharff, M. D. The absence of a detectable G1 phase in a cultured strain of Chinese hamster lung cell. *J. Cell Biol.* (1967). doi:10.1083/jcb.34.2.684
6. O'Connor, C. Cell Division: Stages of Mitosis. *Nature Education* (2008).
7. Barnum, K. J. & O'Connell, M. J. Cell cycle regulation by checkpoints. *Methods in Molecular Biology* (2014). doi:10.1007/978-1-4939-888-2_2
8. Vermeulen, K., Van Bockstaele, D. R. & Berneman, Z. N. The cell cycle: A review of regulation, deregulation and therapeutic targets in cancer. *Cell Proliferation* (2003). doi:10.1046/j.1365-2184.2003.00266.x
9. King, K. L. & Cidlowski, J. A. Cell cycle regulation and apoptosis. *Annual Review of Physiology* (1998). doi:10.1146/annurev.physiol.60.1.601
10. Topacio, B. R. *et al.* Cyclin D-Cdk4,6 Drives Cell-Cycle Progression via the Retinoblastoma Protein's C-Terminal Helix. *Mol. Cell* (2019). doi:10.1016/j.molcel.2019.03.020
11. Draetta, G. & Beach, D. Activation of cdc2 protein kinase during mitosis in human cells:

Cell cycle-dependent phosphorylation and subunit rearrangement. *Cell* (1988). doi:10.1016/0092-8674(88)90175-4

12. Slangy, A. *et al.* Phosphorylation by p34cdc2 regulates spindle association of human Eg5, a kinesin-related motor essential for bipolar spindle formation in vivo. *Cell* (1995). doi:10.1016/0092-8674(95)90142-6
13. Kimura, K., Hirano, M., Kobayashi, R. & Hirano, T. Phosphorylation and activation of 13S condensin by Cdc2 in vitro. *Science (80-.).* (1998). doi:10.1126/science.282.5388.487
14. Rhind, N. & Russell, P. Signaling pathways that regulate cell division. *Cold Spring Harb. Perspect. Biol.* (2012). doi:10.1101/cshperspect.a005942
15. Salaun, P., Rannou, Y. & Claude, P. Cdk1, plks, auroras, and neks: The mitotic bodyguards. in *Advances in Experimental Medicine and Biology* (2008). doi:10.1007/978-0-387-69080-3_4
16. Willems, E. *et al.* The functional diversity of Aurora kinases: A comprehensive review. *Cell Division* (2018). doi:10.1186/s13008-018-0040-6
17. Barr, F. A., Silljé, H. H. W. & Nigg, E. A. Polo-like kinases and the orchestration of cell division. *Nature Reviews Molecular Cell Biology* (2004). doi:10.1038/nrm1401
18. Caglar, H. O. & Biray Avci, C. Alterations of cell cycle genes in cancer: unmasking the role of cancer stem cells. *Molecular Biology Reports* (2020). doi:10.1007/s11033-020-05341-6
19. Hanahan, D. & Weinberg, R. A. The hallmarks of cancer. *Cell* (2000). doi:10.1016/S0092-8674(00)81683-9
20. Hanahan, D. & Weinberg, R. A. Hallmarks of cancer: The next generation. *Cell* **144**, 646–

674 (2011).

21. Shortt, J. & Johnstone, R. W. Oncogenes in cell survival and cell death. *Cold Spring Harb. Perspect. Biol.* (2012). doi:10.1101/cshperspect.a009829

22. Martin, G. S. Rous sarcoma virus: A function required for the maintenance of the transformed state. *Nature* (1970). doi:10.1038/2271021a0

23. Duesberg, P. H. & Vogt, P. K. Differences between the ribonucleic acids of transforming and nontransforming avian tumor viruses. *Proc. Natl. Acad. Sci. U. S. A.* (1970). doi:10.1073/pnas.67.4.1673

24. Barbosa, M. S. *et al.* The region of the HPV E7 oncoprotein homologous to adenovirus E1a and SV40 large T antigen contains separate domains for Rb binding and casein kinase II phosphorylation. *EMBO J.* (1990). doi:10.1002/j.1460-2075.1990.tb08091.x

25. Hall, A. Oncogenes - implications for human cancer: A review. *Journal of the Royal Society of Medicine* (1984).

26. Marco A. Pierotti, PhD, Gabriella Sozzi, PhD, and Carlo M. Croce, M. Discovery and identification of oncogenes. in *Holland-Frei Cancer Medicine. 6th edition.* (ed. Kufe DW, Pollock RE, Weichselbaum RR, et al.) (BC Decker, 2003).

27. Mantovani, F., Collavin, L. & Del Sal, G. Mutant p53 as a guardian of the cancer cell. *Cell Death and Differentiation* (2019). doi:10.1038/s41418-018-0246-9

28. Courtois-Cox, S., Jones, S. L. & Cichowski, K. Many roads lead to oncogene-induced senescence. *Oncogene* **27**, 2801–2809 (2008).

29. White, E. Regulation of the cell cycle and apoptosis by the oncogenes of adenovirus. *Oncogene* **20**, 7836–7846 (2001).

30. Castel, P., Rauen, K. A. & McCormick, F. The duality of human oncoproteins: drivers of

cancer and congenital disorders. *Nature Reviews Cancer* (2020). doi:10.1038/s41568-020-0256-z

31. De Visser, K. E., Eichten, A. & Coussens, L. M. Paradoxical roles of the immune system during cancer development. *Nat. Rev. Cancer* **6**, 24–37 (2006).

32. Jin, M. H. & Oh, D. Y. ATM in DNA repair in cancer. *Pharmacology and Therapeutics* (2019). doi:10.1016/j.pharmthera.2019.07.002

33. Levine, A. J. p53: 800 million years of evolution and 40 years of discovery. *Nat. Rev. Cancer* (2020). doi:10.1038/s41568-020-0262-1

34. Godet, I. & M. Gilkes, D. BRCA1 and BRCA2 mutations and treatment strategies for breast cancer. *Integr. Cancer Sci. Ther.* (2017). doi:10.15761/icst.1000228

35. Fradet-Turcotte, A., Sitz, J., Grapton, D. & Orthwein, A. BRCA2 functions: From DNA repair to replication fork stabilization. *Endocrine-Related Cancer* (2016). doi:10.1530/ERC-16-0297

36. Meek, D. W. The p53 response to DNA damage. *DNA Repair* (2004). doi:10.1016/j.dnarep.2004.03.027

37. Brady, C. A. & Attardi, L. D. P53 At a Glance. *J. Cell Sci.* **123**, 2527–2532 (2010).

38. Chen, J. The cell-cycle arrest and apoptotic functions of p53 in tumor initiation and progression. *Cold Spring Harb. Perspect. Med.* (2016). doi:10.1101/cshperspect.a026104

39. Lens, S. M. A. & Medema, R. H. Cytokinesis defects and cancer. *Nature Reviews Cancer* (2019). doi:10.1038/s41568-018-0084-6

40. Elmore, S. Apoptosis: A Review of Programmed Cell Death. *Toxicologic Pathology* (2007). doi:10.1080/01926230701320337

41. Boutelle, A. M. & Attardi, L. D. p53 and Tumor Suppression: It Takes a Network. *Trends*

in Cell Biology **31**, 298–310 (2021).

42. Watters, D. Molecular mechanisms of ionizing radiation-induced apoptosis. in *Immunology and Cell Biology* **77**, 263–271 (1999).

43. Morales, J. C. *et al. Review of Poly (ADP-ribose) Polymerase (PARP) Mechanisms of Action and Rationale for Targeting in Cancer and Other Diseases*.

44. Goodwin, J. F. & Knudsen, K. E. Beyond DNA repair: DNA-PK function in cancer. doi:10.1158/2159-8290.CD-14-0358

45. Vávrová, J. & Řezáčová, M. *The Importance of Senescence in Ionizing Radiation-Induced Tumour Suppression (review / senescence / ionizing radiation / cytokine expression)*. *Folia Biologica (Praha)* **57**, (2011).

46. Moldovan, G. L., Pfander, B. & Jentsch, S. PCNA, the Maestro of the Replication Fork. *Cell* (2007). doi:10.1016/j.cell.2007.05.003

47. Lee, S. & Schmitt, C. A. The dynamic nature of senescence in cancer. *Nature Cell Biology* (2019). doi:10.1038/s41556-018-0249-2

48. Kastenhuber, E. R. & Lowe, S. W. Putting p53 in Context. *Cell* (2017). doi:10.1016/j.cell.2017.08.028

49. Reinhardt, H. C. & Schumacher, B. The p53 network: Cellular and systemic DNA damage responses in aging and cancer. *Trends in Genetics* (2012). doi:10.1016/j.tig.2011.12.002

50. Jung, R., Radko, S. & Pelka, P. The Dual Nature of Nek9 in Adenovirus Replication. *J. Virol.* **90**, 1931–1943 (2016).

51. Sanz, G., Singh, M., Peuget, S. & Selivanova, G. Inhibition of p53 inhibitors: Progress, challenges and perspectives. *Journal of Molecular Cell Biology* **11**, 586–599 (2019).

52. Donehower, L. A. The p53-deficient mouse: A model for basic and applied cancer studies.

Seminars in Cancer Biology **7**, 269–278 (1996).

53. Aubrey, B. J., Kelly, G. L., Janic, A., Herold, M. J. & Strasser, A. How does p53 induce apoptosis and how does this relate to p53-mediated tumour suppression? *Cell Death Differ.* **25**, 104–113 (2018).

54. Petroulakis, E. *et al.* p53-Dependent Translational Control of Senescence and Transformation via 4E-BPs. *Cancer Cell* **16**, 439–446 (2009).

55. Bunz, F. *et al.* Disruption of p53 in human cancer cells alters the responses to therapeutic agents. *J. Clin. Invest.* **104**, 263–269 (1999).

56. Wang, Y., Zhu, S., Cloughesy, T. F., Liau, L. M. & Mischel, P. S. p53 disruption profoundly alters the response of human glioblastoma cells to DNA topoisomerase I inhibition. *Oncogene* **23**, 1283–1290 (2004).

57. Muz, B., De La Puente, P., Azab, F. & Azab, A. K. Hypoxia Dovepress The role of hypoxia in cancer progression, angiogenesis, metastasis, and resistance to therapy. (2015). doi:10.2147/HP.S93413

58. Sermeus, A. & Michiels, C. Reciprocal influence of the p53 and the hypoxic pathways. **2**, (2011).

59. Koumenis, C. *et al.* Regulation of p53 by Hypoxia: Dissociation of Transcriptional Repression and Apoptosis from p53-Dependent Transactivation. *Mol. Cell. Biol.* **21**, 1297–1310 (2001).

60. Vander Heiden, M. G., Cantley, L. C. & Thompson, C. B. Understanding the Warburg Effect: The Metabolic Requirements of Cell Proliferation NIH Public Access. *Science (80-.).* **324**, 1029–1033 (2009).

61. Cross, T. G. *et al.* Serine/threonine protein kinases and apoptosis. *Exp. Cell Res.* **256**, 34–

41 (2000).

62. Kale, J., Osterlund, E. J. & Andrews, D. W. BCL-2 family proteins: Changing partners in the dance towards death. *Cell Death and Differentiation* (2018). doi:10.1038/cdd.2017.186

63. Toshiyuki, M. & Reed, J. C. Tumor suppressor p53 is a direct transcriptional activator of the human bax gene. *Cell* (1995). doi:10.1016/0092-8674(95)90412-3

64. Haldar, S., Negrini, M., Monne, M., Sabbioni, S. & Croce, C. M. Down-Regulation of bcl-2 by p53 in Breast Cancer Cells. *Cancer Res.* (1994).

65. Giam, M., Huang, D. & Bouillet, P. BH3-only proteins and their roles in programmed cell death. *Oncogene* **27**, 128–136 (2009).

66. Hemann, M. T. & Lowe, S. W. The p53-Bcl-2 connection. *Cell Death Differ.* (2006). doi:10.1038/sj.cdd.4401962

67. Czabotar, P. E., Lessene, G., Strasser, A. & Adams, J. M. Control of apoptosis by the BCL-2 protein family: Implications for physiology and therapy. *Nat. Rev. Mol. Cell Biol.* **15**, 49–63 (2014).

68. Shikama, N. *et al.* A novel cofactor for p300 that regulates the p53 response. *Mol. Cell* (1999). doi:10.1016/S1097-2765(00)80338-X

69. Silva, M. T., Do Vale, A. & Dos Santos, N. M. N. Secondary necrosis in multicellular animals: An outcome of apoptosis with pathogenic implications. *Apoptosis* (2008). doi:10.1007/s10495-008-0187-8

70. Shalini, S., Dorstyn, L., Dawar, S. & Kumar, S. Old, new and emerging functions of caspases. *Cell Death Differ.* **22**, 526–539 (2015).

71. Dewson, G. & Kluck, R. M. Mechanisms by which Bak and Bax permeabilise

mitochondria during apoptosis. *J. Cell Sci.* **122**, 2801–2808 (2009).

72. Silva, M. T. Secondary necrosis: The natural outcome of the complete apoptotic program. *FEBS Letters* (2010). doi:10.1016/j.febslet.2010.10.046

73. Rydell-Törmänen, K., Uller, L. & Erjefält, J. S. Neutrophil cannibalism - A back up when the macrophage clearance system is insufficient. *Respir. Res.* (2006). doi:10.1186/1465-9921-7-143

74. He, S. & Sharpless, N. E. Senescence in Health and Disease. *Cell* (2017). doi:10.1016/j.cell.2017.05.015

75. Campisi, J. Cellular senescence : when bad things. **8**, (2007).

76. Shay, J. W. & Roninson, I. B. Hallmarks of senescence in carcinogenesis and cancer therapy. *Oncogene* **23**, 2919–2933 (2004).

77. Noureddine, H. *et al.* Pulmonary artery smooth muscle cell senescence is a pathogenic mechanism for pulmonary hypertension in chronic lung disease. *Circ. Res.* (2011). doi:10.1161/CIRCRESAHA.111.241299

78. Kurioka, D. *et al.* NEK9-dependent proliferation of cancer cells lacking functional p53. *Sci. Rep.* **4**, 3–10 (2014).

79. Braig, M. & Schmitt, C. A. Oncogene-induced senescence: Putting the brakes on tumor development. *Cancer Res.* **66**, 2881–2884 (2006).

80. Kowalski, P., Dihel, N. & Garcia, M. Chapter 8. *World* **1**, 283–331 (2008).

81. Humphreys, D., Elghazaly, M. & Frisan, T. Senescence and Host–Pathogen Interactions. 1–17 (2020).

82. Chandeck, C. & Mooi, W. J. Oncogene-induced cellular senescence. *Adv. Anat. Pathol.* **17**, 42–48 (2010).

83. Roskoski, R. A historical overview of protein kinases and their targeted small molecule inhibitors. *Pharmacological Research* (2015). doi:10.1016/j.phrs.2015.07.010

84. BURNETT, G. & KENNEDY, E. P. The enzymatic phosphorylation of proteins. *J. Biol. Chem.* (1954).

85. McCubrey, J. A., May, W. S., Duronio, V. & Mufson, A. Serine/threonine phosphorylation in cytokine signal transduction. *Leukemia* **14**, 9–21 (2002).

86. Ardito, F., Giuliani, M., Perrone, D., Troiano, G. & Muzio, L. Lo. The crucial role of protein phosphorylation in cell signalingand its use as targeted therapy (Review). *International Journal of Molecular Medicine* (2017). doi:10.3892/ijmm.2017.3036

87. Shi, X. *et al.* Research progress on the PI3K/AKT signaling pathway in gynecological cancer (Review). *Mol. Med. Rep.* (2019). doi:10.3892/mmr.2019.10121

88. Ma, Q., Gabelli, S. B. & Raben, D. M. Diacylglycerol kinases: Relationship to other lipid kinases. *Advances in Biological Regulation* (2019). doi:10.1016/j.jbior.2018.09.014

89. Franklin, R. A. & McCubrey, J. A. Kinases: Positive and negative regulators of apoptosis. *Leukemia* (2000). doi:10.1038/sj.leu.2401967

90. Deshpande, A., Sicinski, P. & Hinds, P. W. Cyclins and cdks in development and cancer: A perspective. *Oncogene* (2005). doi:10.1038/sj.onc.1208618

91. Meirelles, G. V. *et al.* 'Stop Ne(c)king around': How interactomics contributes to functionally characterize Nek family kinases. *World J. Biol. Chem.* (2014). doi:10.4331/wjbc.v5.i2.141

92. Peppelenbosch, M. P. Kinome Profiling. *Scientifica (Cairo).* (2012). doi:10.6064/2012/306798

93. Cicenas, J., Zalyte, E., Bairoch, A. & Gaudet, P. Kinases and cancer. *Cancers* (2018).

doi:10.3390/cancers10030063

94. Malumbres, M. & Barbacid, M. Cell cycle kinases in cancer. *Current Opinion in Genetics and Development* (2007). doi:10.1016/j.gde.2006.12.008

95. Takai, N., Hamanaka, R., Yoshimatsu, J. & Miyakawa, I. Polo-like kinases (Plks) and cancer. *Oncogene* (2005). doi:10.1038/sj.onc.1208272

96. Lee, J. W. *et al.* Combined Aurora kinase A (AURKA) and WEE1 inhibition demonstrates synergistic antitumor effect in squamous cell carcinoma of the head and neck. *Clin. Cancer Res.* (2019). doi:10.1158/1078-0432.CCR-18-0440

97. Fang, Y. & Zhang, X. Targeting NEK2 as a promising therapeutic approach for cancer treatment. *Cell Cycle* **15**, 895–907 (2016).

98. O'Connell, M. J., Krien, M. J. E. & Hunter, T. Never say never. The NIMA-related protein kinases in mitotic control. *Trends in Cell Biology* (2003). doi:10.1016/S0962-8924(03)00056-4

99. O'Regan, L., Blot, J. & Fry, A. M. Mitotic regulation by NIMA-related kinases. *Cell Div.* (2007). doi:10.1186/1747-1028-2-25

100. Casey, J. P. *et al.* Recessive NEK9 mutation causes a lethal skeletal dysplasia with evidence of cell cycle and ciliary defects. *Hum. Mol. Genet.* (2016). doi:10.1093/hmg/ddw054

101. Fry, A. M., Bayliss, R. & Roig, J. Mitotic regulation by NEK kinase networks. *Front. Cell Dev. Biol.* **5**, 1–13 (2017).

102. Chen, Y., Craigen, W. J. & Riley, D. J. Nek1 regulates cell death and mitochondrial membrane permeability through phosphorylation of VDAC1. *Cell Cycle* (2009). doi:10.4161/cc.8.2.7551

103. De Donato, M. *et al.* Nek6 and Hif-1α cooperate with the cytoskeletal gateway of drug resistance to drive outcome in serous ovarian cancer. *Am. J. Cancer Res.* (2015).

104. Lee, M. Y. *et al.* Nek6 is involved in G2/M phase cell cycle arrest through DNA damage-induced phosphorylation. *Cell Cycle* **7**, 2705–2709 (2008).

105. Kim, S., Lee, K. & Rhee, K. NEK7 is a centrosomal kinase critical for microtubule nucleation. *Biochem. Biophys. Res. Commun.* (2007). doi:10.1016/j.bbrc.2007.05.206

106. Salem, H. *et al.* Nek7 kinase targeting leads to early mortality, cytokinesis disturbance and polyploidy. *Oncogene* **29**, 4046–4057 (2010).

107. Miller, S. L., Antico, G., Raghunath, P. N., Tomaszewski, J. E. & Clevenger, C. V. Nek3 kinase regulates prolactin-mediated cytoskeletal reorganization and motility of breast cancer cells. *Oncogene* (2007). doi:10.1038/sj.onc.1210264

108. Bowers, A. J. & Boylan, J. F. Nek8, a NIMA family kinase member, is overexpressed in primary human breast tumors. *Gene* (2004). doi:10.1016/j.gene.2003.12.002

109. Christodoulou, E. *et al.* NEK11 as a candidate high-penetrance melanoma susceptibility gene. *J. Med. Genet.* **57**, 203–210 (2020).

110. Fry, A. M., O'Regan, L., Sabir, S. R. & Bayliss, R. Cell cycle regulation by the NEK family of protein kinases. *J. Cell Sci.* **125**, 4423–4433 (2012).

111. Kaneta, Y. & Ullrich, A. NEK9 depletion induces catastrophic mitosis by impairment of mitotic checkpoint control and spindle dynamics. *Biochem. Biophys. Res. Commun.* **442**, 139–146 (2013).

112. Eibes, S. *et al.* Nek9 Phosphorylation Defines a New Role for TPX2 in Eg5-Dependent Centrosome Separation before Nuclear Envelope Breakdown. *Curr. Biol.* (2018). doi:10.1016/j.cub.2017.11.046

113. Sdelci, S. *et al.* Nek9 phosphorylation of NEDD1/GCP-WD contributes to Plk1 control of γ-tubulin recruitment to the mitotic centrosome. *Curr. Biol.* **22**, 1516–1523 (2012).

114. Roig, J., Groen, A., Caldwell, J. & Avruch, J. Active Nercc1 protein kinase concentrates at centrosomes early in mitosis and is necessary for proper spindle assembly. *Mol. Biol. Cell* (2005). doi:10.1091/mbc.E05-04-0315

115. O'Regan, L. & Fry, A. M. The Nek6 and Nek7 Protein Kinases Are Required for Robust Mitotic Spindle Formation and Cytokinesis. *Mol. Cell. Biol.* **29**, 3975–3990 (2009).

116. Haq, T. *et al.* Mechanistic basis of Nek7 activation through Nek9 binding and induced dimerization. *Nat. Commun.* **6**, 8771 (2015).

117. Bertran, M. T. *et al.* Nek9 is a Plk1-activated kinase that controls early centrosome separation through Nek6/7 and Eg5. *EMBO J.* **30**, 2634–2647 (2011).

118. Yang, S. W. *et al.* Nek9 regulates spindle organization and cell cycle progression during mouse oocyte meiosis and its location in early embryo mitosis. *Cell Cycle* **11**, 4366–4377 (2012).

119. Gallego, P., Velazquez-Campoy, A., Regue, L., Roig, J. & Reverter, D. Structural analysis of the regulation of the DYNLL/LC8 binding to Nek9 by phosphorylation. *J. Biol. Chem.* (2013). doi:10.1074/jbc.M113.459149

120. Regué, L. *et al.* DYNLL/LC8 protein controls signal transduction through the Nek9/Nek6 signaling module by regulating Nek6 binding to Nek9. *J. Biol. Chem.* (2011). doi:10.1074/jbc.M110.209080

121. Sdelci, S. *et al.* Nek9 phosphorylation of NEDD1/GCP-WD contributes to Plk1 control of γ-tubulin recruitment to the mitotic centrosome. *Curr. Biol.* (2012). doi:10.1016/j.cub.2012.06.027

122. Hadjebi, O., Casas-Terradellas, E., Garcia-Gonzalo, F. R. & Rosa, J. L. The RCC1 superfamily: From genes, to function, to disease. *Biochimica et Biophysica Acta - Molecular Cell Research* (2008). doi:10.1016/j.bbamcr.2008.03.015

123. O'Regan, L. *et al.* EML4-ALK V3 Drives Cell Migration Through NEK9 and NEK7 Kinases in Non-Small-Cell Lung Cancer. *SSRN Electron. J.* (2019). doi:10.2139/ssrn.3377373

124. Roig, J., Mikhailov, A., Belham, C. & Avruch, J. Nercc1, a mammalian NIMA-family kinase, binds the Ran GTPase and regulates mitotic progression. *Genes Dev.* (2002). doi:10.1101/gad.972202

125. Tan, B. C. M. & Lee, S. C. Nek9, a Novel FACT-associated Protein, Modulates Interphase Progression. *J. Biol. Chem.* (2004). doi:10.1074/jbc.M311477200

126. Roig, J., Mikhailov, A., Belham, C. & Avruch, J. Nercc1, a mammalian NIMA-family kinase, binds the Ran GTPase and regulates mitotic progression. *Genes Dev.* (2002). doi:10.1101/gad.972202

127. Yamamoto, Y. *et al.* NEK9 regulates primary cilia formation by acting as a selective autophagy adaptor for MYH9/myosin IIA. *Nat. Commun.* **12**, 3292 (2021).

128. Consortium, I. M. P. Nek9 Knockout Mice. *IMPC* (2019). Available at: https://www.mousephenotype.org/data/genes/MGI:2387995#phenotypesTab.

129. Mundt, F. *et al.* Mass spectrometry–based proteomics reveals potential roles of NEK9 and MAP2K4 in resistance to PI3K inhibition in triple-negative breast cancers. *Cancer Res.* (2018). doi:10.1158/0008-5472.CAN-17-1990

130. Xu, Z. *et al.* Decreased Nek9 expression correlates with aggressive behaviour and predicts unfavourable prognosis in breast cancer. *Pathology* **52**, 329–335 (2020).

131. Phadke, M. *et al.* Dabrafenib inhibits the growth of *BRAF-WT* cancers through CDK16 and NEK9 inhibition. *Mol. Oncol.* 1–15 (2017). doi:10.1002/1878-0261.12152

132. Phadke, M. *et al.* Dabrafenib inhibits the growth of BRAF-WT cancers through CDK16 and NEK9 inhibition. *Mol. Oncol.* **12**, 74–88 (2018).

133. de Oliveira, A. P. *et al.* Checking neks: Overcoming a bottleneck in human diseases. *Molecules* **25**, 1–32 (2020).

134. Jung, R., Radko, S. & Pelka, P. The Dual Nature of Nek9 in Adenovirus Replication. *J. Virol.* **90**, 1931–1943 (2016).

135. Pelka, P. *et al.* Adenovirus E1A proteins direct subcellular redistribution of Nek9, a NimA-related kinase. *J. Cell. Physiol.* (2007). doi:10.1002/jcp.20983

136. Ea, A. *et al.* crossm Hacking the Cell : Network Intrusion and Exploitation by MANIPULATION OF CELLULAR PROTEIN INTERACTION NETWORKS BY VIRAL. 1–18 (2018).

137. Ghebremedhin, B. Human adenovirus: Viral pathogen with increasing importance. *Eur. J. Microbiol. Immunol.* (2014). doi:10.1556/eujmi.4.2014.1.2

138. Khanal, S., Ghimire, P. & Dhamoon, A. S. The repertoire of adenovirus in human disease: The innocuous to the deadly. *Biomedicines* (2018). doi:10.3390/biomedicines6010030

139. Lynch, J. P. & Kajon, A. E. Adenovirus: Epidemiology, Global Spread of Novel Serotypes, and Advances in Treatment and Prevention. *Semin. Respir. Crit. Care Med.* (2016). doi:10.1055/s-0036-1584923

140. Nedelman, M. 30 sickened in adenovirus outbreak in New Jersey, including 10 children who have died. *CNN* (2018). Available at: https://www.cnn.com/2018/11/06/health/adenovirus-outbreak-new-jersey/index.html.

141. Steinwaerder, D. S., Carlson, C. A. & Lieber, A. Human papilloma virus E6 and E7 proteins support DNA replication of adenoviruses deleted for the E1A and E1B genes. *Mol. Ther.* **4**, 211–216 (2001).

142. Balagué, C., Noya, F., Alemany, R., Chow, L. T. & Curiel, D. T. Human Papillomavirus E6E7-Mediated Adenovirus Cell Killing: Selectivity of Mutant Adenovirus Replication in Organotypic Cultures of Human Keratinocytes. *J. Virol.* **75**, 7602–7611 (2001).

143. Pipas, J. M. DNA Tumor Viruses and Their Contributions to Molecular Biology. (2019). doi:10.1128/JVI.01524-18

144. Weinmann, R., Raskas, H. J. & Roeder, R. G. Role of DNA dependent RNA polymerases II and III in transcription of the adenovirus genome late in productive infection. *Proc. Natl. Acad. Sci. U. S. A.* **71**, 3426–3430 (1974).

145. Gallimore, P. H. & Turnell, A. S. Adenovirus E1A: remodelling the host cell, a life or death experience. *Oncogene* (2001). doi:10.1038/sj.onc.1204913

146. Fessler, S. P. & Young, C. S. H. Control of Adenovirus Early Gene Expression during the Late Phase of Infection. *J. Virol.* (1998). doi:10.1128/jvi.72.5.4049-4056.1998

147. Mangel, W. F. & Martín, C. S. Structure, function and dynamics in adenovirus maturation. *Viruses* **6**, 4536–4570 (2014).

148. Berka, A. J. Discovery of RNA splicing and genes in pieces. *Proceedings of the National Academy of Sciences of the United States of America* (2016). doi:10.1073/pnas.1525084113

149. Berk, A. J. & Sharp, P. A. Sizing and mapping of early adenovirus mRNAs by gel electrophoresis of S1 endonuclease-digested hybrids. *Cell* (1977). doi:10.1016/0092-8674(77)90272-0

150. Flint, S. J., Berget, S. M. & Sharp, P. A. Characterization of single-stranded viral DNA sequences present during replication of adenovirus types 2 and 5. *Cell* **9**, 559–571 (1976).

151. Chow, L. T., Roberts, J. M., Lewis, J. B. & Broker, T. R. A map of cytoplasmic RNA transcripts from lytic adenovirus type 2, determined by electron microscopy of RNA:DNA hybrids. *Cell* (1977). doi:10.1016/0092-8674(77)90294-X

152. Flint, S. J. & Sharp, P. A. Adenovirus transcription. V. Quantitation of viral RNA sequences in adenovirus 2-infected and transformed cells. *J. Mol. Biol.* (1976). doi:10.1016/0022-2836(76)90263-1

153. Radko, S., Jung, R., Olanubi, O. & Pelka, P. Effects of adenovirus type 5 E1A isoforms on viral replication in arrested human cells. *PLoS One* **10**, 1–18 (2015).

154. Winberg, G. & Shenk, T. Dissection of overlapping functions within the adenovirus type 5 E1A gene. *EMBO J.* **3**, 1907–1912 (1984).

155. Glenn, G. M. & Ricciardi, R. P. Detailed kinetics of adenovirus type-5 steady-state transcripts during early infection. *Virus Res.* **9**, 73–91 (1988).

156. Binger, M. H. & Flint, S. J. Accumulation of early and intermediate mRNA species during subgroup C adenovirus productive infections. *Virology* **136**, 387–403 (1984).

157. Vetrini, F. & Ng, P. Gene therapy with helper-dependent adenoviral vectors: Current advances and future perspectives. *Viruses* (2010). doi:10.3390/v2091886

158. Han, J. *et al.* The E1B 19K protein blocks apoptosis by interacting with and inhibiting the p53-inducible and death-promoting Bax protein. *Genes Dev.* (1996). doi:10.1101/gad.10.4.461

159. Yew, P. R. & Berk, A. J. Inhibition of p53 transactivation required for transformation by adenovirus early 1B protein. *Nature* (1992). doi:10.1038/357082a0

160. Dallaire, F. *et al.* The Human Adenovirus Type 5 E4orf6/E1B55K E3 Ubiquitin Ligase Complex Can Mimic E1A Effects on E2F. *mSphere* (2016). doi:10.1128/msphere.00014-15

161. Cheng, C. Y. *et al.* Role of E1B55K in E4orf6/E1B55K E3 Ligase Complexes Formed by Different Human Adenovirus Serotypes. *J. Virol.* (2013). doi:10.1128/jvi.00384-13

162. Hidalgo, P., Ip, W. H., Dobner, T. & Gonzalez, R. A. The biology of the adenovirus E1B 55K protein. *FEBS Letters* (2019). doi:10.1002/1873-3468.13694

163. Hoeben, R. C. & Uil, T. G. Adenovirus DNA replication. *Cold Spring Harb. Perspect. Biol.* **5**, 1–11 (2013).

164. Mysiak, M. E., Holthuizen, P. E. & van der Vliet, P. The adenovirus priming protein pTP contributes to the kinetics of initiation of DNA replication. *Nucleic Acids Res.* (2004). doi:10.1093/nar/gkh726

165. De Jong, R. N. & Van Der Vliet, P. C. Mechanism of DNA replication in eukaryotic cells: Cellular host factors stimulating adenovirus DNA replication. *Gene* (1999). doi:10.1016/S0378-1119(99)00249-8

166. Chang, L. S. & Shenk, T. The adenovirus DNA-binding protein stimulates the rate of transcription directed by adenovirus and adeno-associated virus promoters. *J. Virol.* (1990). doi:10.1128/jvi.64.5.2103-2109.1990

167. Mul, Y. M. & Van Der Vliet, P. C. Nuclear factor I enhances adenovirus DNA replication by increasing the stability of a preinitiation complex. *EMBO J.* (1992). doi:10.1002/j.1460-2075.1992.tb05108.x

168. van Breukelen, B., Brenkman, A. B., Holthuizen, P. E. & van der Vliet, P. C. Adenovirus Type 5 DNA Binding Protein Stimulates Binding of DNA Polymerase to the Replication

Origin. *J. Virol.* (2003). doi:10.1128/jvi.77.2.915-922.2003

169. Lichtenstein, D. L., Toth, K., Doronin, K., Tollefson, A. E. & Wold, W. S. M. Functions and mechanisms of action of the adenovirus E3 proteins. *International Reviews of Immunology* (2004). doi:10.1080/08830180490265556

170. Ginsberg, H. S. *et al.* Role of early region 3 (E3) in pathogenesis of adenovirus disease. *Proc. Natl. Acad. Sci. U. S. A.* (1989). doi:10.1073/pnas.86.10.3823

171. McNees, A. L., Garnett, C. T. & Gooding, L. R. The Adenovirus E3 RID Complex Protects Some Cultured Human T and B Lymphocytes from Fas-Induced Apoptosis. *J. Virol.* (2002). doi:10.1128/jvi.76.19.9716-9723.2002

172. Virtanen, A. *et al.* mRNAs from human adenovirus 2 early region 4. *J. Virol.* (1984). doi:10.1128/jvi.51.3.822-831.1984

173. Freyer, G. A., Katoh, Y. & Roberts, R. J. Characterization of the major mRNAs from adenovirus 2 early region 4 by cDNA cloning and sequencing. *Nucleic Acids Res.* (1984). doi:10.1093/nar/12.8.3503

174. Weitzman, M. D. Functions of the adenovirus E4 proteins and their impact on viral vectors. *Frontiers in bioscience : a journal and virtual library* (2005). doi:10.2741/1604

175. O'Shea, C. C., Choi, S., McCormick, F. & Stokoe, D. Adenovirus overrides cellular checkpoints for protein translation. *Cell Cycle* (2005). doi:10.4161/cc.4.7.1791

176. Kong, K., Kumar, M., Taruishi, M. & Javier, R. T. The Human Adenovirus E4-ORF1 Protein Subverts Discs Large 1 to Mediate Membrane Recruitment and Dysregulation of Phosphatidylinositol 3-Kinase. *PLoS Pathog.* (2014). doi:10.1371/journal.ppat.1004102

177. Täuber, B. & Dobner, T. Adenovirus early E4 genes in viral oncogenesis. *Oncogene* (2001). doi:10.1038/sj/onc/1204914

178. Nakahara, T. & Lambert, P. F. Induction of promyelocytic leukemia (PML) oncogenic domains (PODs) by papillomavirus. *Virology* (2007). doi:10.1016/j.virol.2007.04.032

179. Ullman, A. J., Reich, N. C. & Hearing, P. Adenovirus E4 ORF3 Protein Inhibits the Interferon-Mediated Antiviral Response. *J. Virol.* (2007). doi:10.1128/jvi.02385-06

180. Soriano, A. M. *et al.* Adenovirus 5 E1A interacts with E4orf3 to regulate viral chromatin organization. *J. Virol.* **93**, (2019).

181. Shtrichman, R. & Kleinberger, T. Adenovirus Type 5 E4 Open Reading Frame 4 Protein Induces Apoptosis in Transformed Cells. *J. Virol.* (1998). doi:10.1128/jvi.72.4.2975-2982.1998

182. Branton, P. E. & Roopchand, D. E. The role of adenovirus E4orf4 protein in viral replication and cell killing. *Oncogene* (2001). doi:10.1038/sj.onc.1204862

183. Cress, W. D., Johnson, D. G. & Nevins, J. R. A genetic analysis of the E2F1 gene distinguishes regulation by Rb, p107, and adenovirus E4. *Mol. Cell. Biol.* (1993). doi:10.1128/mcb.13.10.6314

184. Huang, M. M. & Hearing, P. The adenovirus early region 4 open reading frame 6/7 protein regulates the DNA binding activity of the cellular transcription factor, E2F, through a direct complex. *Genes Dev.* (1989). doi:10.1101/gad.3.11.1699

185. Schaley, J., O'Connor, R. J., Taylor, L. J., Bar-Sagi, D. & Hearing, P. Induction of the Cellular E2F-1 Promoter by the Adenovirus E4-6/7 Protein. *J. Virol.* (2000). doi:10.1128/jvi.74.5.2084-2093.2000

186. O'Connor, R. J. & Hearing, P. The E4-6/7 Protein Functionally Compensates for the Loss of E1A Expression in Adenovirus Infection. *J. Virol.* (2000). doi:10.1128/jvi.74.13.5819-5824.2000

187. Siekierka, J., Mariano, T. M., Reichel, P. A. & Mathews, M. B. Translational control by adenovirus: Lack of virus-associated RNA(I) during adenovirus infection results in phosphorylation of initiation factor eIF-2 and inhibition of protein synthesis. *Proc. Natl. Acad. Sci. U. S. A.* **82**, 1959–1963 (1985).

188. O'Malley, R. P., Mariano, T. M., Siekierka, J. & Mathews, M. B. A mechanism for the control of protein synthesis by adenovirus VA RNAI. *Cell* (1986). doi:10.1016/0092-8674(86)90460-5

189. Launer-Felty, K., Wong, C. J. & Cole, J. L. Structural analysis of adenovirus VAI RNA defines the mechanism of inhibition of PKR. *Biophys. J.* (2015). doi:10.1016/j.bpj.2014.12.014

190. Thimmappaya, B., Weinberger, C., Schneider, R. J. & Shenk, T. Adenovirus VAI RNA is required for efficient translation of viral mRNAs at late times after infection. *Cell* (1982). doi:10.1016/0092-8674(82)90310-5

191. Ma, Y. & Mathews, M. B. Structure, function, and evolution of adenovirus-associated RNA: a phylogenetic approach. *J. Virol.* **70**, 5083–5099 (1996).

192. Maekawa, A. *et al.* Efficient production of adenovirus vector lacking genes of virus-associated RNAs that disturb cellular RNAi machinery. *Sci. Rep.* (2013). doi:10.1038/srep01136

193. Aparicio, O., Razquin, N., Zaratiegui, M., Narvaiza, I. & Fortes, P. Adenovirus Virus-Associated RNA Is Processed to Functional Interfering RNAs Involved in Virus Production. *J. Virol.* (2006). doi:10.1128/jvi.80.3.1376-1384.2006

194. Farley, D. C., Brown, J. L. & Leppard, K. N. Activation of the Early-Late Switch in Adenovirus Type 5 Major Late Transcription Unit Expression by L4 Gene Products. *J.*

Virol. **78**, 1782–1791 (2004).

195. Ahi, Y. S. & Mittal, S. K. Components of adenovirus genome packaging. *Frontiers in Microbiology* (2016). doi:10.3389/fmicb.2016.01503

196. Tribouley, C., Lutz, P., Staub, A. & Kedinger, C. The product of the adenovirus intermediate gene IVa2 is a transcriptional activator of the major late promoter. *J. Virol.* (1994). doi:10.1128/jvi.68.7.4450-4457.1994

197. Parks, R. J. Adenovirus protein IX: A new look at an old protein. *Molecular Therapy* (2005). doi:10.1016/j.ymthe.2004.09.018

198. Zhang, W. & Imperiale, M. J. Requirement of the Adenovirus IVa2 Protein for Virus Assembly. *J. Virol.* (2003). doi:10.1128/jvi.77.6.3586-3594.2003

199. Morris, S. J., Scott, G. E. & Leppard, K. N. Adenovirus Late-Phase Infection Is Controlled by a Novel L4 Promoter. *J. Virol.* (2010). doi:10.1128/jvi.00107-10

200. Wu, K., Guimet, D. & Hearing, P. The Adenovirus L4-33K Protein Regulates both Late Gene Expression Patterns and Viral DNA Packaging. *J. Virol.* (2013). doi:10.1128/jvi.00652-13

201. Reddy, V. S., Natchiar, S. K., Stewart, P. L. & Nemerow, G. R. Crystal structure of human adenovirus at 3.5 Å resolution. *Science (80-.).* (2010). doi:10.1126/science.1187292

202. Reddy, V. S. & Nemerow, G. R. Structures and organization of adenovirus cement proteins provide insights into the role of capsid maturation in virus entry and infection. *Proc. Natl. Acad. Sci. U. S. A.* (2014). doi:10.1073/pnas.1408462111

203. Anderson, C. W., Young, M. E. & Flint, S. J. Characterization of the adenovirus 2 virion protein, Mu. *Virology* (1989). doi:10.1016/0042-6822(89)90193-1

204. Russell, W. C. Adenoviruses: Update on structure and function. *Journal of General Virology* (2009). doi:10.1099/vir.0.003087-0

205. Webster, A., Leith, I. R., Nicholson, J., Hounsell, J. & Hay, R. T. Role of preterminal protein processing in adenovirus replication. *J. Virol.* **71**, 6381–6389 (1997).

206. Gupta, S. P., Shaik, B. & Prabhakar, Y. S. Advances in studies on adenovirus proteases and their inhibitors. in *Viral Proteases and Their Inhibitors* (2017). doi:10.1016/B978-0-12-809712-0.00003-4

207. Greber, U. F., Webster, P., Weber, J. & Helenius, A. The role of the adenovirus protease in virus entry into cells. *EMBO J.* (1996). doi:10.1002/j.1460-2075.1996.tb00525.x

208. Smith, S. C. *et al.* A gemcitabine sensitivity screen identifies a role for NEK9 in the replication stress response. *Nucleic Acids Res.* **42**, 11517–11527 (2014).

209. Miller, D. L., Myers, C. L., Rickards, B., Coller, H. A. & Flint, S. J. Adenovirus type 5 exerts genome-wide control over cellular programs governing proliferation, quiescence, and survival. *Genome Biol.* **8**, (2007).

210. Hsu, E., Pennella, M. A., Zemke, N. R., Eng, C. & Berk, A. J. Adenovirus E1A Activation Domain Regulates H3 Acetylation Affecting Varied Steps in Transcription at Different Viral Promoters. *J. Virol.* **92**, e00805-18 (2018).

211. Pelka, P. *et al.* Adenovirus E1A proteins direct subcellular redistribution of Nek9, a NimA-related kinase. *J. Cell. Physiol.* **212**, 13–25 (2007).

212. Hardy, S., Kitamura, M., Harris-Stansil, T., Dai, Y. & Phipps, M. L. Construction of adenovirus vectors through Cre-lox recombination. *J. Virol.* **71**, 1842–1849 (1997).

213. Addgene. General transfection. Available at: https://www.addgene.org/protocols/transfection/.

214. Radko, S., Jung, R., Olanubi, O. & Pelka, P. Effects of adenovirus type 5 E1A isoforms on viral replication in arrested human cells. *PLoS One* (2015). doi:10.1371/journal.pone.0140124

215. Peter Pelka. Characterization of the Interaction between the NIMA-Related Kinase Nek9 and Adenovirus E1A proteins. (McMaster University, 2006).

216. Numbers, C. SYBR ® Select Master Mix for CFX. **2012**, 7500 (2012).

217. Protocols., C. S. H. NP-40 Lysis Buffer. *Cold Spring Harbor Protocols.* (2006). Available at: http://cshprotocols.cshlp.org/content/2006/1/pdb.rec10423.full?text_only=true.

218. Protocols., C. S. H. SDS 2X Sample Buffer. *Cold Spring Harbor Protocols.* (2009). Available at: http://cshprotocols.cshlp.org/content/2009/10/pdb.rec11975.full.

219. Shen, W., Han, Q., Sun, F., Li, Z. & Li, L. Nek9,a sensitive immunohistochemical marker for Schwannian, melanocytic and myogenic tumours. *J. Clin. Pathol.* jclinpath-2020-206864 (2020). doi:10.1136/jclinpath-2020-206864

220. Moniz, L., Dutt, P., Haider, N. & Stambolic, V. Nek family of kinases in cell cycle, checkpoint control and cancer. *Cell Div.* **6**, 18 (2011).

221. Koba, M. & Konopa, J. [Actinomycin D and its mechanisms of action]. *Postepy Hig. Med. Dosw. (Online)* (2005).

222. Debacq-Chainiaux, F., Erusalimsky, J. D., Campisi, J. & Toussaint, O. Protocols to detect senescence-associated beta-galactosidase (SA-βgal) activity, a biomarker of senescent cells in culture and in vivo. *Nat. Protoc.* **4**, 1798–1806 (2009).

223. Riss, T. L. *et al. Cell Viability Assays*. *Assay Guidance Manual* (2004).

224. Kurioka, D. *et al.* NEK9-dependent proliferation of cancer cells lacking functional p53. *Sci. Rep.* **4**, 3–10 (2014).

225. Riccardi, C. & Nicoletti, I. Analysis of apoptosis by propidium iodide staining and flow cytometry. *Nat. Protoc.* **1**, 1458–1461 (2006).

226. Hayano, T. *et al.* Molecular characterization of an intact p53 pathway subtype in high-grade serous ovarian cancer. *PLoS One* **9**, 1–18 (2014).

227. Quarmby, L. M. & Mahjoub, M. R. Caught Nek-ing: Cilia and centrioles. *J. Cell Sci.* (2005). doi:10.1242/jcs.02681

228. Noguchi, K., Fukazawa, H., Murakami, Y. & Uehara, Y. Nek11, a new member of the NIMA family of kinases, involved in DNA replication and genotoxic stress responses. *J. Biol. Chem.* **277**, 39655–39665 (2002).

229. Liu, X. & Marmorstein, R. Structure of the retinoblastoma protein bound to adenovirus E1A reveals the molecular basis for viral oncoprotein inactivation of a tumor suppressor. *Genes Dev.* **21**, 2711–2716 (2007).

230. Jeon, Y. J. *et al.* Role of NEK6 in tumor promoter-induced transformation in JB6 C141 mouse skin epidermal cells. *J. Biol. Chem.* (2010). doi:10.1074/jbc.M110.137190

231. Choi, B. K. *et al.* Literature-based automated discovery of tumor suppressor p53 phosphorylation and inhibition by NEK2. *Proc. Natl. Acad. Sci. U. S. A.* (2018). doi:10.1073/pnas.1806643115

232. Haider, N. *et al.* NEK10 tyrosine phosphorylates p53 and controls its transcriptional activity. *Oncogene* (2020). doi:10.1038/s41388-020-1361-x

233. Chahal, J. S. & Flint, S. J. The p53 Protein Does Not Facilitate Adenovirus Type 5 Replication in Normal Human Cells. *J. Virol.* **87**, 6044–6046 (2013).

234. Gobeil, S., Boucher, C. C., Nadeau, D. & Poirier, G. G. Characterization of the necrotic cleavage of poly (ADP-ribose) polymerase (PARP-1): Implication of lysosomal proteases.

Cell Death Differ. (2001). doi:10.1038/sj.cdd.4400851

235. Liu, X. ling, Ding, J. & Meng, L. hua. Oncogene-induced senescence: a double edged sword in cancer. *Acta Pharmacologica Sinica* (2018). doi:10.1038/aps.2017.198

236. Tan, R. *et al.* Nek7 Protects Telomeres from Oxidative DNA Damage by Phosphorylation and Stabilization of TRF1. *Mol. Cell* (2017). doi:10.1016/j.molcel.2017.01.015

237. Jee, H. J. *et al.* Nek6 suppresses the premature senescence of human cancer cells induced by camptothecin and doxorubicin treatment. *Biochem. Biophys. Res. Commun.* (2011). doi:10.1016/j.bbrc.2011.04.083

238. Jee, H. J. *et al.* Nek6 overexpression antagonizes p53-induced senescence in human cancer cells. *Cell Cycle* (2010). doi:10.4161/cc.9.23.14059

239. Adib, R. *et al.* Mitotic phosphorylation by NEK6 and NEK7 reduces the microtubule affinity of EML4 to promote chromosome congression. *Sci. Signal.* **12**, (2019).

240. Kaneta, Y. & Ullrich, A. NEK9 depletion induces catastrophic mitosis by impairment of mitotic checkpoint control and spindle dynamics. *Biochem. Biophys. Res. Commun.* **442**, 139–146 (2013).

241. Morillo-Huesca, M. *et al.* FACT prevents the accumulation of free histones evicted from transcribed chromatin and a subsequent cell cycle delay in G1. *PLoS Genet.* (2010). doi:10.1371/journal.pgen.1000964

242. Takahata, S., Yu, Y. & Stillman, D. J. The E2F functional analogue SBF recruits the Rpd3(L) HDAC, via Whi5 and Stb1, and the FACT chromatin reorganizer, to yeast G1 cyclin promoters. *EMBO J.* (2009). doi:10.1038/emboj.2009.270

243. Shah, G. M., Shah, R. G. & Poirier, G. G. Different cleavage pattern for poly(ADP-ribose) polymerase during necrosis and apoptosis in HL-60 cells. *Biochem. Biophys. Res.*

Commun. (1996). doi:10.1006/bbrc.1996.1889

244. Petrova, V., Annicchiarico-Petruzzelli, M., Melino, G. & Amelio, I. The hypoxic tumour microenvironment Hypoxia and hypoxia-inducible factors. **7**, 10 (2018).

245. Shigaki, S. *et al.* A peptide microarray for the detection of protein kinase activity in cell lysate. *Anal. Sci.* **23**, 271–5 (2007).

246. Xue, L. & Tao, W. A. Current technologies to identify protein kinase substrates in high throughput. *Front. Biol. (Beijing).* **8**, 216–227 (2013).

247. Mok, J., Im, H. & Snyder, M. Global identification of protein kinase substrates by protein microarray analysis. *Nat. Protoc.* (2009). doi:10.1038/nprot.2009.194

248. Parikh, K. & Peppelenbosch, M. P. Kinome profiling of clinical cancer specimens. *Cancer Research* (2010). doi:10.1158/0008-5472.CAN-09-3989

249. Ma, H., Deacon, S. & Horiuchi, K. The challenge of selecting protein kinase assays for lead discovery optimization. *Expert Opinion on Drug Discovery* (2008). doi:10.1517/17460441.3.6.607

250. Corporation, K. B. Kinase Net. Available at: http://www.kinasenet.ca/.

251. Belham, C. *et al.* A mitotic cascade of NIMA family kinases: Nercc1/Nek9 activates the Nek6 and Nek7 kinases. *J. Biol. Chem.* **278**, 34897–34909 (2003).

252. Richards, M. W. *et al.* An Autoinhibitory Tyrosine Motif in the Cell-Cycle-Regulated Nek7 Kinase Is Released through Binding of Nek9. *Mol. Cell* **36**, 560–570 (2009).

253. Crisostomo, L., Soriano, A. M., Mendez, M., Graves, D. & Pelka, P. Correction: Temporal dynamics of adenovirus 5 gene expression in normal human cells(PLoS ONE (2019) 14:1 (e0211192) DOI: 10.1371/journal.pone.0211192). *PLoS One* **14**, 1–18 (2019).

254. Crisostomo, L., Soriano, A. M., Mendez, M., Graves, D. & Pelka, P. Temporal dynamics

of adenovirus 5 gene expression in normal human cells. *PLoS One* **14**, (2019).

255. Ziff, E. B. & Evans, R. M. Coincidence of the promoter and capped 5′ terminus of RNA from the adenovirus 2 major late transcription unit. *Cell* **15**, 1463–1475 (1978).

256. Shaw, A. R. & Ziff, E. B. Transcripts from the adenovirus-2 major late promoter yield a single early family of 3′ coterminal mRNAs and five late families. *Cell* **22**, 905–916 (1980).

257. Söderlund, H., Pettersson, U., Vennström, B., Philipson, L. & Mathews, M. B. A new species of virus-coded low molecular weight RNA from cells infected with adenovirus type 2. *Cell* **7**, 585–593 (1976).

258. Control, Q., Setup, R. & Equipment, R. ddPCR Supermix for Probes (Bio-Rad). 1–6 (2009).

259. BIO-RAD. SsoAdvanced Universal SYBR Green Supermix. 6101 (2017).

260. Aparicio, O., Razquin, N., Zaratiegui, M., Narvaiza, I. & Fortes, P. Adenovirus Virus-Associated RNA Is Processed to Functional Interfering RNAs Involved in Virus Production. *J. Virol.* **80**, 1376–1384 (2006).

261. Akusjärvi, G. Anatomy of region L1 from adenovirus type 2. *J. Virol.* **56**, 879–886 (1985).

262. Källsten, M. *et al.* Temporal characterization of the non-structural Adenovirus type 2 proteome and phosphoproteome using high-resolving mass spectrometry. *Virology* (2017). doi:10.1016/j.virol.2017.08.032

263. Masters, J. R. HeLa cells 50 years on: The good, the bad and the ugly. *Nature Reviews Cancer* (2002). doi:10.1038/nrc775

264. Krzywkowski, T., Ciftci, S., Assadian, F., Nilsson, M. & Punga, T. Simultaneous Single-

Cell In Situ Analysis of Human Adenovirus Type 5 DNA and mRNA Expression Patterns in Lytic and Persistent Infection. *J. Virol.* (2017). doi:10.1128/jvi.00166-17

265. Miller, M. S. *et al.* Characterization of the 55-Residue Protein Encoded by the 9S E1A mRNA of Species C Adenovirus. *J. Virol.* (2012). doi:10.1128/jvi.06399-11

266. Liao, H. J., Kobayashi, R. & Mathews, M. B. Activities of adenovirus virus-associated RNAs: Purification and characterization of RNA binding proteins. *Proc. Natl. Acad. Sci. U. S. A.* (1998). doi:10.1073/pnas.95.15.8514

267. Parsons, J. T. & Green, M. Biochemical studies on adenovirus multiplication. XVIII. Resolution of early virus-specific RNA species in Ad 2 infected and transformed cells. *Virology* (1971). doi:10.1016/0042-6822(71)90122-X

268. Cross, F. R. & Darnell, J. E. Cycloheximide stimulates early adenovirus transcription if early gene expression is allowed before treatment. *J. Virol.* (1983). doi:10.1128/jvi.45.2.683-692.1983

269. Akusjarvi, G. & Persson, H. Controls of RNA splicing and termination in the major late adenovirus transcription unit. *Nature* **292**, 420–426 (1981).

270. Yamashita, T. & Green, M. Adenovirus DNA Replication I. Requirement for Protein Synthesis and Isolation of Nuclear Membrane Fractions Containing Newly Synthesized Viral DNA and Proteins. *J. Virol.* **14**, 412–420 (1974).

271. Charman, M., Herrmann, C. & Weitzman, M. D. Viral and cellular interactions during adenovirus DNA replication. *FEBS Letters* (2019). doi:10.1002/1873-3468.13695

272. Hidalgo, P. & Gonzalez, R. A. Formation of adenovirus DNA replication compartments. *FEBS Lett.* (2019). doi:10.1002/1873-3468.13672

273. Schmid, M., Speiseder, T., Dobner, T. & Gonzalez, R. A. DNA Virus Replication

Compartments. *J. Virol.* (2014). doi:10.1128/jvi.02046-13

274. Schreiner, S., Wimmer, P. & Dobner, T. Adenovirus degradation of cellular proteins. *Future Microbiology* (2012). doi:10.2217/fmb.11.153

275. Miller, C. J. & Turk, B. E. Homing in: Mechanisms of Substrate Targeting by Protein Kinases. *Trends in Biochemical Sciences* (2018). doi:10.1016/j.tibs.2018.02.009

276. Bhat, R. A. & Thimmappaya, B. Construction and analysis of additional adenovirus substitution mutants confirm the complementation of VAI RNA function by two small RNAs encoded by Epstein-Barr virus. *J. Virol.* (1985). doi:10.1128/jvi.56.3.750-756.1985

277. Cascalló, M., Capellà, G., Mazo, A. & Alemany, R. Ras-dependent oncolysis with an adenovirus VAI mutant. *Cancer Res.* (2003).

278. Reichel, R. *et al.* The adenovirus E4 gene, in addition to the E1A gene, is important for trans-activation of E2 transcription and for E2F activation. *J. Virol.* (1989). doi:10.1128/jvi.63.9.3643-3650.1989

279. Komatsu, T. *et al.* Tracking adenovirus genomes identifies morphologically distinct late DNA replication compartments. *Traffic* (2016). doi:10.1111/tra.12429

280. Genoveso, M. J. *et al.* Formation of adenovirus DNA replication compartments and viral DNA accumulation sites by host chromatin regulatory proteins including NPM1. *FEBS J.* (2020). doi:10.1111/febs.15027